MOLECULAR-SCALE ENERGETIC EVENTS IN ORGANIC MOLECULAR CRYSTALS

A Dissertation

Presented to the Faculty of the Graduate School

of Cornell University

in Partial Fulfillment of the Requirements for the Degree of

Doctor of Philosophy

by

Joseph Edward Goose

February 2010

MOLECULAR-SCALE ENERGETIC EVENTS IN ORGANIC MOLECULAR CRYSTALS

Joseph Edward Goose, Ph.D.

Cornell University 2010

This thesis is broken up into two main parts: firstly, the characterisation of Ehrlich–Schwöebel barriers for some common organic molecules and secondly an examination of the hyperthermal deposition of pentacene. The Ehrlich–Schwöebel barrier of the sexiphenyl molecule was examined in detail and the system was used as a test case in the evaluation of the ability of potential models to capture accurate molecular conformation. The MM3π potential was found to be the best choice and even compared favourably to the best *ab initio* models. In the subsequent search for an Ehrlich–Schwöebel barrier the flexible backbone of the sexiphenyl molecule was observed to promote a “Fosbury Flop” type mechanism where the molecule rolls off the step edge with a minimum barrrier of 30-35 kJ/mol. After the introduction of six further small organic molecules (anthracene, tetracene, pentacene, diindenoperylene, C_{60} and rubrene), both homo–epitaxial and hetero–epitaxial barriers were studied and a correlation was found between the Ehrlich–Schwöebel barrier and the binding energy of the molecule to the terrace surface. Finally, the process of hyperthermal deposition of pentacene was examined using Molecular Dynamics simulations concentrating on mechanisms such as molecular insertion and adsorption. The behaviour of the system was documented as a function of incident energy (0-10eV), incident angle and molecular orientation and compared to published experimental data.

BIOGRAPHICAL SKETCH

Joseph Goose was born in Huddersfield in 1981 and moved to Grimsby at the age of five. Following the completion of his A-Levels at Franklin Sixth Form College he enrolled in undergraduate Chemical Engineering at Imperial College, London. Here after spending his third year abroad at the National University of Singapore he received a first class honours degree and was awarded the Shell Research Prize for his final year work with Professor George Jackson. The following year whilst applying for Graduate School he spent time as a teaching assistant at St. Mary's Roman Catholic School, working in fish factories and travelling to the Orient. The summer of 2004 saw his arrival at Cornell where he pursued his PhD under the tutelage of Professor Paulette Clancy. He was awarded the Hoey Prize for Research in 2009.

This document is dedicated to Shamoni and the Chapter House and all those wonderful friends within.

ACKNOWLEDGEMENTS

I would firstly like to acknowledge my committee, Paulette, Mike and Fernando for their expertise and guiding hand throughout my studies. They were always approachable both academically and as an invaluable source of support during those hard times when despondency seems to take an upper hand.

Thanks also go to Jim Engstrom and his research group who provided the most meticulous experimental work and invaluable insight into the field of organic electronics. George Malliaras and his research group helped train me in experimental techniques whilst Cornell Centre for Materials Research provided the funding for my PhD and Intel provided much of the computing power which was relied upon so heavily.

My research was made so much easier by colleagues and friends; Leonard Harris, Krishna Iyengar, Becky Cantrell, Ananth, Michelle Giron, Ben Nicholson, and Jay Catherwood all played an important part both within our group and as friends. Mohit Haran deserves a special mention for both his academic mentorship and his invaluable friendship throughout hard times; this thesis certainly would not be written were it not for him. Also, a mention must go to my squash partners over the years, John, Vikram, Eric and Camilo, without whom I would not have been able to vent any pent up frustration upon an inanimate object.

Finally, a thank you to all those who, after arriving on the continent not knowing a soul, I now have the pleasure of a calling friends. Amongst the myriad others, Matthias Kormaksson was there throughout and shared many adventures which will bring a smile to my face in remembrance for many a year. The Chapter House and its coterie ably led by Jon Schaeffer provided me not just with liquid sustenance, but also a home from home and friends for life. Cheers guys.

TABLE OF CONTENTS

LIST OF TABLES

LIST OF FIGURES

CHAPTER 1

INTRODUCTION

1.1 Organic molecules and thin film growth

Small organic molecules (MW<1000) have attracted considerable interest over the past decade mainly due to their promising electrical performance in thin film applications such as transistors [1, 2, 3, 4, 5, 6, 7] and LEDs [8, 9, 10] as a component in flexible displays, and for their role as a component in photovoltaic cells [11, 12].

The most widely studied of these molecules has been pentacene [13, 14, 15] which expresses many of qualities typical of these molecules and which has demonstrated, for a considerable time, the best electrical properties (*e.g.*, with mobilities $\sim 10^0 \mathrm{cm}^2\mathrm{V}^{-1}\mathrm{s}^{-1}$) [13, 16]. In addition, pentacene, like many small organic molecules, exhibits polymorphism (many crystalline phases differing only by a few tenths of an eV of free energy) [17, 18, 19, 20], and is a frustratingly difficult material to grow as a smooth thin film beyond a few monolayers [21, 14]. The crystal cohesive energy (the energy difference between an isolated molecule and one existing within the crystalline state) for these relatively large molecules is only on the order of a few eV [22, 23], with the intermolecular forces being dominated by weak long–range van der Waals type interactions. The need to grow well–ordered crystalline thin films is driven by electrical performance (currently on the cusp of that required for viable commercial products), but much of the research into the production of good quality *inorganic* thin films is not directly transferable to organics: The anisotropic interactions that result from either geometric or chemical anisotropies among the organic molecules create a very different "phase space" to explore, and the almost infinite number of candidate molecules (achievable by "tweaking" the chemical composition of organic molecules) is daunting. These

physico–chemical differences are compounded by the fact that even small changes in deposition conditions, or post–deposition annealing, can have a very strong affect on the final morphology and topology of the deposited film [24, 25, 26, 27, 14, 28, 29].

Despite this knowledge of the anisotropy of molecule–molecule interactions for these materials, there has been very little examination of the fundamental *growth processes* themselves, particularly at a molecular–level, with the result that speculation into the causes of experimentally observed variations in final morphologies of grown films often remains just speculation. Processes such as surface diffusion have until recently have not been investigated although this is changing [30]. Recent simulation work in our group using molecular mechanics potentials has highlighted how small organic molecules diffuse over surfaces, for instance, how pentacene and C_{60} molecules diffuse on organic molecular crystals [31]. These results illustrate that diffusion is not easily characterised within any established diffusion regime, complicated -for instance- by the tendency for isolated pentacene molecules to diffuse face down over the surface, while islands above a critical size spontaneously stand up to take advantage of the face–to–face like–like interactions among themselves. The net result is that there is considerable difference between the modes of diffusion of an organic molecule over a surface, depending on the diffusing species and the surface. Other simulation work in our group has looked at the role of molecular insertion in hyperthermal deposition of pentacene and diindenoperylene (DIP) on a variety of surfaces including pentacene films [32, 33] or self–assembled monolayers of alkane thiols [34]. In addition to this, the Ehrlich–Schwöebel barrier has been characterised by other research groups for two organic molecules which we will discuss in detail later. Once these fundamental processes have been investigated, the objective is to devise an overall framework (either a Kinetic Monte Carlo or continuum model) in which thin film growth can be modelled over large time–scales [35].

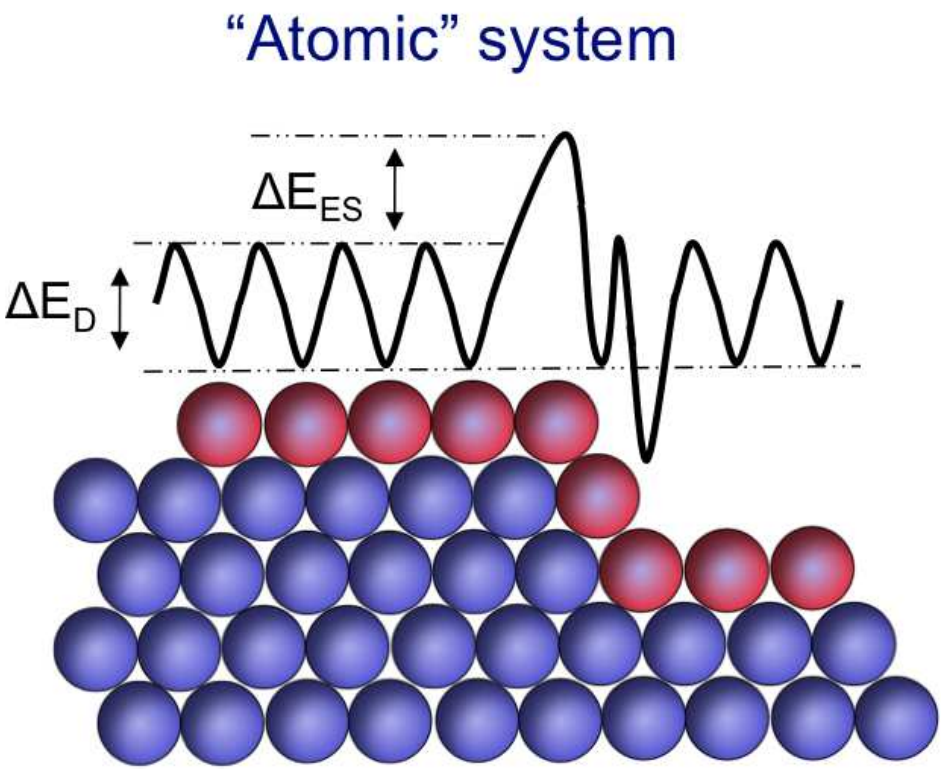

Figure 1.1: Schematic of the 3–dimensional Ehrlich–Schwöebel barrier of an atom descending down two monolayers as encountered in an 'atomic system'

1.2 Ehrlich–Schwöebel barrier

1.2.1 The Schwöebel barrier for atomic systems

The Ehrlich–Schwöebel barrier (hereafter called the Schwöebel barrier) is the energy required for an atom or molecule to descend a mono–layer step–edge *extra to that* of the conventional surface diffusion barrier and was originally proposed by Schwöebel and Ehrlich in separate papers in 1966 [36, 37]. Figure 1.1 shows a typical 3D Schwöebel barrier.

The existence and size of the Schwöebel barrier plays an important role when considering the growth and nucleation of thin films. The existence of a large Schwöebel barrier suppresses the downward flux of particles between crystalline layers, inhibiting the layer–by–layer growth that would promote favoured 2D growth over the unwanted 3D growth that results when one layer starts growing before the one below it has completed a full monolayer. It is therefore of considerable interest to quantify these barriers in order to understand the inherent limitations of thin growth of a system.

The Schwöebel barrier was first observed for tungsten ad–atoms on various tungsten surfaces [37] and continued to be classified for a range of inorganic substances of interest to the field of thin film deposition. Computationally, this barrier has been observed and quantified for monatomic crystals such as copper and silicon where the atom's coordination number decreases as it negotiates the step–edge, resulting in an increase in potential energy. Experimentally, the Schwöebel barrier is impossible to measure directly due to the multitude of competing events and growth processes, but some diffusional moves can be observed through scanning tunnelling microscopy. What results from these experimental observations is largely an ensemble average of many different step–edge barriers

corresponding to different exposed steps, whether classifiable as identifiable edges or as a collection of defective edges. The advent of more accurate experimental [38, 39] and modelling techniques and larger computational power has increased our understanding of these processes. Self–diffusion barriers of Al ad–atoms have been calculated using high level *ab initio* and Density Functional Theory for kinks, steps and corners [40, 41] including some novel atom exchange mechanisms. Xiang *et al.* [42] have extended this to *ab initio* calculations of three–dimensional barriers of the Cu{111} system where the barriers are elevated when the ad–atom diffuses down more than one layer of steps.

1.2.2 The Schwöebel barrier for organic molecules

The inherent symmetry and size of *atomic* systems make the calculation of a Schwöebel barrier tractable, even with fairly sophisticated potential energy models. For organic molecules, the situation is far more complicated. The Schwöebel barrier is defined as the *additional* energy required for a particle to diffuse down a step–edge on top of the 2D surface diffusional energy. For organic molecules, even the 2D diffusion pathway on the surface is not easily defined as the molecules often do not occupy single sites at any given time [31]. The diffusion cannot be characterised as being either "site–site" jumping or continuum random walks and there can be considerable bias in the direction of diffusion. Systems containing small organic molecules are also more complicated due to the conformational freedom provided by the nature of their chemical bonds, the anisotropic interactions associated with "π–stacking," and the molecular shape and flexibility. Experimental routes to this energy barrier are only indirect; typically, they involve scaling models fitted to experimental data such as AFM or *in situ* X–ray diffraction leading to an inferred overall barrier averaged over all possible step types. In contrast, molecular–scale modelling and simulation offer a more direct and insightful view of the

barrier facing molecules as they approach step–edges.

1.2.3 Prior Work: The Schwöebel barrier of sexiphenyl and PTCDA

In order to study a molecule descending over an organic molecular step–edge, the minimum system size quickly spirals upwards with molecular size (on the order of one to ten thousand atoms for this study). This automatically precludes the direct calculation of the Schwöebel barrier through *ab initio* methods or semi–empirical DFT methods. Instead, previous quantification of the Schwöebel barrier for organic molecules (and inorganic, until recently) has been confined to the use of empirical potentials for two systems, PTCDA (3,4,9,10-perylene-tetracarboxylic-3,4,9,10-dianhydride) [43] and sexiphenyl [44] for which barriers of 80 kJ/mol and 60 kJ/mol, were obtained as the step–edge barriers, respectively.

Both of these previous attempts to quantify Schwöebel barriers of small organic molecules *via* molecular modelling used a Nudged Elastic Band method for energy minimisation. The use of a Nudged Elastic Band search method requires that the number of degrees of freedom is kept low, necessitating that, in both cases, the step–edges were frozen and the internal degrees of freedom reduced — in the case of PTCDA a rigid molecule was enforced, whilst -for sexiphenyl- a single parameter described the bending of the molecular backbone with all other internal degrees of freedom frozen. A gradient search algorithm was then employed in the remaining rotational and translational degrees of freedom giving rise to a total of 6 and 7 degrees of freedom for PTDCA and sexiphenyl, respectively. For PTCDA, where the fused ring backbone of the molecule is almost certain to remain rigid and the molecule to remain planar throughout the step

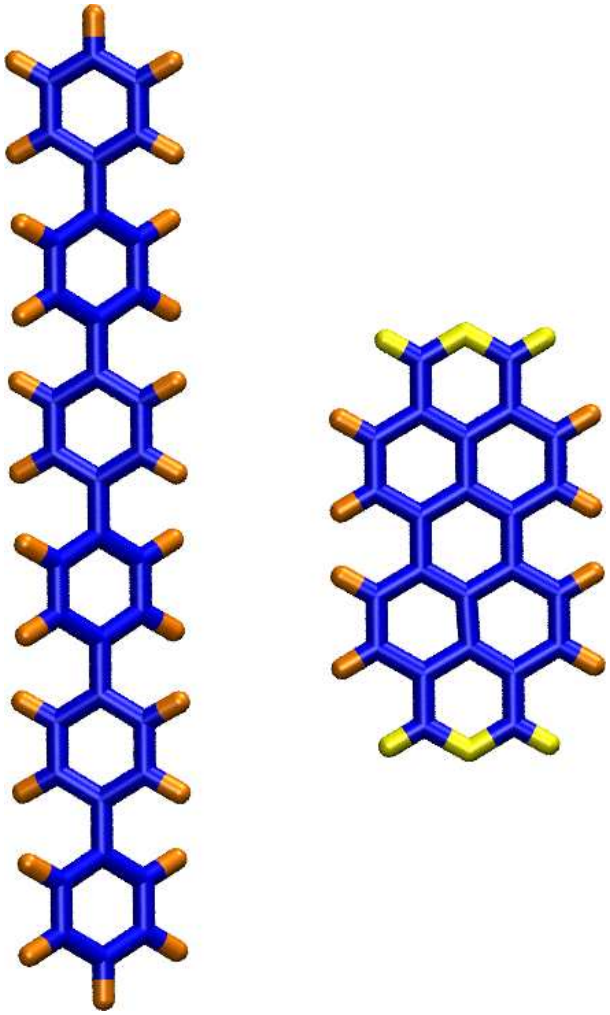

Figure 1.2: Chemical structure of sexiphenyl ($C_{36}H_{26}$) and PTCDA ($C_{24}H_8O_6$)

edge descent, we assert that this is a valid assumption. For sexiphenyl, concerns remain regarding the validity of these constraints. We address this and other concerns in Chapter 3.

1.3 Hyperthermal deposition of organic molecules

The adsorption of atoms and molecules on solid surfaces has been studied extensively for the past century and in increasing detail with the advent of ultrahigh vacuum techniques starting about four decades ago [45]. In parallel, developments in computing resources and algorithms allow consideration of problems that lie at the heart of molecular dynamics: what is the nature of the trajectories (with ps– and Å–scale precision) that describe the gas–surface interactions that lead to adsorption? [46] Early work in this area emphasised the non–dissociative adsorption of monatomic and diatomic species, and many general rules emerged from these works [47]. The dissipation of the particle's incident energy is, of course, essential to adsorption, and is often achieved via momentum exchange with the lattice (phonon excitation), which results in the effective reduced mass of the collision partners and the gas–surface interaction potential playing key roles as factors. The angle of incidence (θ_i) also plays a role, and is often coupled to the incident kinetic energy (E_i) as a factor in terms of energy scaling arguments, the simplest of which involve either normal energy scaling ($E_i cos^2\theta_i$) or total energy scaling ($E_i cos^0\theta_i$) [48]. Many of the studies conducted to date have been of rather simple, high symmetry molecules interacting with similarly simple, high symmetry low–index crystal planes of transition metals or main group semiconductors. In these cases, particularly at low to modest energies, trajectories are typically single collision events, or a collision followed by short–lived diffusion across the surface.

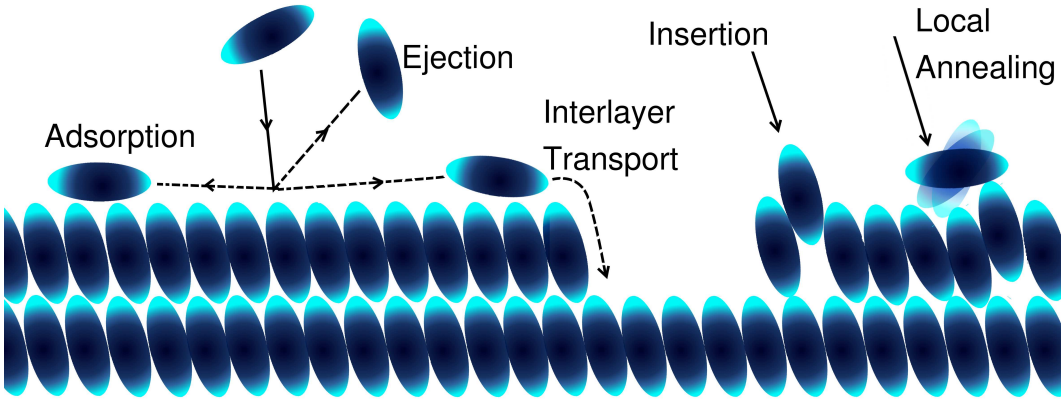

Figure 1.3: Schematic of some possible mechanisms in the hyperthermal deposition of organic thin films.

Examination of the dynamics of adsorption of more complicated molecules (beyond, say, CH_4) and the examination of more complex surfaces such as those provided by liquids [49] and surfaces terminated with self–assembled monolayers (SAMs) [50] is much less often reported. As molecules grow in complexity, excitation of internal degrees of freedom can increasingly play a role in the adsorption process. On the other hand, for surfaces such as liquids and SAMs, new mechanisms of adsorption emerge, including penetration of the surface, and, in the case of liquids, absorption. The crystals formed by small organic molecules offer an interesting, and largely unexplored, middle ground between these surfaces and high symmetry inorganic crystals: They can form surfaces that possess both short– and long–range order, while their constituents are bound together by weak van der Waals forces. Thus, one may expect contributions from mechanisms arising from both of these disparate systems.

1.4 Organisation of this thesis

This thesis is broken up into two main parts: firstly, the characterisation of Schwöebel barriers for some common organic molecules and secondly an examination of the hyperthermal deposition of pentacene. The Schwöebel barrier of sexiphenyl is examined in detail in Chapter 3 particularly in light of the recent results published by Hlawacek *et al.* [44] before moving onto six other common organic molecules in Chapter 4 where we attempt to discover some general rules and correlations for both the self Schwöebel barriers and some heteroepitaxial Schwöebel barriers. A Molecular Dynamics study of the hyperthermal deposition of pentacene follows in Chapter 5 looking at one way of overcoming the barriers we have observed in previous chapters. The study concentrates on mechanisms such as molecular insertion and adsorption. Finally, Chapter 6 summarises the achievements of this work and presents recommendations for future studies.

BIBLIOGRAPHY

[1] C. Dimitrakopoulos and P. Malenfant, "Organic thin film transistors for large area electronics," *Adv. Materials*, vol. 14, no. 2, p. 99, **2002**.

[2] C. Dimitrakopoulos and D. Mascaro, "Organic thin-film transistors: A review of recent advances," *IBM J. of Res. and Dev.*, vol. 45, no. 1, p. 11, **2001**.

[3] J. H. Lee, S. H. Kim, G. H. Kim, S. C. Lim, H. Lee, J. Jang, and T. Zyung, "Pentacene thin film transistors fabricated on plastic substrates," *Synthetic Metals*, vol. 139, no. 2, p. 445, **2003**.

[4] L. Torsi, N. Cioffi, C. D. Franco, L. Sabbatini, P. G. Zambonin, and T. Bleve-Zacheo, "Organic thin film transistors: from active materials to novel applications," *Solid-State Electronics*, vol. 45, no. 8, p. 1479, **2001**.

[5] M. Shtein, J. Mapel, J. B. Benziger, and S. R. Forrest, "Effects of film morphology and gate dielectric surface preparation on the electrical characteristics of organic-vapor-phase-deposited pentacene thin-film transistors," *Appl. Phys. Lett.*, vol. 81, no. 2, p. 268, **2002**.

[6] C. H. Hsu, J. Deng, C. R. Staddon, and P. H. Beton, "Growth front nucleation of rubrene thin films for high mobility organic transistors," *Appl. Phys. Lett.*, vol. 91, no. 19, p. 193505, **2007**.

[7] Z. Bao and J. Locklin, eds., *Organic Field-Effect Transistors*. Optical Science and Engineering, CRC, **2007**.

[8] H. Yanagi and T. Morikawa, "Self-waveguided blue light emission in *p*-sexiphenyl crystals epitaxially grown by mask-shadowing vapor deposition," *Appl. Phys. Lett.*, vol. 75, no. 2, p. 187, **1999**.

[9] A. Piaggi, G. Lanzani, G. Bongiovanni, A. Mura, W. Graupner, F. Meghdadi, G. Leising, and M. Nisoli, "Emission properties of *para*-hexaphenyl polycrystalline films," *Phys. Rev. B*, vol. 56, no. 16, p. 10133, **1997**.

[10] G. Grem, V. Martin, F. Meghdadi, C. Paar, J. Stampfl, J. Sturm, S. Tasch, and G. Leising, "Stable poly(*para*-phenylene)s and their application in organic light emitting devices," *Synthetic Metals*, vol. 71, no. 1-3, p. 2193, **1995**. Proceedings of the International Conference on Science and Technology of Synthetic Metals (ICSM '94).

[11] C. J. Brabec, "Organic photovoltaics: technology and market," *Solar Energy Materials and Solar Cells*, vol. 83, no. 2-3, p. 273, **2004**. The development of organic and polymer photovoltaics.

[12] M. T. Lloyd, A. C. Mayer, A. S. Tayi, A. M. Bowen, T. G. Kasen, D. J. Herman, D. A. Mourey, J. E. Anthony, and G. G. Malliaras, "Photovoltaic cells from a soluble pentacene derivative," *Organic Electronics*, vol. 7, p. 243, **2006**.

[13] R. Ruiz, D. Choudhary, B. Nickel, T. Toccoli, K.-C. Chang, A. Mayer, P. Clancy, J. Blakely, R. Headrick, S. Iannotta, and G. Malliaras, "Pentacene thin film growth," *Chem. Mater.*, vol. 16, no. 23, p. 4497, **2004**.

[14] F. J. Meyer zu Heringdorf, M. C. Reuter, and R. M. Tromp, "Growth dynamics of pentacene thin films," *Nature*, vol. 412, p. 517, **2001**.

[15] R. Ruiz, A. C. Mayer, G. G. Malliaras, B. Nickel, G. Scoles, A. Kazimirov, H. Kim, R. L. Headrick, and Z. Islam, "Structure of pentacene thin films," *Appl. Phys. Lett.*, vol. 85, p. 4926, **2004**.

[16] D. J. Gundlach, "Organic thin film transistors with field effect mobility $> 2cm^2/$ Vs," *57th device research conference digest.*, vol. 1, p. 164, **1999**.

[17] C. C. Mattheus, A. B. Dros, J. Baas, A. Meetsma, J. L. d. Boer, and T. T. M. Palstra, "Polymorphism in pentacene," *Acta Crysta. C*, vol. 57, no. 8, p. 939, **2001**.

[18] C. C. Mattheus, A. B. Dros, J. Baas, G. T. Oostergetel, A. Meetsma, J. L. de Boer, and T. T. M. Palstra, "Identification of polymorphs of pentacene," *Synthetic Metals*, vol. 138, p. 475, **2003**.

[19] B. D. P Parisse, L Ottaviano and S. Picozzi, "First-principles approach to the electronic structure in the pentacene thin film polymorph," *J. Physics: Condensed Matter*, vol. 19, no. 10, p. 106209, **2007**.

[20] I. P. M. Bouchoms, W. A. Schoonveld, J. Vrijmoeth, and T. M. Klapwijk, "Morphology identification of the thin film phases of vacuum evaporated pentacene on SiO_2 substrates," *Synthetic Metals*, vol. 104, p. 175, **1999**.

[21] S. Zorba, Y. Shapir, and Y. Gao, "Fractal-mound growth of pentacene thin films," *Phys. Rev. B*, vol. 74, no. 24, p. 245410, **2006**.

[22] J. E. Northrup, M. L. Tiago, and S. G. Louie, "Surface energetics and growth of pentacene," *Phys. Rev. B*, vol. 66, no. 12, p. 121404, **2002**.

[23] D. Nabok, P. Puschnig, and C. Ambrosch-Draxl, "Cohesive and surface energies of π-conjugated organic molecular crystals: A first-principles study," *Phys. Rev. B*, vol. 77, no. 24, p. 245316, **2008**.

[24] R. Ruiz, B. Nickel, N. Koch, L. C. Feldman, R. F. Haglund, A. Kahn, and G. Scoles, "Pentacene ultrathin film formation on reduced and oxidized Si surfaces," *Phys. Rev. B*, vol. 67, no. 12, p. 125406, **2003**.

[25] R. Ye, M. Baba, K. Suzuki, Y. Ohishi, and K. Mori, "Effect of thermal annealing on morphology of pentacene thin films," *Jpn. J. Appl. Phys.*, vol. 42, p. 4473, **2003**.

[26] D. Guo, S. Ikeda, K. Saiki, H. Miyazoe, and K. Terashima, "Effect of annealing on the mobility and morphology of thermally activated pentacene thin film transistors," *J. Appl. Phys.*, vol. 99, no. 9, p. 094502, **2006**.

[27] S. Iannotta and T. Toccoli, "Supersonic molecular beam growth of thin films of organic materials: A novel approach to controlling the structure, morphology, and functional properties," *J. Polymer Science Part B: Polymer Physics*, vol. 41, no. 21, p. 2501, **2003**.

[28] R. Ruiz, B. Nickel, N. Koch, L. C. Feldman, R. F. Haglund, A. Kahn, F. Family, and G. Scoles, "Dynamic scaling, island size distribution, and morphology in the aggregation regime of submonolayer pentacene films," *Phys. Rev. Lett.*, vol. 91, no. 13, p. 136102, **2003**.

[29] A. Amassian, V. A. Pozdin, T. V. Desai, S. Hong, A. R. Woll, J. D. Ferguson, J. D. Brock, G. G. Malliaras, and J. R. Engstrom, "Post-deposition reorganization of pentacene films deposited on low-energy surfaces," *J. Materials Chemistry*, vol. 19, no. 31, p. 5580, **2009**.

[30] K. A. Fichthorn and J. S. Raut, *The Diffusion of Large, Adsorbed Molecules on Solid Surfaces*. In: M. C. Tringides (ed.), *Surface Diffusion: Atomistic and Collective Processes*, NATO Science Series B: Physics, vol. 360, p. 409, Plenum Press, **1997**.

[31] R. Cantrell and P. Clancy, "A computational study of surface diffusion of C_{60} on pentacene," *Surface Science*, vol. 602, no. 22, p. 3499, **2008**.

[32] J. Goose and P. Clancy, "Exploring the energetic deposition of pentacene on pentacene through molecular dynamics simulations," *J. Phys. Chem. C*, vol. 111, no. 43, p. 15653, **2007**.

[33] J. Goose, A. Killampalli, P. Clancy, and J. Engstrom, "Molecular-scale events in hyperthermal deposition of organic semiconductors implicated from experiment and molecular simulation," *J. Phys. Chem. C*, vol. 113, no. 14, p. 6068, **2009**.

[34] T. Desai, P. Ananth, P. Clancy, and J. Engstrom, "In preparation," **2009**.

[35] D. Choudhary, P. Clancy, R. Shetty, and F. Escobedo, "A computational study of the sub-monolayer growth of pentacene," *Adv. Funct. Mater.*, vol. 16, no. 13, p. 1768, **2006**.

[36] R. L. Schwoebel and E. J. Shipsey, "Step motion on crystal surfaces," *J. Appl. Phys.*, vol. 37, no. 10, p. 3682, **1966**.

[37] G. Ehrlich and F. G. Hudda, "Atomic view of surface self-diffusion: Tungsten on tungsten," *J. Chem. Phys.*, vol. 44, no. 3, p. 1039, **1966**.

[38] G. Ehrlich, "Atomic events at lattice steps and clusters: A direct view of crystal growth processes," *Surface Science*, vol. 331-333, no. Part 2, p. 865, **1995**. Proceedings of the 14th European Conference on Surface Science.

[39] P. Weiss, M. Abrams, M. Cygan, J. Ferris, M. Kamna, K. Krom, S. Stranick, and M. Y. Youngquist, "Atomic-scale view of motion on surfaces," *Analytica Chimica Acta*, vol. 307, no. 2-3, p. 355, **1995**. Looking to the Future of Analytical Chemistry – 1995.

[40] A. Bogicevic, J. Strömquist, and B. I. Lundqvist, "Low-symmetry diffusion barriers in homoepitaxial growth of Al(111)," *Phys. Rev. Lett.*, vol. 81, no. 3, p. 637, **1998**.

[41] R. Stumpf and M. Scheffler, "*Ab initio* calculations of energies and self-diffusion on flat and stepped surfaces of Al and their implications on crystal growth," *Phys. Rev. B*, vol. 53, no. 8, p. 4958, **1996**.

[42] S. K. Xiang and H. Huang, "*Ab initio* determination of Ehrlich–Schwoebel barriers on Cu{111}," *Appl. Phys. Lett.*, vol. 92, no. 10, p. 101923, **2008**.

[43] M. Fendrich and J. Krug, "Ehrlich-Schwöebel effect for organic molecules: Direct calculation of the step-edge barrier using empirical potentials," *Phys. Rev. B*, vol. 76, no. 12, p. 121302, **2007**.

[44] G. Hlawacek, P. Puschnig, P. Frank, A. Winkler, C. Ambrosch-Draxl, and C. Te-

ichert, “Characterization of step-edge barriers in organic thin-film growth,” *Science*, vol. 321, no. 5885, p. 108, **2008**.

[45] C. B. Duke, ed., *Surface Science: The first thirty years*. North Holland, **1994**.

[46] C. T. Reeves, B. A. Ferguson, C. B. Mullins, G. O. Sitz, B. A. Helmer, and D. B. Graves, “Trapping dynamics of ethane on Si(100)-(2 x 1): Molecular beam experiments and molecular dynamics simulations,” *J. Chem. Phys.*, vol. 111, no. 16, p. 7567, **1999**.

[47] C. Rettner, D. Auerbach, J. Tully, and A. Kleyn, “Chemical dynamics at the gas-surface interface,” *J. Phys. Chem.*, vol. 100, no. 31, p. 13021, **1996**.

[48] L.-Q. Xia and J. R. Engstrom, “The role of surface corrugation in direct translationally activated dissociative adsorption,” *J. Chem. Phys.*, vol. 101, no. 6, p. 5329, **1994**.

[49] G. M. Nathanson, “Molecular beam studies of gas-liquid interfaces,” *Annu. Rev. of Phys. Chem.*, vol. 55, no. 1, p. 231, **2004**.

[50] S. R. Cohen, R. Naaman, and J. Sagiv, “Translational energy transfer from molecules and atoms to adsorbed organic monolayers of long-chain amphiphiles,” *Phys. Rev. Lett.*, vol. 58, no. 12, p. 1208, **1987**.

CHAPTER 2

SIMULATION METHODS

In this work, we use a variety of modelling and simulation methods to describe the interactions within the systems of small organic molecules that we have studied. The models chosen for each task reflect the size and complexity of the system. They range from electronic structure calculations that take into account the positions of electrons within a small system that is modelled extremely accurately, to molecular simulations in which every atom in the molecule is explicitly modelled and the system followed as it evolves in time and space using Molecular Dynamics, to mesoscale Kinetic Monte Carlo methods where molecular detail is replaced by a series of "events" that describe the evolution of a larger system (in time and space but in which the representation of the system is at a coarser level. As a general rule of thumb, the more accurate the level of representation of the molecular system, the more intense the computational effort, leading to compromises in system size and the length– and time–scales that can be covered. We now provide some background for each of these approaches as used in the calculations described in later chapters.

2.1 Electronic structure calculations

In cases where we needed the highest accuracy, typically as a "baseline" against which to measure the less accurate property determination of semi–empirical models, we are able to use *ab initio*, or "electronic structure," methods such as HF (Hartree–Fock) –based or DFT (Density Functional Theory) methods which require no empirical data. These computations are sufficiently onerous in use of resources that we are typically only able to consider a small number of atoms (actually, a consideration of the electrons in the system), typically on the order of a hundred atoms or so. These methods give us, poten-

tially, a very high accuracy in terms of predictions of structural and energetic properties but they still must be used with extreme caution: Both the level of theory used and the basis sets chosen need to be investigated carefully to ensure that the system is being properly described. All of the calculations involve a certain degree of approximation in solving the Schrödinger equation:

$$H\Psi = E\Psi \tag{2.1}$$

The two main sub–divisions of electronic structure calculations -those which are based on a Hartree–Fock approach and those which rely on Density Functionals to relate the electron density to the total energy- are, in essence, less separate than it may appear. Traditionally, Hartree–Fock based methods [1] approximate the solution to the Schrödinger equation by assuming a linear approximation of atomic orbitals each represented by a basis function which as a whole describes the molecular orbitals. This method, being a "mean–field" method, neglects electron correlations, producing errors which are then addressed either by introducing corrections for electron correlation such as the so–called MPn methods [2], or by including excited states such as CI (configurational interaction) calculations [3]. It is these corrections which result in large computational time as the Hartree–Fock calculation is *relatively* simple.

DFT, on the other hand, uses the variational principle to solve for a minimum energy. A representation of an initial molecular orbital is estimated which is then used to calculate the total energy Hamiltonian from the Kohn–Sham equations [4]. From this, a new molecular orbital is constructed, and the procedure repeated until a self–consistent solution has been reached. The Kohn–Sham equations which underlie this method and the techniques used to solve them are very similar in principle to those in the Hartree–Fock calculations yet, in general, DFT methods are more computationally efficient than the

higher complexity Hartree Fock based methods needed to retain sufficient accuracy. The explosion in DFT techniques over the past two decades has created an enormous number of functionals describing the electron correlation and exchange part of the Kohn–Sham equations [5, 6, 7]. One of the most popular functional, B3LYP, is actually a hybrid functional where electron exchange contains a contribution from the Hartree–Fock calculation, thus blurring the distinction between the two methods.

To avoid an overly complicated approach to our structural and energetic calculations, we use several standard theories and make use of a large body of work which has already been published to determine the accuracy and applicability of the models used to describe our system. The theories we use are listed below as they appear in Gaussian03 [8]. All methods have analytical derivatives enabling more efficient geometry optimisations.

- HF – (Restricted) Hartree–Fock calculation.
- MP2 [9, 10, 11, 12] Hartree–Fock with 2nd–order Möller–Plesset [2] correction.
- B3LYP [13, 14, 15, 16] A popular hybrid functional.
- PBEPBE [17, 18] The Perdew, Burke and Ernzerhof pure functional.
- PBE1PBE [19] A hybrid functional using 75% correlation and 25% exchange.

The relative computational cost of each method is not always obvious as it depends on system size in terms of electrons (MP2 scales to the fifth power, whereas B3LYP scales to the fourth) and many other things, but, generally, for larger organic molecules, DFT methods are frequently the tool of choice. See, for example, a recent study comparing heats of formation and isomerisation energies calculated with the B3LYP potential to experimental values for over six hundred organic molecules [20]. For a quick comparison of computational effort, Table 2.1 shows a comparison of the CPU time taken for

a single point energy calculation on a planar sexiphenyl and a pentacene molecule using different models. The various models take from 3.5 to over 27 minutes for pentacene (differing by almost an order of magnitude), and from 8.0 to 152 minutes for sexiphenyl (showing a factor of 20 variation). exhibiting the range of execution time that can be found for different models and the impact of even relatively small differences in molecular complexity (pentacene can be modelled in roughly half the time of its similar but more flexible "cousin," sexiphenyl).

Gaussian03 [8] is used for all electronic structure calculations in this thesis as it was specifically designed with chemists in mind to study single molecules or clusters of molecules rather than periodic systems which are more suitable to electronic structure codes that make use of plane waves. The Gaussians used to construct the basis set expansions are easily integrable in discrete space, but the complexity of the basis set expansions must be sufficient to describe the level of theory chosen.

2.2 Semi–empirical potentials

By coarse–graining the electronic structure of the atoms and not describing molecular orbitals explicitly, a common strategy involves constructing a mathematical model for

Table 2.1: CPU time in mins:secs for single point energy calculations of pentacene and sexiphenyl molecules. All calculations were carried out on the same dedicated Intel dual core processor (2.6 GHz) and were allocated 800 MB of physical memory plus up to ≈10 GB of scratch disk space.

Model	**Pentacene**	**Sexiphenyl**
HF/6-31G(d,p)	3:26	8:23
MP2/6-31G(d,p)	27:10	152:05
B3LYP/6-31G(d,p)	5:33	10:10
PBEPBE/6-31G(d,p)	3:50	8:00
PBE1PBE/6-31G(d,p)	7:18	11:48

the potential energy function between two or more molecules that phenomenologically describes, and is often fitted to, experimental and/or electronic structure calculations. Such approaches produce interatomic potentials, where the interactions between two or more atoms can be said to be semi–empirically described. The main advantage of this approach is that interatomic or intermolecular potential models offer the mathematical simplicity and computational efficiency to allow the study of system sizes containing up to around 10000 atoms relatively easily, or to perform smaller sized systems over longer timescales, allowing more detailed searches or dynamic simulations to be undertaken.

2.2.1 MM3 potential

The "Molecular Model", MM3, potential was first devised by Allinger in the early 1970s and has since evolved through a series of reparameterisations and modifications into its present form, described in more detail in this section. The MM3 model is one of a number of intermolecular potentials which ere designed to model systems containing reasonably complex organic molecules of the type that have become increasingly important with the advent of fields such as protein folding and nanofabrication. Codes such as AMBER [21], CHARMM [22] and GROMACS [23] are more suitable for studies of macromolecular studies, whilst the Dreiding [24] and MM group of potentials are employed more successfully for small organic molecules.

We have tested the MM3 potential [25, 26, 27, 28] against several *ab initio*–based methods for the linear fused acenes (naphthalene, anthracene and pentacene), and found that it performs very well in comparison to reference experimental data or those from electronic structure calculations. Other studies have observed the same high quality of the MM–class of models for aromatic molecules [29, 30, 31]. The strength of the MM

series lies in its ability to reproduce experimental minimum energy molecular conformations of a wide variety of hydrocarbon–based molecules, along with vibrational, steric and torsional properties. The latest in the evolutionary set of MM models is MM3(2000) which has been refined with aromatic hydrocarbons in mind and MM4 which increases the chemical functionality of the potential with parameterisations branching away from hydrocarbons. In our case, all the molecules we considered contain only carbon and hydrogen and so the latest MM3 potential is generally satisfactory, although a more sophisticated and costly variant of this model, MM3π, described below, is often a better (more accurate) option if the length of the simulations runs is feasible.

Like most semi–empirical potentials, the total energy of the system can be described by splitting up the contributions of the inter– and intra–molecular energy of the system:

$$E_{tot} = E_{intra} + E_{inter} \tag{2.2}$$

The intramolecular energy is composed of the following terms:

1. Bond Stretching

$$E_S = 71.94 k_s (l - l_o)^2 \left\{ 1 - 2.55 (l - l_o) + \left(\frac{7}{12}\right) [2.55 (l - l_o)]^2 \right\} \tag{2.3}$$

2. Angle Bending

$$E_\theta = 0.021914 k_\theta (\theta - \theta_o)^2 \left[1 - 0.014 (\theta - \theta_o) + 5.6 \times 10^{-5} (\theta - \theta_o)^2 \right. \tag{2.4}$$
$$\left. -7.0 \times 10^{-7} (\theta - \theta_o)^3 + 9.0 \times 10^{-10} (\theta - \theta_o)^4 \right]$$

3. Torsion

$$E_\omega = \left(\frac{V_1}{2}\right) [1 + cos(\omega)] + \left(\frac{V_2}{2}\right) [1 - cos(2\omega)] + \left(\frac{V_3}{2}\right) [1 + cos(3\omega)] \tag{2.5}$$

4. Stretch–Bend Interaction

$$E_{S\theta} = 2.51118 K_{s\theta} \left[(l - l_o) + (l' - l'_o) \right] (\theta - \theta_o) \tag{2.6}$$

5. Torsion–Stretch interaction

$$E_{\omega s} = 11.995 \left(\frac{K_{\omega s}}{2} \right) (l - l_o) \left[1 + cos\,(3\omega) \right] \tag{2.7}$$

6. Bend-Bend Interactions

$$E_{\theta\theta'} = -0.021914 K_{\theta\theta'} \, (\theta - \theta_o) \, (\theta' - \theta'_o) \tag{2.8}$$

The intermolecular energy is composed of the following terms:

1. van der Waals Interactions

$$E_{vdw} = \epsilon \left\{ -2.25 \left(\frac{r_v}{r} \right)^6 + 1.84 \times 10^5 exp \left[-12.00 \left(\frac{r}{r_v} \right) \right] \right\} \tag{2.9}$$

2. Electrostatic and dipole–dipole interactions are also included. Although these terms are not considered as important for saturated hydrocarbons, they do play a role with aromatic structures.

Another important inclusion for some aromatic molecules is the role played by electron correlation in the delocalisation of π electrons [28]. The MM3(2000) release contains a π system correction which uses the same basic theory [2] as the previously mentioned *ab initio* MP2 method. Because the method relies on an iterative process to generate self consistency, it is more computationally expensive and this expense increases rapidly with the number of atoms present. [Note: It is still, however, many orders of magnitude quicker than *ab initio* methods]. Typically the dynamic and minimisation

simulations that are carried out in this thesis limit the π–system atoms in each calculation to under one hundred atoms. The π–system contribution is specified for individual atoms within the system. From here on, we use the term MM3 to denote use of the MM3(2000) potential without the MP2 correction, and MM3π to denote the use of the MM3(2000) potential with the MP2 correction.

All MM3 and MM3π calculations are performed with the TINKER [32] modelling package which is available freely on–line for academic use.

2.2.2 AIREBO potential

This section involves a brief description of the AIREBO potential. We evaluate the ability of this potential to describe the potential energy of a sexiphenyl molecule in Chapter 3. It represents a different class of empirical potentials which rely on local bond order, one of which was used by Hlawacek *et al.* [33] in their quantification of the Ehrlich–Schwöebel barrier for sexiphenyl.

The AIREBO (Adaptive Intermolecular Reactive Empirical Bond Order) potential is a relatively recent development of a form of bond order potential which trace their ancestry back to Tersoff potentials [34]. These potentials describe the interactions between atoms allowing for the formation and dissociation of covalent bonds. The local coordination of each atom affects the strength of the pairwise interactions therefore allowing temporal variation in the hybridisation state or coordination number of the atom. Traditionally, these potentials were used to simulate bulk systems of silicon, carbon and germanium where the intermolecular interactions were less significant than studies for example of interfacial systems, thin films or liquids [35]. This was due to the lack of an appropriate van der Waals–type term to describe the long–range dispersion forces. In

2000, Stuart *et al.* [36] incorporated such a term, with an explicit torsional interaction term, into the established Brenner REBO potential for hydrocarbons.

Although the AIREBO potential model can be a very powerful tool for molecular modelling, the bond breaking and creating aspect of the potential is not particularly relevant to the systems described in this thesis as we do not anticipate any bond–breaking or change in coordination number of any of the molecules we study. [The covalent bond strength in our aromatic fused molecules is on the order of 50-100 kJ/mol.] If the potential is capable of describing the molecular structure and intermolecular interactions effectively, then it will suffice. Here we present the basic equations of the potential without providing too much detail, so that the functional form and underlying theory can be readily understood. For a detailed explanation of the potential see ref. Staurt et al. [36].

The total energy of the system as described by the AIREBO potential is given as:

$$E_{tot} = \frac{1}{2}\sum_{i}\sum_{j\neq i}\left[E_{ij}^{REBO} + E_{ij}^{LJ} + \sum_{k\neq i,j}\sum_{l\neq i,j,k} E_{kijl}^{TORSION}\right] \tag{2.10}$$

The progenitor Reactive Empirical Bond Order, REBO, term describing covalently bonded atoms is very short–ranged (only 2 Å) and takes the form:

$$E_{ij}^{REBO} = V_{ij}^{R}(r_{ij}) + b_{ij}V_{ij}^{A}(r_{ij}) \tag{2.11}$$

where V_{ij}^{R} and V_{ij}^{A} are, respectively, the repulsive and attractive pairwise potentials between atoms i and j. The b_{ij} term is the "bond order" term responsible for taking into account differences in coordination number, bond angles and conjugation effects.

The popular Lennard–Jones 12-6 potential was chosen to model the long–range dis-

persion forces and short–range repulsion forces:

$$V_{ij}^{LJ} = 4\epsilon_{ij}\left[\left(\frac{\sigma_{ij}}{r_{ij}}\right)^{12} - \left(\frac{\sigma_{ij}}{r_{ij}}\right)^{6}\right] \tag{2.12}$$

A switching mechanism is used to integrate the bonded and non–bonded potentials. This prevents interference with the REBO term at short inter–atomic distances and provides a smooth transition between the two. The complete Lennard–Jones term between two atoms i and j is given by:

$$E_{ij}^{LJ} = S(t_r(r_{ij}))S(t_b(b_{ij}^{*}))C_{ij}V_{ij}(r_{ij}) + \left[1 - S(t_r(r_{ij}))\right]C_{ij}V_{ij}(r_{ij}) \tag{2.13}$$

where $S(t)$ is a universal switching function and C_{ij} is a connectivity switch precluding L-J interactions for first and second neighbours. In addition, the torsional interaction for 4th neighbours is described by a separate term dependent on bond weights $w(r)$ with the torsional angle

$$E^{tors} = \frac{1}{2}\sum_{i}\sum_{j\neq i}\sum_{k\neq i,j}\sum_{l\neq i,j,k} w_{ij}(r_{ij})w_{jk}(r_{jk})w_{kl}(r_{kl})V^{tors}(\omega_{ijkl}) \tag{2.14}$$

where the torsional potential of a single torsional angle (ω) is given by:

$$V^{tors}(\omega) = \epsilon\left[\frac{256}{405}cos^{10}\left(\frac{\omega}{2}\right) - \frac{1}{10}\right] \tag{2.15}$$

The well used freeware code, LAMMPS [37, 38], is used to implement the AIREBO potential. LAMMPS provides functionality to switch the torsional term ‘on’ and ‘off’ by a simple switch in the input file; we name these two variants AIREBO and ‘AIREBO

no torsion,' respectively. The significant advantage associated with LAMMPs lies in the parallelisation of the code potentially enabling very large scale simulations.

BIBLIOGRAPHY

[1] P. Echenique and J. L. Alonso, "A mathematical and computational review of Hartree-Fock SCF methods in quantum chemistry," *Molecular Physics*, vol. 105, p. 3057, **2007**.

[2] C. Möller and M. S. Plesset, "Note on an approximation treatment for many-electron systems," *Phys. Rev.*, vol. 46, no. 7, p. 618, **1934**.

[3] I. Shavitt, "The history and evolution of configuration interaction," *Molecular Physics*, vol. 94, p. 3, **1998**.

[4] W. Kohn and L. J. Sham, "Self-consistent equations including exchange and correlation effects," *Phys. Rev.*, vol. 140, no. 4A, p. A1133, **1965**.

[5] R. J. Bartlett, I. Grabowski, S. Hirata, and S. Ivanov, "The exchange-correlation potential in *ab initio* density functional theory," *The Journal of Chemical Physics*, vol. 122, no. 3, p. 034104, **2005**.

[6] A. D. Becke, "Real-space post-Hartree–Fock correlation models," *The Journal of Chemical Physics*, vol. 122, no. 6, p. 064101, **2005**.

[7] S. Kümmel and L. Kronik, "Orbital-dependent density functionals: Theory and applications," *Reviews of Modern Physics*, vol. 80, no. 1, p. 3, **2008**.

[8] M. J. Frisch, G. W. Trucks, H. B. Schlegel, G. E. Scuseria, M. A. Robb, J. R. Cheeseman, J. A. Montgomery, Jr., T. Vreven, K. N. Kudin, J. C. Burant, J. M. Millam, S. S. Iyengar, J. Tomasi, V. Barone, B. Mennucci, M. Cossi, G. Scalmani, N. Rega, G. A. Petersson, H. Nakatsuji, M. Hada, M. Ehara, K. Toyota, R. Fukuda, J. Hasegawa, M. Ishida, T. Nakajima, Y. Honda, O. Kitao, H. Nakai, M. Klene, X. Li, J. E. Knox, H. P. Hratchian, J. B. Cross, V. Bakken, C. Adamo, J. Jaramillo, R. Gomperts, R. E. Stratmann, O. Yazyev, A. J. Austin, R. Cammi, C. Pomelli, J. W. Ochterski, P. Y. Ayala, K. Morokuma, G. A. Voth, P. Salvador, J. J. Dannenberg, V. G. Zakrzewski, S. Dapprich, A. D. Daniels, M. C. Strain, O. Farkas, D. K. Malick, A. D. Rabuck, K. Raghavachari, J. B. Foresman, J. V. Ortiz, Q. Cui, A. G. Baboul, S. Clifford, J. Cioslowski, B. B. Stefanov, G. Liu, A. Liashenko, P. Piskorz, I. Komaromi, R. L. Martin, D. J. Fox, T. Keith, M. A. Al-Laham, C. Y. Peng, A. Nanayakkara, M. Challacombe, P. M. W. Gill, B. Johnson, W. Chen, M. W. Wong, C. Gonzalez, and J. A. Pople, "Gaussian 03, Revision C.02." Gaussian, Inc., Wallingford, CT, 2004.

[9] M. Head-Gordon, J. A. Pople, and M. J. Frisch, "MP2 energy evaluation by direct methods," *Chem. Phys. Lett.*, vol. 153, no. 6, p. 503, **1988**.

[10] M. J. Frisch, M. Head-Gordon, and J. A. Pople, "Semi-direct algorithms for the MP2 energy and gradient," *Chem. Phys. Lett.*, vol. 166, no. 3, p. 281, **1990**.

[11] M. J. Frisch, M. Head-Gordon, and J. A. Pople, "A direct MP2 gradient method," *Chem. Phys. Lett.*, vol. 166, no. 3, p. 275, **1990**.

[12] S. Sæbø and J. Almlöf, "Avoiding the integral storage bottleneck in LCAO calculations of electron correlation," *Chem. Phys. Lett.*, vol. 154, no. 1, p. 83, **1989**.

[13] A. D. Becke, "Density-functional thermochemistry. III. The role of exact exchange," *The Journal of Chemical Physics*, vol. 98, no. 7, p. 5648, **1993**.

[14] C. Lee, W. Yang, and R. G. Parr, "Development of the Colle-Salvetti correlation-energy formula into a functional of the electron density," *Phys. Rev. B*, vol. 37, no. 2, p. 785, **1988**.

[15] S. H. Vosko, L. Wilk, and M. Nusair, "Accurate spin-dependent electron liquid correlation energies for local spin density calculations: A critical analysis," *Can. J. Phys.*, vol. 58, p. 1200, **1980**.

[16] P. J. Stephens, F. J. Devlin, C. F. Chabalowski, and M. J. Frisch, "*Ab initio* calculation of vibrational absorption and circular dichroism spectra using functional force fields," *J. Phys. Chem.*, vol. 98, no. 45, p. 11623, **1994**.

[17] J. P. Perdew, K. Burke, and M. Ernzerhof, "Generalized gradient approximation made simple," *Phys. Rev. Lett.*, vol. 77, p. 3865, **1996**.

[18] J. P. Perdew, K. Burke, and M. Ernzerhof, "Errata: Generalized gradient approximation made simple," *Phys. Rev. Lett.*, vol. 78, p. 1396, **1997**.

[19] C. Adamo and V. Barone, "Toward reliable density functional methods without adjustable parameters: The PBE0 model," *J. Chem. Phys.*, vol. 110, no. 13, p. 6158, **1999**.

[20] J. Tirado-Rives and W. L. Jorgensen, "Performance of B3LYP density functional methods for a large set of organic molecules," *J. Comp. Theo. & Comp.*, vol. 4, no. 2, p. 297, **2008**.

[21] D. A. Case, T. A. Darden, T. E. Cheatham, III, C. L. Simmerling, J. Wang, R. E. Duke, R. Luo, M. Crowley, R. C. Walker, W. Zhang, K. M. Merz, B. Wang, S. Hayik, A. Roitberg, G. Seabra, I. Kolossvry, K. F. Wong, F. Paesani, J. Vanicek, X. Wu, S. R. Brozell, T. Steinbrecher, H. Gohlke, L. Yang, C. Tan, J. Mongan,

V. Hornak, G. Cui, D. H. Mathews, M. G. Seetin, C. Sagui, V. Babin, and P. A. Kollman, "AMBER 10, *University of California, San Francisco*," **2008**.

[22] B. R. Brooks, R. E. Bruccoleri, D. J. Olafson, D. J. States, S. Swaminathan, and M. Karplus, "CHARMM: A program for macromolecular energy, minimization, and dynamics calculations," *J. Comp. Chem.*, vol. 4, pp. 187–217, **1983**.

[23] B. Hess, C. Kutzner, D. van der Spoel, and E. Lindahl, "GROMACS 4: Algorithms for highly efficient, load-balanced, and scalable molecular simulation," *J. Chemical Theory and Computation*, vol. 4, p. 435, **2008**.

[24] S. Mayo, B. Olafson, and W. Goddard, "DREIDING: A generic force field for molecular simulations," *J. Phys. Chem.*, vol. 94, no. 26, p. 8897, **1990**.

[25] N. L. Allinger, Y. H. Yuh, and J. H. Lii, "Molecular mechanics. the MM3 force field for hydrocarbons. 1.," *J. Amer. Chem. Soc.*, vol. 111, pp. 8551–8566, **1989**.

[26] J. H. Lii and N. L. Allinger, "Molecular mechanics. the MM3 force field for hydrocarbons. 2. Vibrational frequencies and thermodynamics," *J. Amer. Chem. Soc.*, vol. 111, p. 8566, **1989**.

[27] J. H. Lii and N. L. Allinger, "Molecular mechanics. the MM3 force field for hydrocarbons. 3. The van der waals' potentials and crystal data for aliphatic and aromatic hydrocarbons," *J. Amer. Chem. Soc.*, vol. 111, p. 8576, **1989**.

[28] J. C. Tai and N. L. Allinger, "Effect of inclusion of electron correlation in MM3 studies of cyclic conjugated compounds," *J. Comp. Chem.*, vol. 19, p. 475, **1998**.

[29] C. Gonzalez and E. C. Lim, "*Ab initio* and MM3 studies of the conformational structures of naphthalene trimer: Comparison with experiment," *J. Phys. Chem. A*, vol. 103, no. 11, p. 1437, **1999**.

[30] L. Claes, S. Kwasniewski, M. S. Deleuze, and J. P. Francois, "Comparative study of the molecular structure of stilbene using molecular mechanics, Hartree–Fock and density functional theories," *J. Mol. Struct.: THEOCHEM*, vol. 549, no. 1-2, p. 63, **2001**.

[31] L. Claes, J. P. Francois, and M. S. Deleuze, "Molecular packing of oligomer chains of poly(*p*-phenylene vinylene)," *Chem. Phys. Lett.*, vol. 339, no. 3-4, p. 216, **2001**.

[32] J. W. Ponder, "Tinker - software tools for molecular design," **2004**.

[33] G. Hlawacek, P. Puschnig, P. Frank, A. Winkler, C. Ambrosch-Draxl, and C. Teichert, "Characterization of step-edge barriers in organic thin-film growth," *Science*, vol. 321, no. 5885, p. 108, **2008**.

[34] J. Tersoff, "New empirical approach for the structure and energy of covalent systems," *Physical Review B*, vol. 37, no. 12, p. 6991, **1988**.

[35] D. W. Brenner, "Empirical potential for hydrocarbons for use in simulating the chemical vapor deposition of diamond films," *Phys. Rev. B*, vol. 42, no. 15, p. 9458, **1990**.

[36] S. J. Stuart, A. B. Tutein, and J. A. Harrison, "A reactive potential for hydrocarbons with intermolecular interactions," *J. Chem. Phys.*, vol. 112, no. 14, p. 6472, **2000**.

[37] S. Plimpton, "Fast parallel algorithms for short-range molecular dynamics," *J. Comp. Phys.*, vol. 117, no. 1, p. 1, **1995**.

[38] S. Plimpton, R. Pollock, and M. Stevens, "Particle-mesh ewald and rRESPA for parallel molecular dynamics simulations," in *Proceedings of the Eighth SIAM Conference on Parallel Processing for Scientific Computing*, p. 8, Citeseer, **1997**.

CHAPTER 3

THE EHRLICH–SCHWÖEBEL BARRIER OF SEXIPHENYL MOLECULES

3.1 Introduction

As introduced in Chapter 1 (section 1.3), the Ehrlich–Schwöebel barrier is the additional energy required for a species to descend a monolayer step edge. In our studies of thin film growth of organic semiconductor molecules, we made a detailed study of the sexiphenyl molecule as it presented a particular challenge due to its configurational flexibility in terms of its ability not only for the phenyl groups to rotate but for the entire molecule to bend. As such, it incorporates some key configurational degrees of freedom most likely to be observed across a wide range of organic molecules. One final inducement to study sexiphenyl was the existence of a prior computational study that offered both a point of comparison and a challenge to reproduce.

The only previous work attempting to directly calculate the Schwöebel barrier of sexiphenyl (Hlawacek *et al.* [1, 2]) proposed a mechanism whereby the descending sexiphenyl molecule approached the step–edge orthogonally and descended by bending (essentially draping itself) continuously over the step–edge. The molecule remained "planar" at all times (*i.e.*, all five torsional angles $\phi_i = 0^o$; see definitions in Figure 3.3) leading to a relatively high Schwöebel barrier of 60 kJ/mol (0.63 eV). Further, it was claimed that a completely rigid molecule (one not allowed to bend) experienced an energy barrier of 85kJ/mol (0.9 eV) representing a loss of seventy percent of the binding energy with the (001) surface. Our experience modelling the Schwöebel barrier of small rigid organic molecules with a somewhat similar structure (*i.e.*, pentacene, anthracene, diindenoperylene as will be seen in the next chapter) produced Schwöebel barriers that were considerably smaller than either of Hlawacek's reported values for sexiphenyl. In

addition, our studies for these relatively rigid molecules showed that the point of their transition over the step–edge occurred with their molecular axis almost parallel to the step–edge (and not orthogonal to the step, as seen in the Hlawacek *et al.* study of sexiphenyl). This caused us to investigate both the mode of descent and the cause of the larger than expected magnitude of the Schwöebel barrier for sexiphenyl.

Initially, our interest centred on the effect of the free rotation of benzene rings around the C-C bonds in the sexiphenyl molecule as a possible cause of the high barrier reported by Hlawacek *et al.* Our approach was to begin with a search for an appropriately accurate intermolecular potential model for sexiphenyl for isolated molecules and then to observe step descent of a single molecule over a crystalline thin film of sexiphenyl.

3.2 Molecular structure of sexiphenyl

In order to accurately describe the energy of a molecule descending a step–edge the intermolecular potential must be able to model both (i) the intermolecular interactions between the molecule and the step–edge surfaces and (ii) the internal energy due to the geometrical conformation of the molecule. The model also needs to be computationally efficient enough to allow sufficient sampling of step–edge descent both in terms of time and system size (we typically use $\approx$ 2000-3000 atoms to describe the step and underlying substrate). We started by examining how well certain potentials were able to describe the conformational phase space of the isolated molecule, specifically its propensity to twist and bend.

There have been a number of papers on the degree of planarity and structure of sexiphenyl [3] and similar molecules [4, 5, 6, 7, 8, 9, 10, 11]. However, these issues are still far from resolved, even for the relatively simple isolated biphenyl molecule. We

Table 3.1: Torsional energy barriers for the biphenyl molecule comparing experimental values to results using a semi–empirical potential model, MM3π and *ab initio* based estimates. a) Taken from Ref. [14] and [15] b) Taken from Ref. [6]

Model	Δ**E**$_0$ **(kJ/mol)**	Δ**E**$_{90}$ **(kJ/mol)**	ϕ_{min}
Experiment[a]	6.0±2.1	6.5±2.0	44.4^o
MM3π	6.3	6.6	35.8^o
'Best Estimates'[b]	8.0	8.3	45.8^o

will show below that the MM3π potential describes the torsional potential of biphenyl as accurately as the latest electronic structure calculations.

3.2.1 Molecular structure notation

We first define some notation to describe the conformation of the molecules (see Figure 3.1). Bending of the molecule is described by a normalised molecular length, $\theta = l/L$, where l is the distance between the terminal carbon atoms and L is the length at the minimum energy structure. We use the term "planar" to correspond to molecules where all torsional angles across the C-C single bond are zero, *i.e.*, $\phi_i = 0^o$. We use the term "twisted" to correspond to molecules in which all the torsional angles are $\neq 0^o$. The difference in energy between the twisted and planar configurations of the sexiphenyl molecule is ΔE_{p-t}. The torsional potential around one C-C single bond is described by ϕ_{min}. The transition energy from ϕ_{min} to the planar and orthogonal configuration are designated by ΔE_0 and ΔE_{90}, respectively.

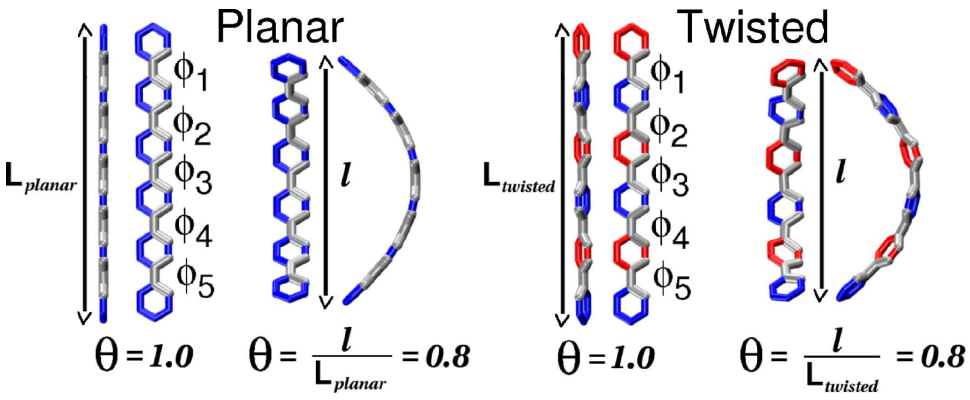

Figure 3.1: Structure and nomenclature of planar molecules ($\phi_i = 0$) and twisted molecules ($\phi_i \neq 0$).

3.2.2 Torsional potentials

Torsional potential of biphenyl

Biphenyl has become something of a *cause célèbre* when considering the ability of electronic structure calculations to predict the geometry of isolated molecules because this relatively simple molecule does not behave as would be expected and the task of explaining this has been given a considerable amount of effort by researchers. The relatively large amount of published literature proved very helpful when interpreting our results and predicting the accuracy of the larger sexiphenyl system. Because of the internal rigidity of the phenyl rings, the complete minimum energy structure can be summarised by one value — the torsional angle between the two phenyl rings (ϕ_{min}). It has been suggested that this angle is thought to be defined by the competing contributions of steric hindrance within a planar molecule and the tendency of the conjugated π system to prefer planarity. Yet even this is debatable [12].

Sexiphenyl being in the same homologous series as biphenyl can be thought of a series of five of these torsional potentials. A combination of electronic structure calculations [6, 7, 8, 9, 10, 11, 12, 13] and experimental measurements [14, 15] examining the torsional potential of biphenyl have highlighted the strong dependence of the predicted values ΔE_0, ΔE_{90} and ϕ_{min} on the choice of theory and basis set used in the calculation. The MP2 level of theory which is normally the chemistry of choice for organic molecules performs unexpectedly poorly. It predicts the incorrect relative magnitude of ΔE_0 and ΔE_{90}, and gives a general over–prediction of both values of ΔE by this large basis set, sophisticated theory calculation. The values for ϕ_{min} are generally within an acceptable range. Most recently, Johansson *et al.* [6] have examined the simple biphenyl system in great detail and have reproduced the latest experimental val-

ues [14, 15] through a very sophisticated treatment and a comprehensive analysis of the theoretical errors and their origins. One of the important conclusions is that some Density Functional Theory (DFT) methods (*i.e.*, B3LYP) agree well, although probably fortuitously, with the highest–level extrapolated *ab initio* results and experiment. From a practical point of view, this enables relatively accurate calculations to be carried out at far less computational cost.

Torsional potential of sexiphenyl

For the longer sexiphenyl molecule, there seems to be consensus that, while neighbouring phenyl rings are twisted along the molecular axis of *isolated* molecules [3, 16, 17, 18], these torsional angles are reduced when the molecules are packed together into a crystalline environment [19, 3, 17, 20, 21, 22]. This effect has also been observed with other conjugated molecules of similar size [5]: An *ab initio* study of poly(*para*-phenylene) [19], for example, predicts a torsional angle of $\phi_{min} \approx 27^o$ and a $\Delta E_0 \approx$ 6 kJ/mol. Previous estimates of ϕ_{min} in an isolated sexiphenyl molecule lie between 30-40^o using empirical potentials [17, 16] and, very recently, using DFT methods [18] with, amongst others, the same Perdew–Burke–Ernzerhof functionals used by Hlawacek *et al*.

MM3π calculation of torsional potentials

The MM3(2000) potential developed by Allinger was parameterised using the structural data of a large number of small organic molecules (biphenyl being among them) but the difficulties in predicting this structure using a simple potential are evident. Without including the MP2 correction for electron correlation (denoted as MM3π), the MM3 potential fails to capture the twisted nature of the molecule and predicts a planar minimum

(as it does for sexiphenyl). A dramatic improvement is observed with the inclusion of the MP2 correction although this significantly increases the computational complexity due to the introduction of SCF iterations. A computational penalty of MM3π over MM3 is about a factor of one hundred in CPU time.

We used MM3π to calculate the torsional potential of biphenyl and the torsional potential of the terminal phenyl ring on an otherwise planar sexiphenyl molecule (Figure 3.2 and Table 3.1) and found that MM3π performs as well as the best *ab initio* calculations in the prediction of ΔE_0 and ΔE_{90} and reasonably well in ϕ_{min}. However, the slight under–prediction of ϕ_{min} is not critical due to the shallowness of the torsional potential around the minimum. It is interesting to note that the maximum energy configuration does not occur exactly at the planar state but instead with a torsional angle of 80^o. When the torsional potential of the terminal phenyl ring on an otherwise planar sexiphenyl molecule is considered, ΔE_0 (6.0 kJ/mol) was found to be very close to the value calculated for biphenyl (6.3 kJ/mol), suggesting the independence of neighbouring twists for the straight molecule, with each twist contributing one–fifth to the total ΔE_{p-t} =30.0 kJ/mol for sexiphenyl. This has been observed by Lukeš *et al.* [18] using DFT methods where only small variations in ϕ_{min} were seen over a range of *para*–phenylene oligomers.

3.2.3 Geometry optimization on the sexiphenyl molecule

Straight molecules

Our first task, then, was to undertake calculations on isolated unbent (straight) molecules using a variety of models ranging from basic Hartree Fock and MP2 corrected methods to Density Functional Theory (DFT) methods, and including some fully atomistic AIREBO [23] and MM3 models. We performed unrestrained geometry optimizations

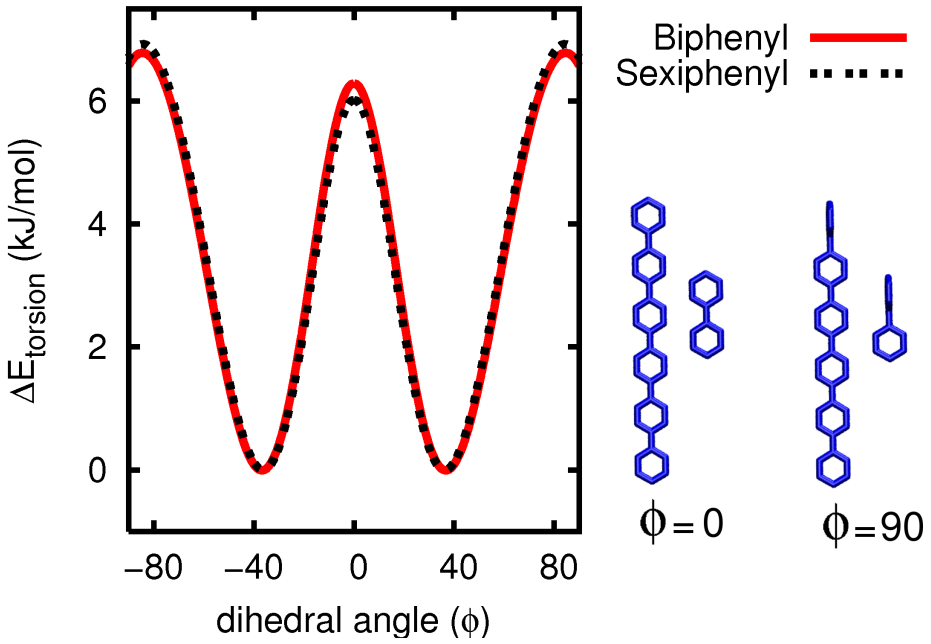

Figure 3.2: Torsional potential calculated with the MM3π potential for biphenyl and sexiphenyl. Constrained geometry optimizations were performed at ϕ intervals of 1^o.

on the molecule to probe the extent of twisting and optimizations constraining $\phi_i = 0$ to examine the planar molecules. The molecular lengths of the planar molecules were very similar irrespective of the potential used. In contrast, AIREBO models tended to slightly under–predict the length of the twisted molecules in comparison to the others presumably because the larger $\phi_{min(i)}$ reduced the steric hindrance between neighbouring phenyl rings.

All of the models predicted an energy minimum in which the molecule was twisted, rather than planar, with the exception of the original MM3 potential. All of the twisted molecules adopted a conformation which we designated as being of type $(+-+-+)$ (see Figure 3.5) where the torsional angle between neighbouring benzene rings alternates between positive and negative offsets along the molecular axis. As shown in Table 3.2, the predicted torsional angles of all the tested models, with the exception of AIREBO(t), fall into the range of 30-50^o which encompasses all of the previous calculations and experimental values for *para*-phenylene oligomers up to *p*-heptaphenyl. The same general behaviour is seen for sexiphenyl, as has been previously for biphenyl [6], in that HF and MP2 (and both AIREBO) over–predict the twist barrier ΔE_{p-t} (ΔE_0) and in that the DFT methods slightly under–predict the torsional angle. We only report the terminal torsional angles ($\phi_{1,5}$) since the variation along the molecule is small.

The Crystal Cohesive Energy we calculate with the MM3π model (183 kJ/mol) is less than that used by Hlawacek *et al.* (272 kJ/mol) reflecting the fact that we use the twisted energy–minimum form of the isolated molecule, whilst they used the planar bulk crystal minimum; the difference between these values being partially attributed to ΔE_{p-t} (planar–to–twisted).

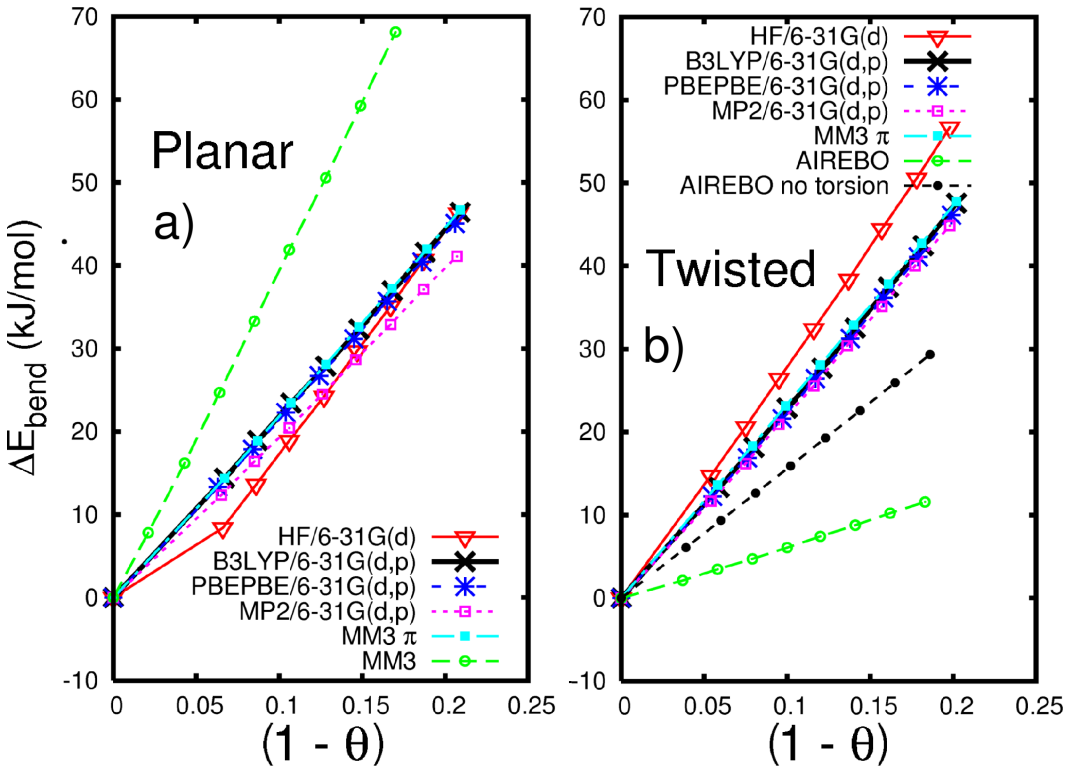

Figure 3.3: The effect of bending on the energy of an isolated (a) planar and (b) twisted molecule.

Table 3.2: Properties of "straight" molecules; Distance between terminal carbon atoms for planar (L_{planar}) and twisted ($L_{twisted}$) sexiphenyl molecules, energy difference between twisted and planar minima (ΔE_{p-t}), cis–torsion angle across the terminal C-C single bond ($\phi_{min(1,5)}$).

Model	$\mathbf{L_{planar}}$ **(Å)**	$\mathbf{L_{twisted}}$ **(Å)**	$\mathbf{\Delta E_{p-t}}$ **(kJ/mol)**	$\phi_{min(1,5)}$
HF/6-31G(d)	24.62	24.33	68.8	44.65^o
B3LYP/6-31G(d,p)	24.65	24.45	36.3	37.22^o
PBEPBE/6-31G(d,p)	24.72	24.53	31.9	35.66^o
MP2/6-31G(d,p)	24.60	24.32	73.1	42.03^o
MM3π	24.65	24.43	30.0	35.30^o
MM3	23.50	n/a	n/a	n/a
AIREBO(t)	24.44	23.88	250.9	66.32^o
AIREBO	24.44	23.95	131.2	40.97^o

Bent molecules

Having shown that the sexiphenyl molecule can twist, we now see if it can bend. The flexibility of the sexiphenyl molecule around its single C-C bonds leads to the expectation that it could bend to some degree as it descends the step–edge, as shown in the Hlawacek paper. The following discussion concerns geometry optimizations on a sexiphenyl molecule under varying degrees of bend starting from both planar and twisted configurations achieved by constraining the end–to–end distance (the distance between terminal carbon atoms). For the planar molecules, it was sometimes necessary to constrain all five torsion angles (ϕ_i) in cases where, otherwise, the optimizations led to the spontaneous formation of the twisted minimum–energy conformation. However, for $\theta > 0.9$, increased steric effects lock the molecules into a planar local minimum. Figure 3.3a shows that *all* the potential models we tested, with the exception of the original MM3, agree that the relationship between the bending energy (ΔE_{bend}) and the reduction in molecular length (1-θ) is roughly linear. A reduction of 20% in the distance between the terminal carbons results in a rise of $\approx$ 45 kJ/mol. The MM3π was a significant improvement over the MM3 potential and almost indistinguishable from the *ab initio* and

DFT calculations which are many orders of magnitude slower in CPU time.

The effect of bending on the energy of the molecule in its minimum–energy, alternating twist (+ − + − +), conformation showed the same qualitative results (Figure 3.3b) as the planar molecule case (all energies are shifted by ΔE_{p-t} over the range of θ): all the *ab initio* and DFT models (with the exception of Hartree–Fock) and the MM3π model are in good agreement. The twisted molecules exhibited an increase in energy of roughly 50 kJ/mol for a reduction in end–to–end distance of 20%. The AIREBO potential was a noticeable outlier, predicting that bending the molecule was not as energetically unfavourable. By removing the torsional term of the AIREBO potential [24], the cost of bending was increased; however, the barrier was still significantly less than all other methods and suggests that this model is not a good choice for sexiphenyl.

Basis sets expansions

We use Gaussian03 for all of our *ab initio* type calculations which was specifically designed for examining isolated molecules or systems, rather than periodic systems, due to the basis set expansions being represented by numerous gaussians instead of plane waves. However, sufficiently complex basis set expansions need to be employed to ensure that the model chemistry is being accurately represented. As can be seen from Figure 3.4, basis set effects are minimal over the range we studied although an anomaly is seen for both MP2 and HF planar molecules with the 6-31G(d) basis sets — the same linear relationship between $(1 - \theta)$ and ΔE_{bend} holds except for the straight molecule where the energy is higher than would be expected. No simple explanation can be offered for this and it is beyond the remit of this thesis but this unusual behaviour is worth noting.

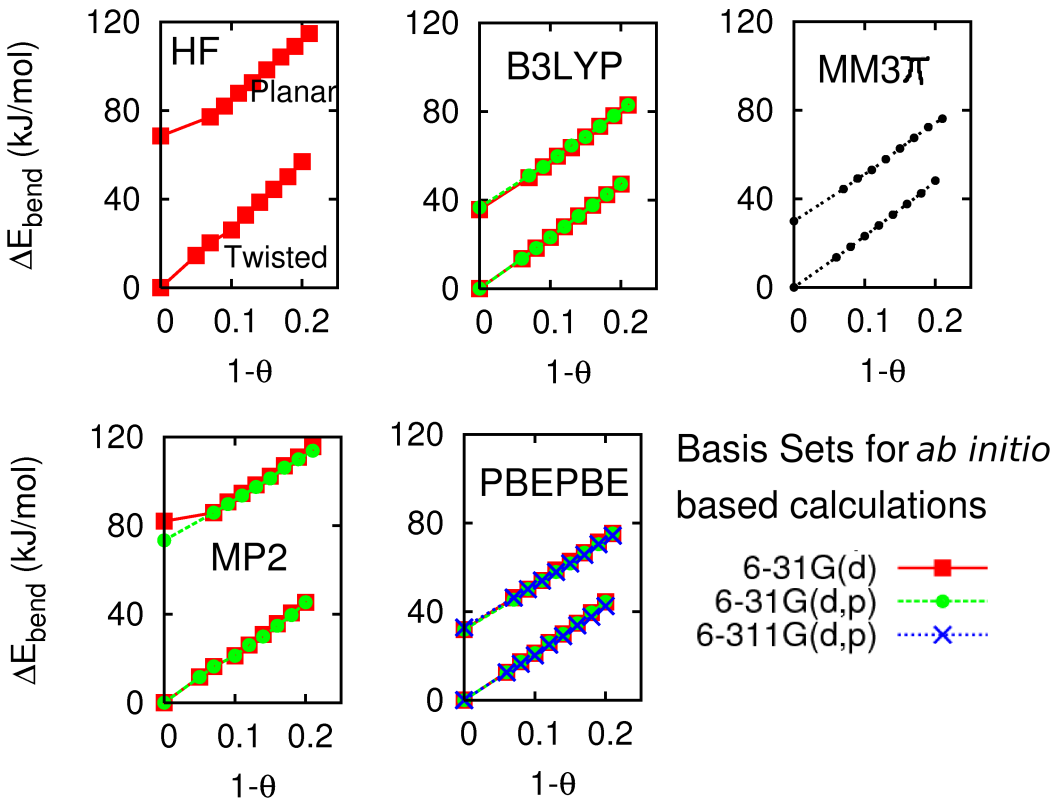

Figure 3.4: ΔE_{bend} for planar and twisted molecules using a variety of model chemistries and basis sets

Alternate configurations of twisted molecules

There are many different ways in which the sexiphenyl molecule can be twisted about its long molecular axis. We use a +− notation to describe the neighbouring twists along the sexiphenyl molecule as shown in Figure 3.5. Preliminary calculations predicted the straight twisted molecule was a global minimum irrespective of the way the molecule was twisted, and the length of the molecule was also constant for any given potential. However, when the twisted molecules are bent, small variations in energy arise due to the exact conformation of the molecule. The two extremes were found to be the alternating twist (+ − + − +) and the helical twist (+ + + + +), as shown in Figure 3.5. In Figure 3.6 we plot the molecular energy for five different twisted configurations and the planar molecules over a range of bending for the MM3π, PBEPBE and B3LYP models. The agreement is quite remarkable considering the difference in model complexity (and hence differences in the CPU time taken). As with all other models, the difference in energy between the twisted (+ − + − +) and planar molecules is roughly constant over the range of bending.

Overall, the ability of the MM3π potential to reproduce the DFT results is very encouraging and leaves us confident that we can use this to examine the Schwöebel barrier of sexiphenyl more accurately than previous efforts. The torsional potential is shallow around ϕ_{min} so the effect of under–predicting the angle slightly will not have a large effect on the system energies. These results suggest that the intermolecular forces are well described by the MM3π potential and, for the rest of this chapter, we concentrate on applying the MM3π potential to model the Schwöebel barrier of sexiphenyl.

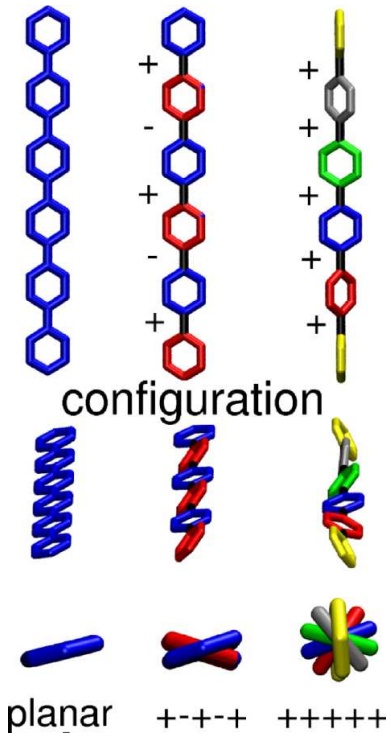

Figure 3.5: Configuration nomenclature for twisted molecules

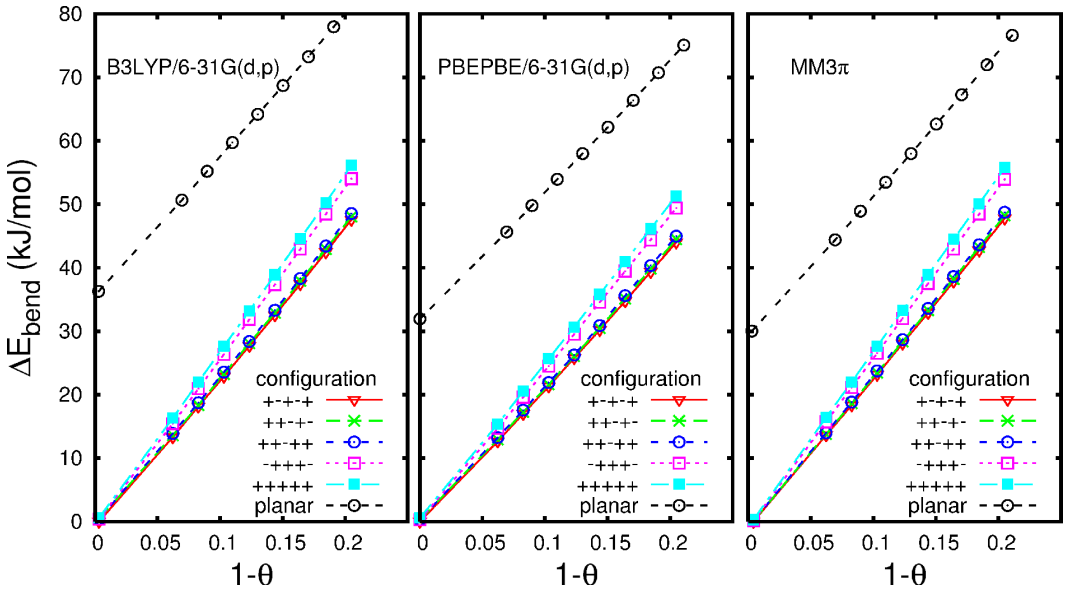

Figure 3.6: Bending energies for five different twisted configurations and planar molecules relative to the global minimum $(+-+-+)$ twisted straight molecule energy. (a) PBEPBE/6-31G(d,p) (b) B3LYP/6-31G(d,p) (c) MM3π

3.3 Descent of the sexiphenyl molecule over a step–edge

We can now turn our attention to simulating the descent of an MM3π–modelled sexiphenyl molecule over a thin film step–edge composed of other sexiphenyl molecules. For all of the following discussion, the crystalline sexiphenyl used to construct the surfaces and step–edges is frozen in place using the bulk crystal parameters [21] with the molecular positions predicted by the MM3π potential. Freezing the substrate in position is done to significantly lower the computational effort involved. Our test case that allowed the molecules in the substrate to move dynamically showed that freezing the substrate molecules in place barely affects the Schwöebel barrier. As will be shown later for pentacene, the difference in barriers for systems in which the substrate molecules are either "frozen" in place or free to move under the influence of the intermolecular forces was just 5 kJ/mol, within the uncertainty in measuring the energy. The long axes of the sexiphenyl molecule form an angle of 14.5^o with the surface normal and the molecules are planar within the crystal, closely matching experimental predictions and the conditions used in the paper by Hlawacek *et al.*

Binding on the (001) surface

To define the energetic baseline for the Schwöebel barrier, we first must know the minimum binding energy on the bulk (001) surface. A search was carried out by generating hundreds of random configurations on the frozen surface and then minimising the total energy. By constraining ϕ_i to lie within $\pm 1^o$ and $\pm 5^o$ (essentially increasing the rigidity of the sexiphenyl molecule and pushing it closer to the domain of molecules such as pentacene and DIP) we have also examined the effect of planarity on the potential energy surface. Figure 3.7 shows all the minimised energies as a function of molecular orien-

tation on the (001) surface and demonstrates the richness of the system. It can be seen that the main origin of this multiplicity of available energies lies in the intermolecular energy, not surprisingly.

For the constrained structures, ϕ_i takes, in the vast majority of cases, the maximum constraint allowed (*i.e.*, $|\phi_i| = 1^o$ and 5^o), while for the unrestrained cases $|\phi_i|$ is between 20^o and 40^o. The minimum binding energy on the surface for the unrestrained molecules is 113 kJ/mol with $|\phi_i| = 36.5 \pm 0.5$ along the molecule and an alternating twist, and its long molecular axis aligned in the [100] direction. For the constrained cases, the minimum structure for $|\phi_i| = 1^o$ has a value for ΔE_{bind} of 111 kJ/mol and, for $|\phi_i| = 5^o$, ΔE_{bind} has a value of 112 kJ/mol. Most importantly, the minimum energy structure switches from an orthogonal (to the [010] direction) position, for the unconstrained case, to a parallel position for the 1^o and 5^o constraints. This critical result is obtained because the unrestrained molecule is able to access configurations prohibited to the planar molecule and in which the intermolecular interactions are greater. The implications of this within a Nudged Elastic Band (NEB) search are substantial and important due to the sensitivity of an NEB search on the initial and final positions chosen. We will later propose that this is the cause of the high energy barrier proposed by Hlawacek *et al.* The sheer number of similar energy local minima on the (001) surface demonstrates the difficulties that will be faced when searching for a saddle point when a step–edge is introduced.

3.3.1 Description of trajectory search

For the trajectory search, we constructed a $6\times12\times1$ super–cell step edge containing 144 sexiphenyl molecules with periodic boundary conditions imposed in the [010] direction. A single sexiphenyl molecule was then placed on this surface with a random orientation

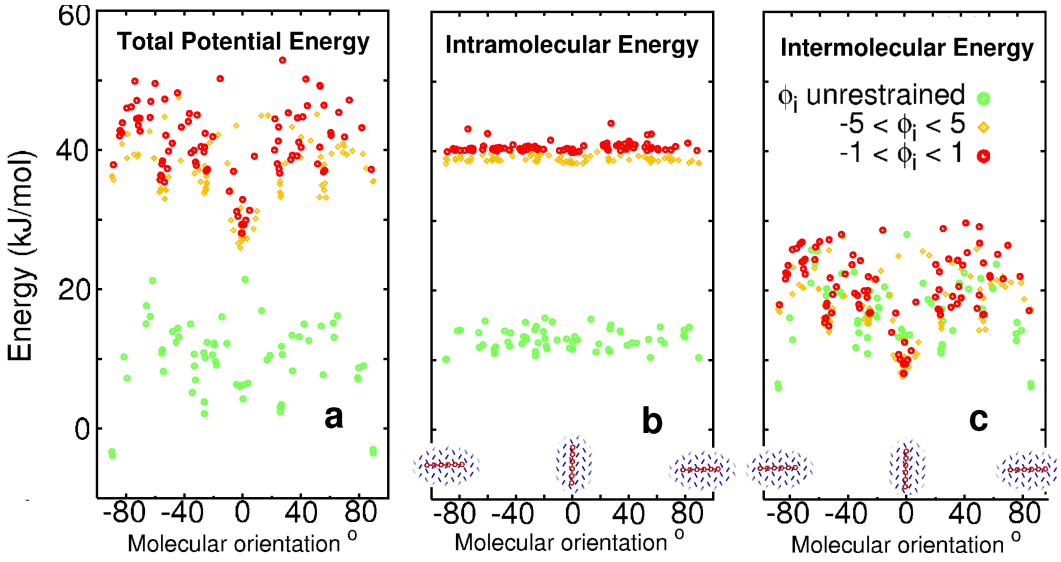

Figure 3.7: The richness of binding energies as a function of molecular orientation on the (001) surface. The binding energy (or "total potential energy") shown in (a) is the sum of the intermolecular energy (shown in (b)) and the intramolecular energy shown in (c)

and with a random lateral position at least 30 Å from the step–edge. The total energy of this set–up was then minimised. Choosing these randomised starting positions assumes that all locally minimised geometries as shown in Figure 3.7 are energetically accessible from the global minimum without compromising the Schwöebel barrier. In other words, the energy required to pass from the global minimum to any starting position is less than the Schwöebel barrier — a condition which we are confident that we have satisfied.

From this starting position, the molecule was then repeatedly translated 0.1 Å towards the step–edge followed by an energy minimization. During the minimization procedure, the molecule was not allowed to move away from the step–edge but, otherwise, any translational, rotational or conformational move was allowed. Although perhaps not as intrinsically elegant as a Nudged Elastic Band (NEB) scheme, we chose to use a full minimization of the atomistic MM3π potential at every point which allows us to probe more of the phase space available to the diffusing sexiphenyl molecule than the more highly constrained NEB method. Each run produces a possible trajectory of the diffusing molecule over the surface; the trajectory with the lowest additional energy is chosen as the predicted Schwöebel barrier. We have used this method successfully to evaluate the Schwöebel barrier for a number of other small organic molecules, but not for a molecule with as many internal degrees of freedom as sexiphenyl. These extra degrees of freedom render it necessary to carry out a larger number of runs to ensure that we are probing as much configurational phase space as possible.

3.3.2 Trajectories constraining ϕ_i

We again examined the effect of planarity by imposing constraints on ϕ_i (unrestrained, and those constrained to ± 1 and ± 5) and, for each constraint case, we examined over

150 trajectories. In Figure 3.8, we show the three minimum energy trajectories for the sexiphenyl molecule descending over the step–edge, giving overall barriers of 35, 40, and 43 kJ/mol, respectively. It is apparent that constraining ϕ_i affects the trajectory in several ways but does not affect the barrier significantly. Constraining $|\phi_i| < 1^o$, produces a trajectory where the molecule 'log–rolls' over the step–edge in a parallel orientation. The molecule remains planar and unbent throughout, therefore, the energetic contributions to the barrier come entirely from the intermolecular energy. We have, in effect, found a barrier for a rigid molecule, roughly half the value predicted by Hlawacek *et al.* (85 kJ/mol), whereby the molecule navigates the step–edge losing less than 40% of the binding energy to the (001) surface (as opposed to the 70% loss proposed by Hlawacek *et al*). By slightly relaxing the constraint on $|\phi_i|$ to $< 5^o$, the same 'log–roll' approach to the step–edge is observed but, at the transition point, a small degree of bending is observed as the molecule twists in a helical conformation, resulting in an overall barrier that is 5 kJ/mol smaller. Again, very little contribution to the barrier comes from the internal energy of the molecule. Only when we lift the constraint on ϕ_i completely, do we see any significant bending of the molecule within the trajectory, yet still only resulting in a normalised molecular length $\theta = 0.93$ (*i.e.*, a 7% bend in the molecule). The internal energy of the molecule, corresponding to the reduction in θ, rises (24 kJ/mol) *as* the transition state is reached. At this point, the increased energy of the system resulting from loss of intermolecular interactions means that it becomes more favourable for the molecule to bend and thereby regain intermolecular interactions with the step–edge. We also see a change in the configuration of the twisted molecule, with a flip in signs of ϕ_3 as the molecule bends. From these three cases, ranging from tight restraint to complete unrestraint, the preferred trajectories always involves the molecule 'log–rolling' off the step–edge. The bending and twisting of the molecule only slightly reduces the barrier by facilitating a complicated "Fosbury Flop"–like mechanism in a near–parallel

approach to the step–edge. However, it must be noted that there are many different trajectories for all three cases. By constraining ϕ_i, we are vastly reducing the phase space and thus all successful trajectories pass through the same transition points shown in Figures 3.8 (a) and (b). The vast majority of molecules were able to re–orient themselves into a near–parallel orientation on the terrace before descending. For the unrestrained case, we observed numerous trajectories of varying energies all passing through slightly different transition points.

3.3.3 Dissimilar (100) step–edges

A further complication in the case of sexiphenyl (and organic molecules in general) arises due to the number of molecules in the monoclinic unit cell and the subtle difference in their orientation. Each 100 surface exposes only one of the two sexiphenyl molecules in each unit cell, so, depending on which molecule is defined at 0 0 0, the (100) surface is cut differently, producing a slightly different step–edge (see Figure 3.9). We arbitrarily denote the step shown in Figure 3.9a as type 'A' and the step shown in Figure 3.9b as type 'B'. Hlawacek *et al.* appeared to exclusively use type 'B'. We used both step edges in our search for the Schwöebel barrier and found a small difference between the two, although this not as significant as we have found for other organic molecules. The lowest barrier we reported (32.5 kJ/mol) was representative of type 'A,' whereas the lowest barrier for type 'B' was 35 kJ/mol, as shown in Figure 3.8. The trajectories shown above were all obtained for type 'B' steps for consistent comparison with previously published material. However, it can be seen from Figure 3.10 that the trajectories are very similar. Indeed, the angles of approach are equivalent, though step 'A' edges produce a trajectory with slightly less bending of the molecule and the molecule undergoes an extra flip within the torsional angles at the transition point.

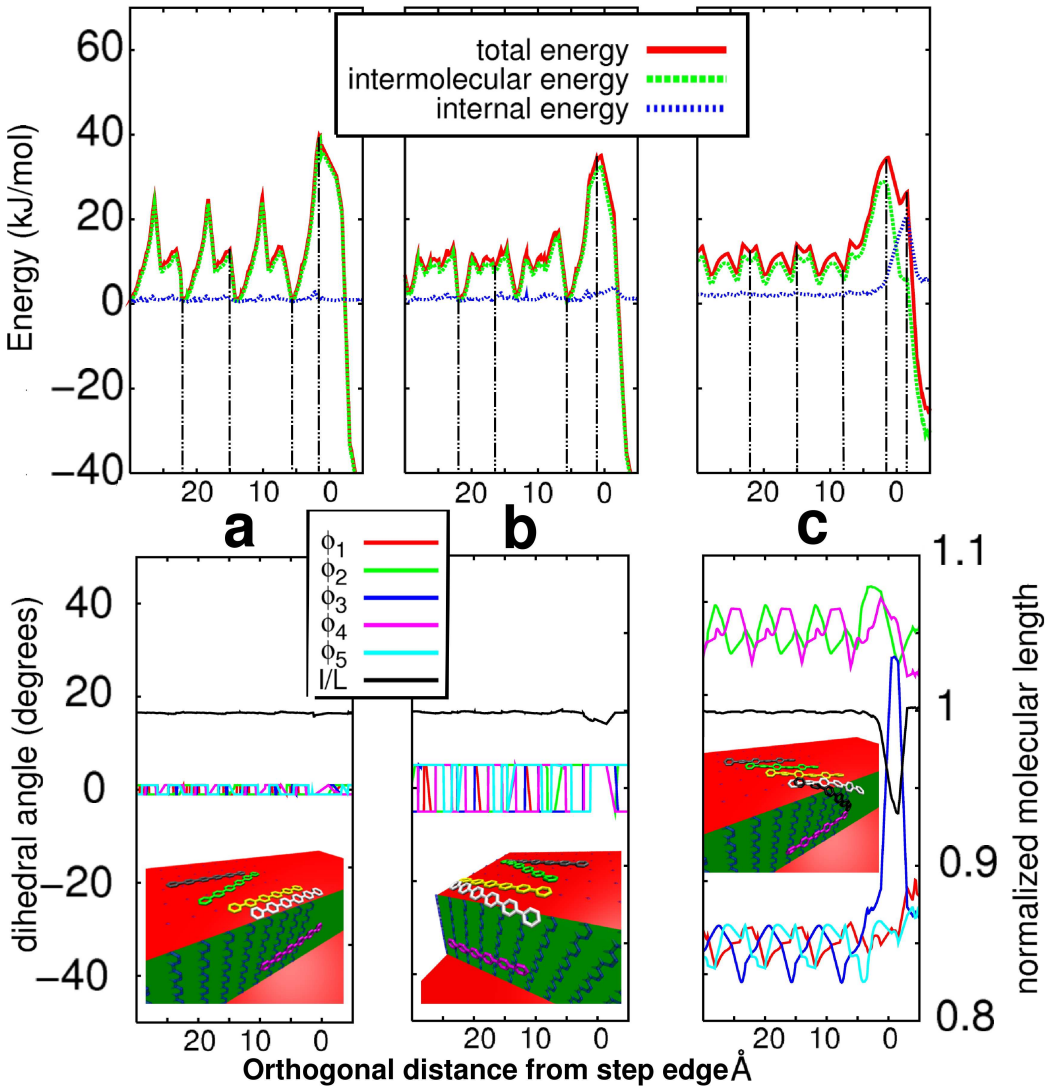

Figure 3.8: Trajectories resulting in the lowest Schwöebel barrier for three cases restraining ϕ_i: (a) Angular rotation constrained to less than 1 degree ($|\phi_i| < 1^o$, (b) angular rotation constrained to less than 5 degrees ($|\phi_i| < 5^o$, and (c) unrestrained molecular rotation. The total energy shown in the plots is the sum of the intermolecular energy and intramolecular energies. The distance axis refers to the orthogonal distance from the centre of the middle phenyl ring to the step–edge.

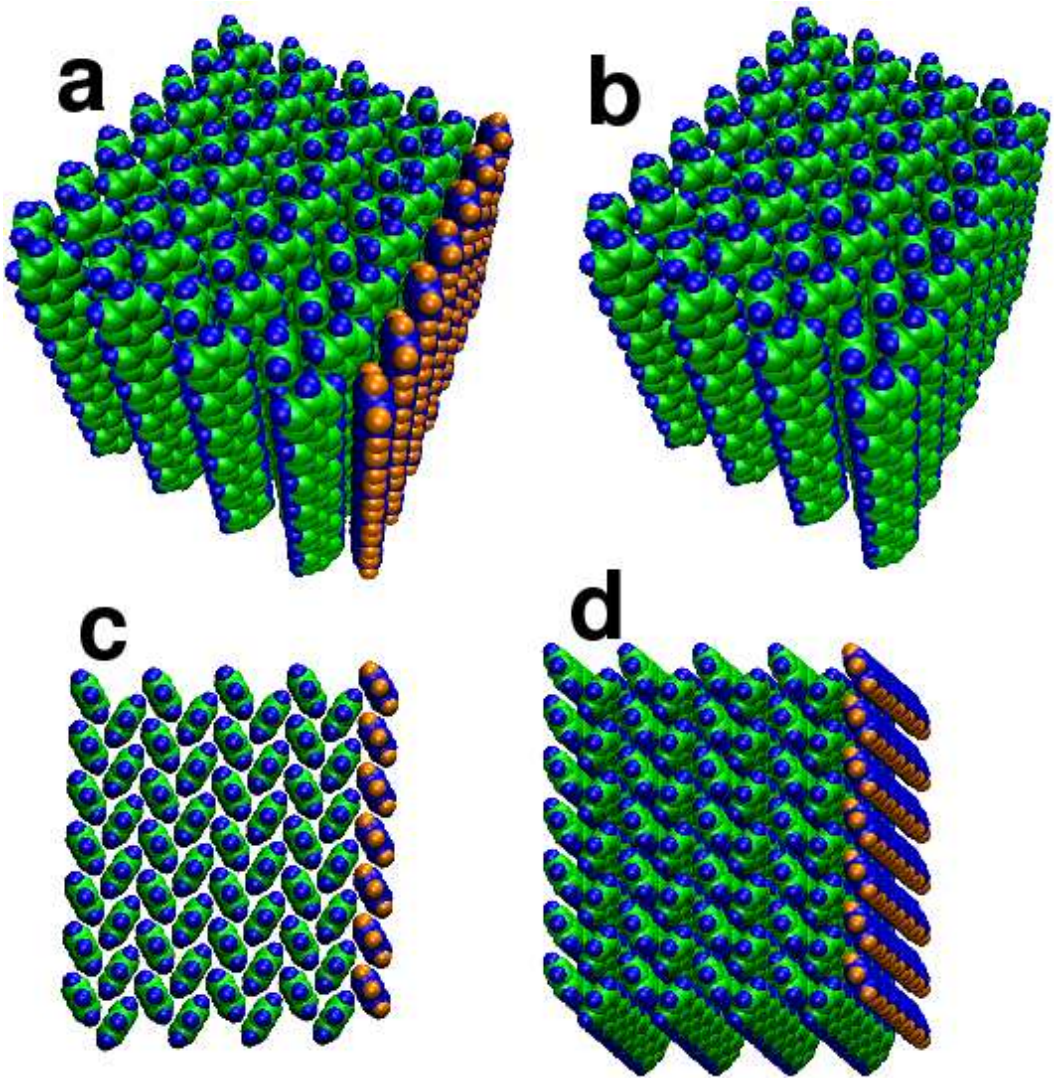

Figure 3.9: The difference between the two possible step–edges in sexiphenyl is illustrated by the presence of the final row of different coloured molecules. a) Step–edge type ‘A’ b) step–edge type ‘B’ c) the view down the long molecular axes d) the view perpendicular to the a and b axes.

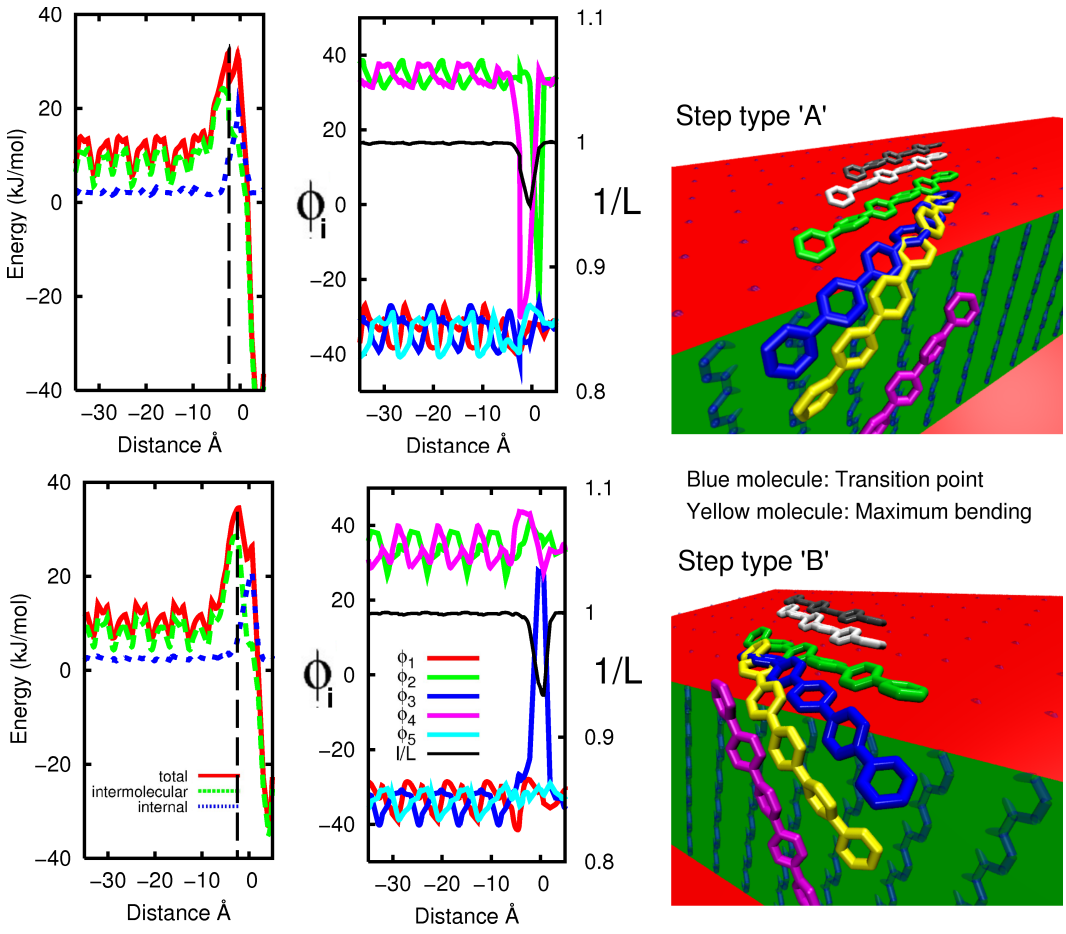

Figure 3.10: Detailed examination of each of the two minimum trajectories for the two step–edges. The distance axis refers to the orthogonal distance from the step–edge and the vertical black dashed line shows the transition points corresponding to the blue molecules. The yellow molecules show the maximum bending throughout the trajectories.

3.3.4 Phase space of unrestrained trajectories

In Figure 3.11, we show the collated results of over 300 simulations to map out values of the Schwöebel barrier that can be explored by the molecule. We examine the orientation of the molecule relative to the step–edge at the transition point and the molecule's normalised molecular length. Significantly, all of the barriers predicted by our method are lower than the previously reported prediction in the literature. The lowest energy trajectories are clustered around two nodes at $\pm\ 20^o$ and $\theta = 0.95$ indicating a strong tendency for the molecules to orient themselves more parallel to the step–edge as they descend. The same qualitative behaviour observed in Figure 3.8(a) is seen for all trajectories except that, in general, if a molecule approaches the step–edge more orthogonally, it is unable to bend in this configuration until the driving force (the loss in intermolecular interactions) is sufficiently large.

The only molecules that undergo significant ($\theta < 0.9$) bending at the transition point approach the edge with an orientation of around $\pm\ 50^o$ and correspond to relatively high Schwöebel barriers. The lowest value of θ that occurs at the transition point is 0.85. However, as we saw from Figure 3.8, the molecule continues to bend directly after the transition point resulting in a slightly lower θ_{min} for each trajectory. We do not see any trajectories in which the molecule continuously drapes itself over the step–edge. The lowest θ_{min} for all trajectories was 0.825; see Figure 3.12.

We include the value due to Hlawacek *et al.* (60 kJ/mol) on Figure 3.11 with the molecule in the orthogonal orientation and the $0.8 < \theta < 0.825$ degree of bending that they report. It is clear that their result fits with our data as one (high energy) point in the much more complex "phase space" that is available to sexiphenyl. It is unclear why parallel orientations were not explored by their search, particularly in light of our results shown in Figure 3.8 (a) and (b) for rotationally constrained molecules. It could

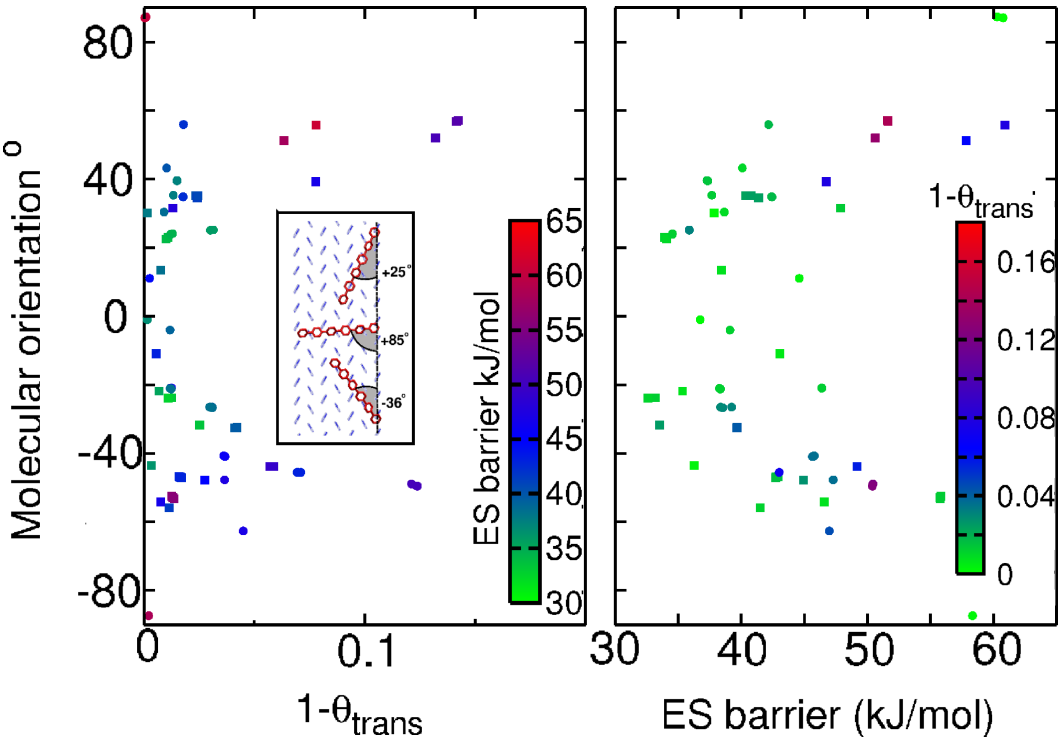

Figure 3.11: Phase space explored during the Schwöebel barrier search. All data relate to the transition state (*i.e.*, the maximum energy within each trajectory). Square points refer to step type 'A,' whilst circle points refer to step type 'B'.

be related to the intermolecular potential energy model they chose, but we believe that the most likely reason is that the constraint implicit in the NEB search only examines trajectories directly between the global minima on each surface. Linear interpolation between the initial and final positions, particularly when they are close together, is not guaranteed to explore all of the phase space available to the molecule.

Orthogonal molecules tethered around the step–edge

In order to ascertain, on a fundamental level, whether the MM3π potential model would allow a trajectory in which the molecule was continually bent over the step–edge we sampled possible transition states by forcing molecules to bend around the step–edge in near orthogonal configurations (angles $> 80^o$), at random positions of descent, and evaluating the minimised locally constrained geometries. In all, over 4000 states were generated by conducting NVT simulations at elevated temperatures (500K) followed by energy minimisations. At every position along the transition path, there should be a configuration with energy less than or equal to 60 kJ/mol and assuming that all neighbouring states are energetically accessible, the trajectory becomes possible. It can be seen from Figure 3.13 that this condition is met with the maximum energy (60 kJ/mol) occurring as the molecule bends around the step–edge with $\theta = 0.825$.

Whilst we are proposing a significantly lower barrier and different mechanism from previous work it is important to note the limitations and assumptions of our own approach. We consider only the (100) faceted step–edge and do not account for mechanisms of descent at kink sites or other facets which will exist as islands form. We assumed that the step–edge was frozen at bulk–optimised coordinates, not allowing molecules closer to the surface the opportunity to twist. Furthermore, mechanisms involving the molecules either hindering or helping the descending molecule were ig-

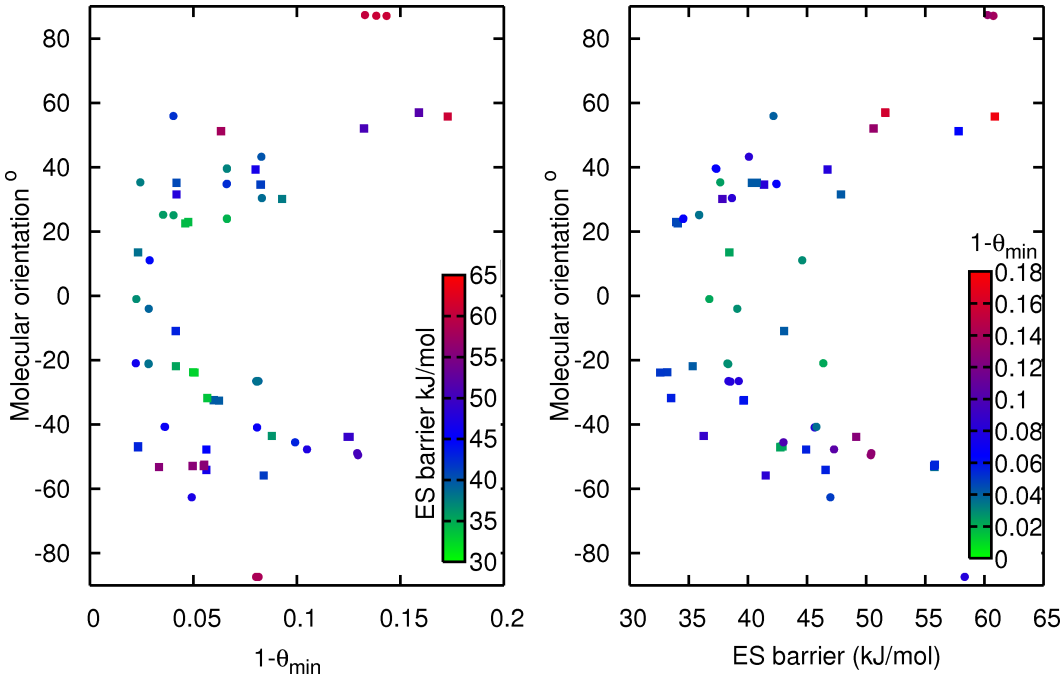

Figure 3.12: Phase space explored during the Schwöebel barrier search. All theta are at the instance of maximum bending of the molecule over the trajectory ($\theta = \theta_{min}$) Square points refer to step type 'A,' whilst circle points refer to step type 'B'.

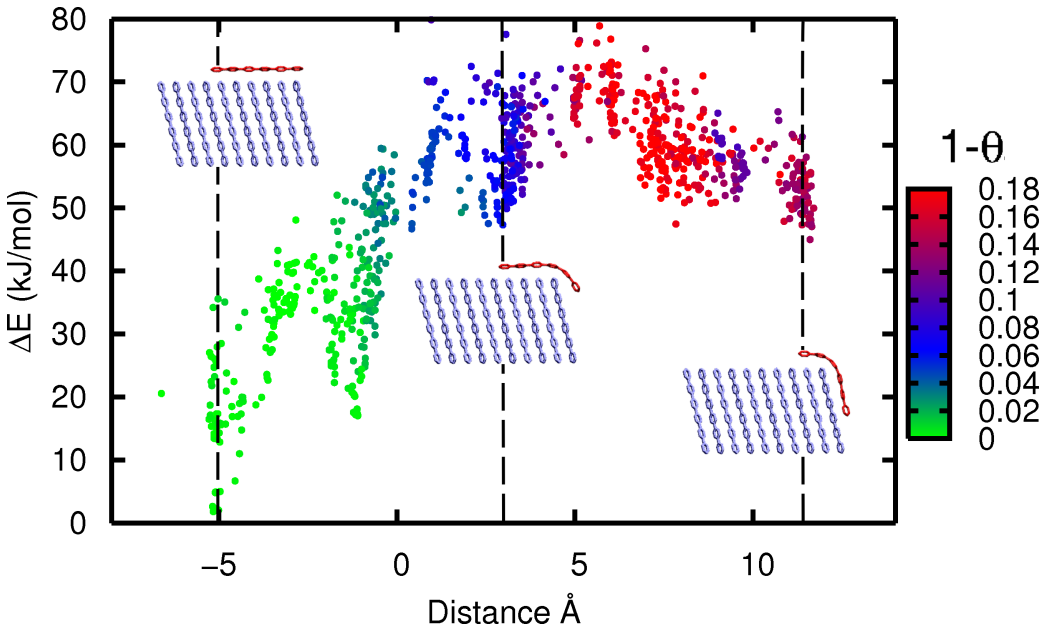

Figure 3.13: Potential energy (intermolecular + intramolecular) of sexiphenyl molecules forcibly bent over the step–edge.

nored. However, we do not believe any of these issues capable of significantly affecting our results, a position taken due to calculations for simpler organic molecules.

3.4 Conclusions

We find, in general, that sexiphenyl molecules prefer to roll over step–edges in a parallel orientation. Allowing rotation around the C-C single bonds vastly increases the phase space of the search and results in a slightly lower energy trajectory where the molecule experiences a kind of Fosbury flop at an angle of 20^o to the step–edge. The sexiphenyl molecule remains twisted as it descends the step–edge, retaining torsional angles of 35 to 45^o. Nearly all of the energetic contribution to the barrier comes from a loss of intermolecular interactions as the unbent molecule tries to navigate the step–edge. Only a small degree of bending occurs at the step–edge and a slight rearrangement of the torsional angles to facilitate the descent and reduce the loss of intermolecular interactions. The lowest energy barrier we found was 32.5 kJ/mol, which is significantly lower than that reported by Hlawacek *et al.*

It is also apparent that previous techniques and assumptions based upon atomic systems do not necessarily hold for systems such as sexiphenyl. The sheer number of local minima on the potential energy surface of the (001) surface create particular problems for a Nudged Elastic Band method when trying to navigate between the global minimum on the terrace and the global minimum bonded to the step as the potentially tortuous route through a number of local minima is not guaranteed to be discovered. These general principles are not confined to sexiphenyl alone, but will hold good for a wide variety of other organic molecules, as we will discuss in the next chapter.

BIBLIOGRAPHY

[1] G. Hlawacek, P. Puschnig, P. Frank, A. Winkler, C. Ambrosch-Draxl, and C. Teichert, "Characterization of step-edge barriers in organic thin-film growth," *Science*, vol. 321, no. 5885, p. 108, **2008**.

[2] P. Puschnig, D. Nabok, and C. Ambrosch-Draxl, *Toward an Ab initio Description of Organic Thin Film Growth*. In: H. G. Rubahn, H. Sitter, G. Horowitz and K. Al-Shamery (eds.), *Interface Controlled Organic Thin Films*, Springer Proceedings in Physics, p. 3, SPVB, **2009**.

[3] S. Guha, W. Graupner, R. Resel, M. Chandrasekhar, H. R. Chandrasekhar, R. Glaser, and G. Leising, "Planarity of *para*-hexaphenyl," *Phys. Rev. Lett.*, vol. 82, no. 18, p. 3625, **1999**.

[4] L. Claes, J. P. Francois, and M. S. Deleuze, "Molecular packing of oligomer chains of poly(*p*-phenylene vinylene)," *Chem. Phys. Lett.*, vol. 339, no. 3-4, p. 216, **2001**.

[5] A. S. Paraskar, A. R. Reddy, A. Patra, Y. H. Wijsboom, O. Gidron, L. J. W. Shimon, G. Leitus, and M. Bendikov, "Rubrenes: Planar and twisted," *Chem. Eur. J.*, vol. 14, no. 34, p. 10639, **2008**.

[6] M. P. Johansson and J. Olsen, "Torsional barriers and equilibrium angle of biphenyl: Reconciling theory with experiment," *J. Chemical Theory and Computation*, vol. 4, no. 9, p. 1460, **2008**.

[7] J. C. Sancho-Garcia and J. Cornil, "Anchoring the torsional potential of biphenyl at the *ab initio* level: The role of basis set versus correlation effects," *J. Chemical Theory and Computation*, vol. 1, no. 4, p. 581, **2005**.

[8] F. Grein, "Influence of diffuse and polarization functions on the second-order Möller-Plesset optimized dihedral angle of biphenyl.," *Theoretical Chemistry Accounts: Theory, Computation, Modeling*, vol. 109, no. 5, pp. 274 – 277, **2003**.

[9] S. Tsuzuki, T. Uchimaru, K. Matsumura, M. Mikami, and K. Tanabe, "Torsional potential of biphenyl: *Ab initio* calculations with the Dunning correlation consisted basis sets," *J. Chem. Phys.*, vol. 110, no. 6, p. 2858, **1999**.

[10] E. Fabiano and F. D. Sala, "Torsional potential of π-conjugated molecules using the localized Hartree-Fock Kohn-Sham exchange potential," *Chem. Phys. Lett.*, vol. 418, no. 4-6, p. 496, **2006**.

[11] F. Grein, "New theoretical studies on the dihedral angle and energy barriers of biphenyl," *J. Mol. Struct.: THEOCHEM*, vol. 624, no. 1-3, p. 23, **2003**.

[12] C. F. Matta, J. Hernández-Trujillo, and T.-H. Tang, "Hydrogen-hydrogen bonding: A stabilizing interaction in molecules and crystals," *Chemistry - A European Journal*, vol. 9, no. 9, p. 1940, **2003**.

[13] L. F. Pacios and L. Gómez, "Conformational changes of the electrostatic potential of biphenyl: A theoretical study," *Chem. Phys. Lett.*, vol. 432, no. 4-6, p. 414, **2006**.

[14] O. Bastiansen and S. Samdal, "Structure and barrier of internal rotation of biphenyl derivatives in the gaseous state : Part 4. Barrier of internal rotation in biphenyl, perdeuterated biphenyl and seven non-ortho-substituted halogen derivatives," *J. Mol. Struct.*, vol. 128, no. 1-3, p. 115, **1985**.

[15] A. Almenningen, O. Bastiansen, L. Fernholt, B. N. Cyvin, S. J. Cyvin, and S. Samdal, "Structure and barrier of internal rotation of biphenyl derivatives in the gaseous state : Part 1. the molecular structure and normal coordinate analysis of normal biphenyl and pedeuterated biphenyl," *J. Mol. Struct.*, vol. 128, no. 1-3, p. 59, **1985**.

[16] E. P. Socci, B. L. Farmer, and W. W. Adams, "Molecular dynamics simulations of a poly(*p*-phenylene) oligomer," *J. Polymer Science Part B: Polymer Physics*, vol. 31, no. 13, p. 1975, **1993**.

[17] K. N. Baker, A. V. Fratini, T. Resch, H. C. Knachel, W. Adams, E. Socci, and B. Farmer, "Crystal structures, phase transitions and energy calculations of poly(*p*-phenylene) oligomers," *Polymer*, vol. 34, no. 8, p. 1571, **1993**.

[18] V. Lukeš, R. Šolc, M. Barbatti, M. Elstner, H. Lischka, and H.-F. Kauffmann, "Torsional potentials and full-dimensional simulation of electronic absorption and fluorescence spectra of para-phenylene oligomers using the semiempirical self-consistent charge density-functional tight binding approach," *J. Chem. Phys.*, vol. 129, no. 16, p. 164905, **2008**.

[19] C. Ambrosch-Draxl, J. A. Majewski, P. Vogl, and G. Leising, "First-principles studies of the structural and optical properties of crystalline poly(*para*-phenylene)," *Phys. Rev. B*, vol. 51, no. 15, p. 9668, **1995**.

[20] K. Saito, Y. Yamamura, and M. Sorai *Bulletin of the Chemical Society of Japan*, vol. 73, no. 12, p. 2713, **2000**.

[21] R. Resel, “Crystallographic studies on hexaphenyl thin films – a review,” *Thin Solid Films*, vol. 433, no. 1-2, p. 1, **2003**. Proceedings from the 12th International Conference on Thin Films.

[22] R. Resel, “Surface induced crystallographic order in sexiphenyl thin films,” *J. Physics: Condensed Matter*, vol. 20, no. 18, p. 184009, **2008**.

[23] S. J. Stuart, A. B. Tutein, and J. A. Harrison, “A reactive potential for hydrocarbons with intermolecular interactions,” *J. Chem. Phys.*, vol. 112, no. 14, p. 6472, **2000**.

[24] The TORSION term is an explicit 4-body potential that describes various dihedral angle preferences in hydrocarbon configurations.

CHAPTER 4

THE EHRLICH–SCHWÖEBEL BARRIER OF SEVEN COMMON ORGANIC MOLECULES

4.1 Introduction

Continuing the theme of the preceding chapter, here we calculate the Schwöebel barrier of seven highly aromatic molecules (see Figure 4.1) which are of significant interest in a wide number of thin film applications [1, 2, 3]. The molecules chosen are similar in many ways but exhibit slight differences which could affect the Schwöebel barrier such as shape effects and the presence of single bonds. The vast array of candidate small organic molecules for thin film growth is daunting and by examining a small number of representative molecules we hope to illuminate some general rules that may lead to a more informed choice of candidate molecules for 2D thin film growth and a better estimate of the step–edge energy barrier. However, it must be noted that here we ignore molecules containing atoms other than carbon and hydrogen and we are still only examining a small subsection of the potential molecules that could be considered, indicating the inherent richness of this field.

Within the molecules studied, there are two distinct subsets: those in which all rings are fused by sharing atoms (anthracene, tetracene, pentacene, DIP, C_{60}) and those in which some rings are joined by external bonds (rubrene and sexiphenyl) allowing far more conformational flexibility, and hence a more complex conformational phase space. The fused–ring molecules can be considered almost as rigid bodies exhibiting a progression of geometric shape from linear molecules of varying aspect ratio to the spherical C_{60} molecule. All of these molecules have been experimentally deposited as thin films on a variety of substrates with varying success from a mobility point of view. Rubrene

Table 4.1: Properties of molecules studied calculated from MM3π–minimised representations

Molecule	ΔE_{bind} (kJ/mol)	ΔE_{CCE} (kJ/mol)	**Length** (Å)	**Width** (Å)	**Ratio**	**Molecular Weight** (g/mol)
Anthracene	39	83	9.25	5.0	1.85	178
Tetracene	52	107	11.72	5.0	2.34	228
Pentacene	65	131	14.14	5.0	2.83	278
DIP	71	149	15.86	6.64	2.39	400
C_{60}	83	155	7.08	7.08	1.00	720
Rubrene	74	154	13.60	11.75	1.16	533
Sexiphenyl	113	174	25.71	4.26	6.03	459

and sexiphenyl contain four and five bonds respectively about which a twist can occur. The extra degrees of freedom that these latter molecules possess may be responsible for the fact that it is harder to deposit these molecules in ordered crystalline films than the fused–ring molecules [4]. The presence of these rotationally free C-C bonds results in a non–planar energy minimum for isolated molecules.

4.2 Method

For each molecule, we constructed a step–edge using the bulk crystal structure [5, 6, 7, 8, 9, 10, 11]. “Thin film” phases were ignored for simplicity (in reality, when they exist, they differ only very slightly from the bulk phase *i.e.*, pentacene). All of the molecules, with the exception of C_{60}, pack in a herringbone structure; their unit cell parameters are given in Table 4.2. The molecules were minimised within the unit cell using the MM3π potential. These unit cells were then used to construct super–cells representing the step–edges which can be visualised in Figure 4.3. The steps consisted of one layer of molecules (except for C_{60}) minimised in the bulk crystalline phase with periodic boundary conditions imposed in the direction parallel to the step–edge. The choice of step–edge was influenced by the preferred growth orientation of the herringbone struc-

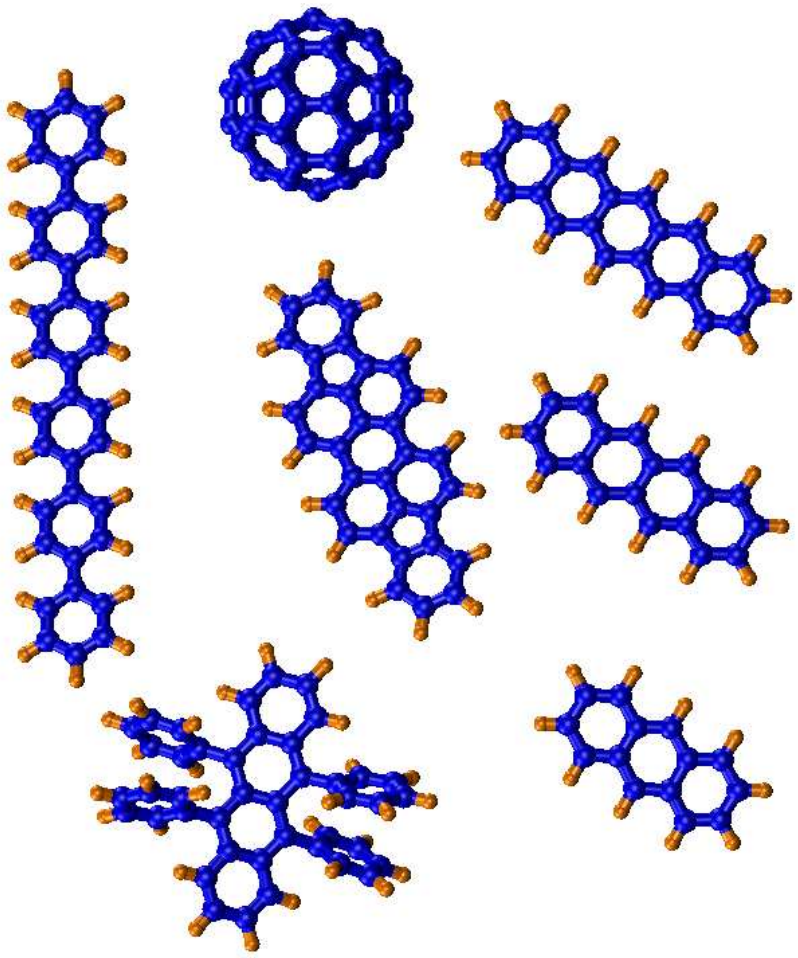

Figure 4.1: Chemical structure of molecules studied. a) Sexiphenyl, b) C_{60}, c) Anthracene, d) Tetracene, e) Pentacene, f) DIP, g) Rubrene

tures.

Pentacene, tetracene, anthracene, DIP and sexiphenyl are almost indistinguishable in the view down the molecular axis and, as a consequence, the (001) surfaces will be energetically similar for any absorbed molecule. The most useful form of these substances in thin film applications occurs on dielectric or inert substrates with the (001) plane parallel to the substrate and orthogonal to the direction of growth. This growth sometimes occurs naturally on dielectric or inert substrates as in the cases of pentacene and DIP [12] but, for others, it can be promoted by the presence of buffer layers. For these molecules, all unit cells, except DIP, are defined with the [100] direction ('a axis') as the long axis in the x-y plane. In DIP, the [010] direction ('b axis') is the longer of the two. From previous work on surface energies of pentacene, oligioacenes and oligiophenylenes [13, 14, 15] it is known that the (100) surface is the more stable of the two. The other surfaces predicted and observed in the equilibrium thin film growth of pentacene and sexiphenyl are (110) and $(1\bar{1}0)$. For consistency, we choose the same direction in relation to the herringbone structure for all molecules. The step–edge is parallel to the furrows of the herringbone structure when viewed down the molecular axis. A further consideration is illustrated by the difference between the (100) and $(\bar{1}00)$ surfaces in pentacene. The (100) surface forms an obtuse interior angle with the (001) plane, whilst the $(\bar{1}00)$ surface forms the corresponding acute angle. We examine only the (100) surfaces for the majority of cases, but will comment on the differences of other surfaces later in the chapter.

The step–edge chosen for rubrene follows the logic of the previous choice consistent with the herringbone structure. Although rubrene is notoriously hard to grow in a crystalline thin film, it has recently been shown to grow where the a-axis of the rubrene unit cell is perpendicular to the substrate surface on a buffer layer of pentacene [16, 17]

with good crystallinity. Here the (010) surface is equivalent to the top surface in the other crystals and the (001) surface is parallel to the furrows created by the herringbone structure.

For C_{60}, the choice was more arbitrary yet simpler due to the symmetry of the molecule. The step–edge is constructed from the bulk fcc structure of C_{60} and we start the molecule on the (111) surface and move it towards a $\{\bar{1}11\}$ micro–facet.

In all cases (except C_{60} where there are no hydrogen atoms), the "top" surface resembles a reasonably smooth hydrogen–rich region. We include the density of exposed hydrogens in Table 4.2 where the density is the number of hydrogens above the highest C atom at the top surface.

Complications for sexiphenyl and rubrene also arise from the question of molecular planarity within the film crystal structure. Both molecules form herringbone type molecular crystals, yet they exhibit different conformations in the crystalline state related to that of the isolated molecule, due to the increased intermolecular interactions in the crystal structure [18, 19]. For both molecules, there still needs to be consensus regarding the degree of planarity within these films. Note, in this regard, that Paraskar *et al.* [19] claim that the molecular tetracene backbone of rubrene is only planar in bulk crystals and not necessarily in thin films (although the deviation is only slight). The twist over the entire tetracene backbone for an isolated molecule is predicted to be roughly 35^o by the MM3π potential, comparing well to the value of 42^o found using B3LYP calculations by Paraskar *et al.* We show the minimum molecular conformation in Figure 4.2. The previous chapter discussed the degree of planarity of sexiphenyl where the isolated molecule is twisted about its long axis and that the crystal structures are, on average, planar. The research community interested in small organic molecule seems slightly unsure how to deal with this. For this work, both the tetracene backbone of rubrene and the

Table 4.2: Unit cells dimensions of molecular crystals. [a] the angle formed between the planes of the top surface and the step edge.

Molecule	**a**	**b**	**c**	α	β	γ	**m**	**Angle**[a]
Anthracene	8.56	6.04	11.16	90.0	124.7	90.0	2	60
Tetracene	7.90	6.03	13.53	100.3	113.2	86.3	2	73
Pentacene	7.90	6.06	16.01	101.9	112.6	85.8	2	73
DIP	7.17	8.55	16.8	90	92.42	90.0	2	69
C_{60}	14.17	14.17	14.17	90.0	90.0	90.0	4	90
Rubrene	26.86	7.19	14.43	90.0	90.0	90.0	4	90
Sexiphenyl	8.09	5.57	26.24	90.0	98.17	90.0	2	76

entire sexiphenyl molecule are considered to be planar when in the crystalline step–edge environment. This is not an assumption but a computational observation when a cluster of proximal molecules are considered. Planarity is predicted by the MM3π potential when the geometries are minimised within the bulk crystal unit cells.

The procedure followed for each search was as outlined in the previous chapter where the molecule was placed on the top surface and pushed continuously (in a sequence of steps of 0.1Å) towards the step–edge, with the total energy minimised at each point. The MM3π potential was employed for the descending molecule only and all the molecules contained within the step–edge were frozen in place.

4.3 Results

4.3.1 Binding energies

The calculation of the maximum binding energies between the top surface of the steps and the descending molecules was achieved by generating hundreds of random starting configurations and then performing a full energy minimisation with the molecules in the crystal frozen in place. All the molecules preferred to lie as flat on the surface as

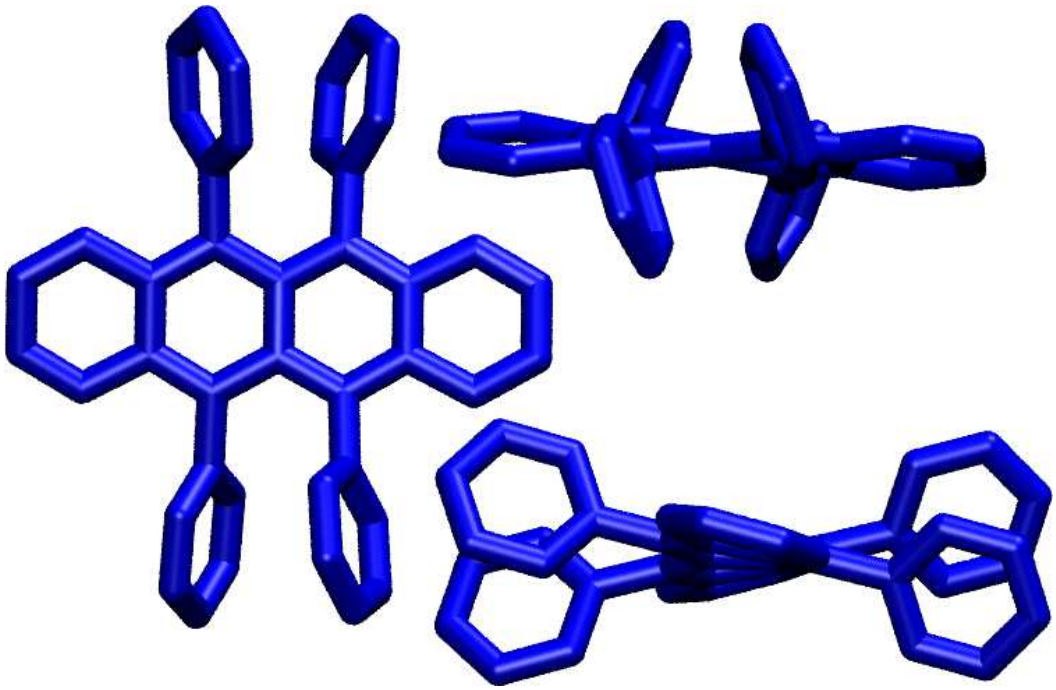

Figure 4.2: Rubrene molecular conformation viewed down the three principal axes of the tetracene backbone as predicted by the MM3π potential

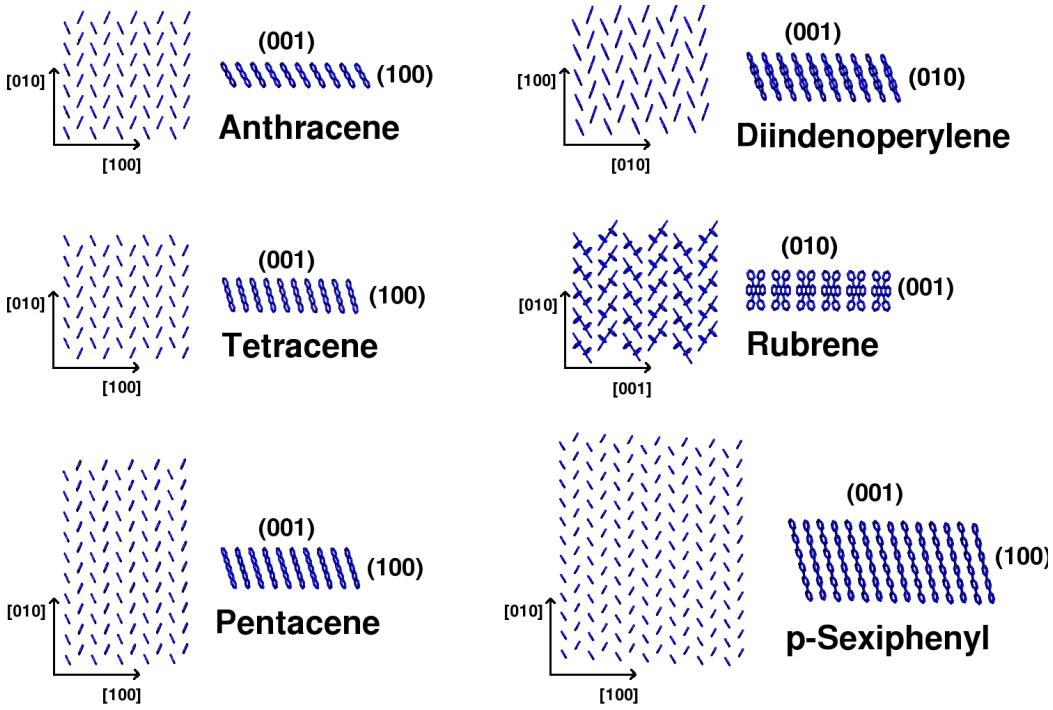

Figure 4.3: Step–edges studied. In each case the step–edge is viewed down the molecular axes (from above), highlighting the herringbone–like structure of the crystals and along the direction of the step–edge.

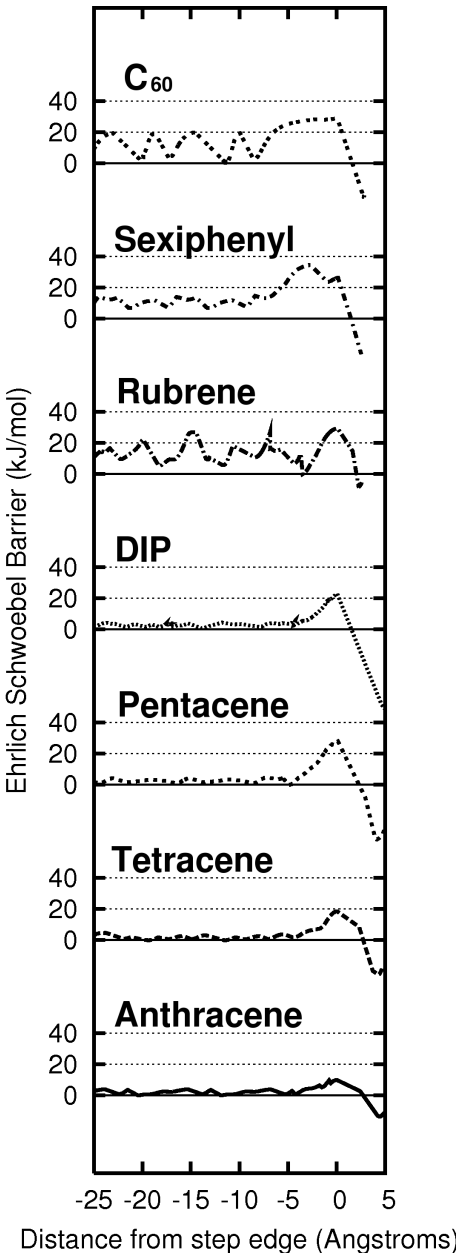

Figure 4.4: Minimum energy trajectories for the self Schwöebel barriers of all the molecules studied.

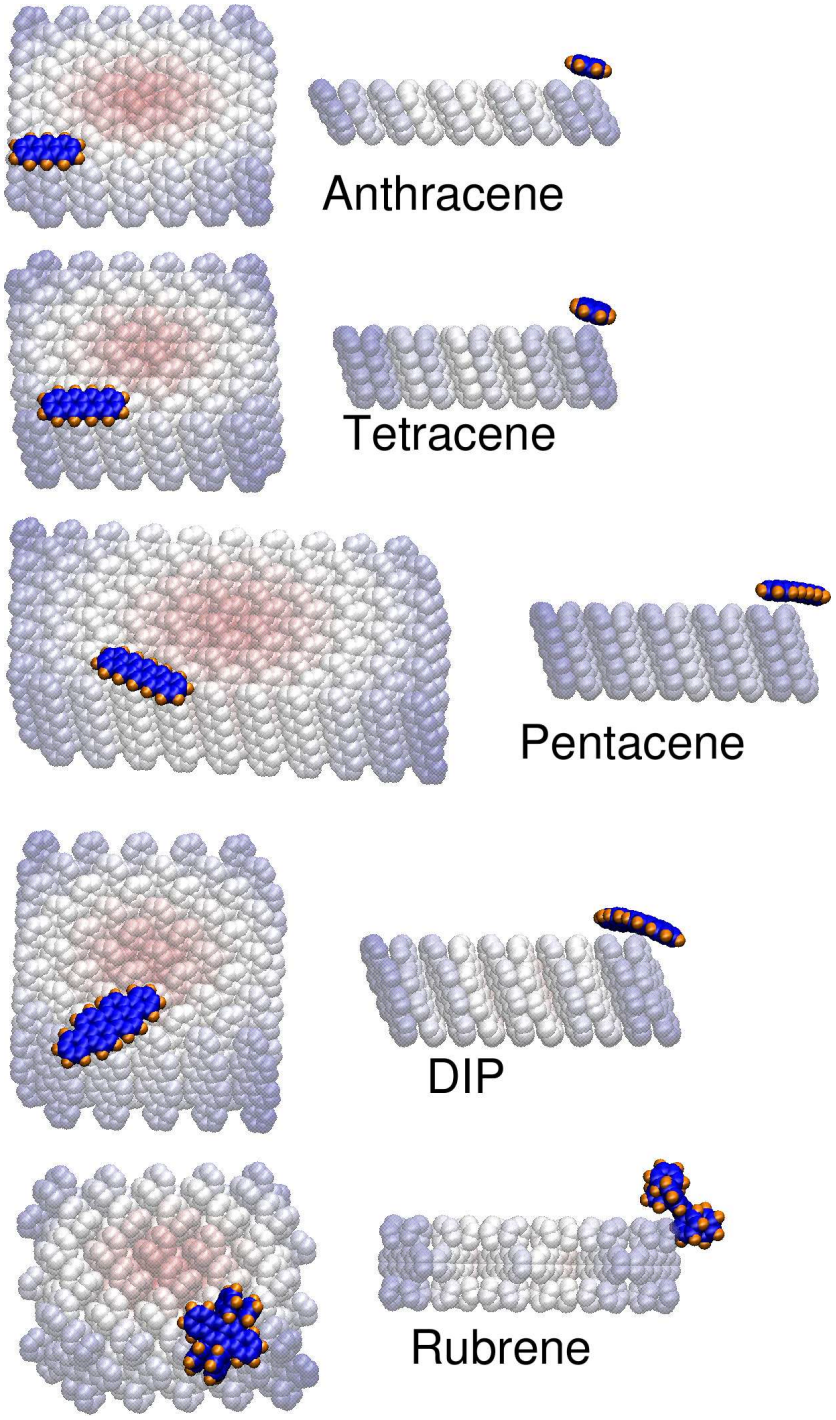

Figure 4.5: Transition points snapshots for the self Schwöebel barriers of anthracene, tetracene, pentacene, DIP and rubrene corresponding to the trajectories in Figure 4.4. The descent of sexiphenyl is examined extensively in the previous chapter whilst the conformation of C_{60} is comparatively uninteresting.

possible maximising the interaction with the surface — this is obviously easier for the planar molecules. In the case of rubrene and sexiphenyl, the strength of the interaction is not strong enough to enforce a planar configuration of the molecular backbone. The density of local minima is also higher for sexiphenyl and rubrene where the internal degrees of freedom are higher, suggesting that the subsequent trajectory search will be more difficult.

4.3.2 Self–Schwöebel barriers

The minimum energy trajectories corresponding to the 'self–' Schwöebel barriers for all seven molecules are shown in Figure 4.4. The transition point for each molecule is also shown in Figure 4.5. The difference between the bottom four trajectories of the 'planar' fused ring molecules and the top three trajectories is quite striking. All of the bottom four trajectories share a similar small (≈5 kJ/mol) 2D diffusion barrier on the approach to the step–edge, followed by a more pronounced rise in energy at the step–edge due to the Schwöebel barrier. In contrast, the top three exhibit larger 2D diffusion barriers on the terrace which are on the same order as the rise at the step–edge. This is due in the case of rubrene and sexiphenyl to the flexibility of the molecules on the surface — the molecules have conformational moves available to them which are prohibited to the fused–ring molecules. By allowing small twists and bending of the single bonds, rubrene and sexiphenyl can adapt more easily to subtle variations in the surface and therefore explore lower energy configurations. Anthracene, tetracene, pentacene and DIP (and C_{60}) experience more of a rigid–body interaction with the surface and, therefore, the surface appears energetically smoother. The exception to this behaviour is C_{60} where the large 2D diffusion barriers in relation to the step–edge barrier exists for different reasons. For the six herringbone type crystals, the top surface on which the molecules

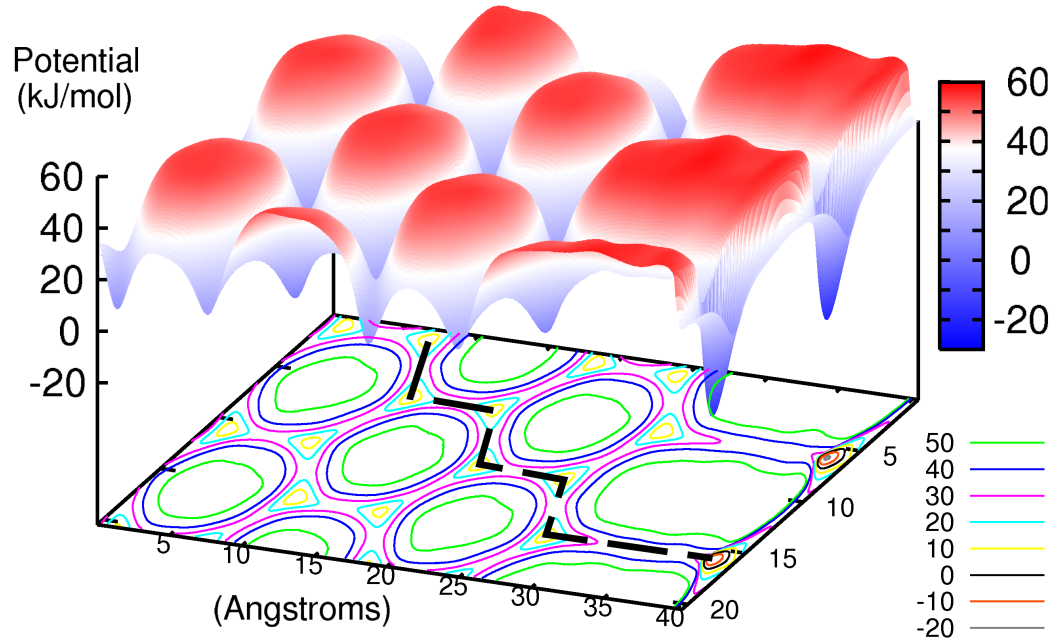

Figure 4.6: Potential energy surface of the C_{60} Schwöebel barrier. The thick black dashed line traces the trajectory shown in Figure 4.4

are adsorbed is relatively flat in comparison to the molecular length of the adsorbed molecules. The large molecular length goes some way to screening out the variations or corrugations in the surface. The C_{60} barrier is more reminiscent of an atomic system, but obviously on a far larger scale. As with atomic systems, the molecular length and the surface corrugations/variations are equivalent, thus, the adsorbed C_{60} molecule is more sensitive to the topological features of the C_{60} surface.

C_{60} potential energy surface

Due to the *relative* simplicity of the C_{60} molecule we were also able to map out the entire potential surface for the molecule approaching the step–edge (Figure 4.6). To do this, we used a technique recently employed by Cantrell *et al.* [20] where the adsorbed C_{60} molecule is used as a probe on the C_{60} surface. A fine mesh of points (with a grid size of 0.1Å) is generated and the energy is minimised with respect to the z-coordinate at each point. In this case, the internal coordinates of the probe molecule (and the rotational degrees of freedom) were "frozen" and the molecule is simply lowered towards the surface until a potential minimum is found. Cantrell *et al.* showed that the rotational degrees of freedom only have a small effect on the potential energy of the system. The non–redundant rotational degrees of freedom in the other molecules prevent them from being used as a probe for their respective surfaces. A comparison of Figures 4.6 and 4.4 indicates that the minimum trajectory corresponds to the minimum energy path through the Potential Energy Surface. C_{60} is also the only case where there exists a clear diffusion barrier that can be separated from the Schwöebel barrier. (The traditional value of each would have $\Delta E_{diff} = 20 kJ/mol$ and $\Delta E_{ES} = 10 kJ/mol$ but, for ease of comparison to the other molecular species, we report the combination of the two.) The diffusion barrier compares well to a study by Liu *et al.* [21] where they assume Arrhenius–like behaviour

to calculate various C_{60} diffusion barriers from coarse–grained Molecular Dynamics simulations. They inferred a value of $\Delta E_{diff} = 17 kJ/mol$ for simple 2D diffusion; however, there was no direct comparison available for the Schwöebel barrier.

Transition points

The trajectories of the five molecules with aspect ratio over 1.5 all share similar modes of descent with the transition point occurring with the long molecular axis close to parallel to the step–edge (Figure 4.5). Only sexiphenyl has the ability to bend significantly and all the other molecules we studied may be considered more or less rigid. If these molecules were to approach the step–edge orthogonally, then the energy penalty would be greater, as more of the molecule would be estranged from the molecular crystal. As reported in the previous chapter, sexiphenyl is able to bend slightly but the cost of bending around the step–edge orthogonally is still prohibitive and therefore a more parallel conformation is observed.

It can be anticipated that rubrene will provide the least reliable estimate of the Schwöebel barrier due mainly to the inherent complexity arising from its conformational freedom to adopt many rotational states. Throughout this work, we observe that the rubrene molecule often experiences a 2D diffusion barrier to traverse the surface that can be of equal or greater magnitude to the Schwöebel barrier to descend the step–edge. This presents a conceptual problem in that the major assumption that all local minima on the top surface are energetically available at a cost lower than the Schwöebel barrier may not hold for highly and dynamically non–planar molecules like rubrene. Due to its lack of planarity, the rubrene molecule is not as geometrically bound to the surface (in the sense that there is not a clear energetic advantage to lie on the surface in one particular orientation since the rest of the molecule can adopt so many other non–planar confor-

mational variations) and thus, overall, rubrene finds steps no less difficult to navigate over than relatively flat surfaces.

4.3.3 Correlations

In an attempt to understand how the self–Schwöebel barrier is related to physical characteristics of the molecule and, more practically speaking, providing a means to estimate the self–Schwöebel barrier *without* performing these lengthy simulations, we plotted the value of the self–Schwöebel barrier that we calculated as a function of several different geometric and physical characteristics that we imagined might play a role. with the results shown in Figure 4.7. The characteristics we chose was molecular length, molecular width, aspect ratio (length to width), molecular weight, crystal cohesive energy, binding energy, and the angle the step forms with the top surface (see Tables 4.1 & 4.2) .

However, even defining simple variables such as molecular length and width poses some problems: For example, for molecular length, a choice must be made between the absolute greatest end–to–end length and the length of the molecular "backbone" (defined by the molecular symmetry of the molecule). We chose the latter and then defined the width based on the next largest axis of symmetry. This choice of width was easy to define for the planar molecules and C_{60}, but was not quite so unambiguous for sexiphenyl or rubrene. For sexiphenyl, the molecule in its isolated state is not planar, as we have reported previously, so although the molecular length is self–explanatory, the width is not. The rubrene molecule suffers from being inherently three–dimensional, and from having a reduced symmetry in its isolated state caused by a twist in the tetracene backbone. Further, the tetracene backbone is slightly smaller than the orthogonal distance between the phenyl appendages across the backbone. Fortunately, in this case, the

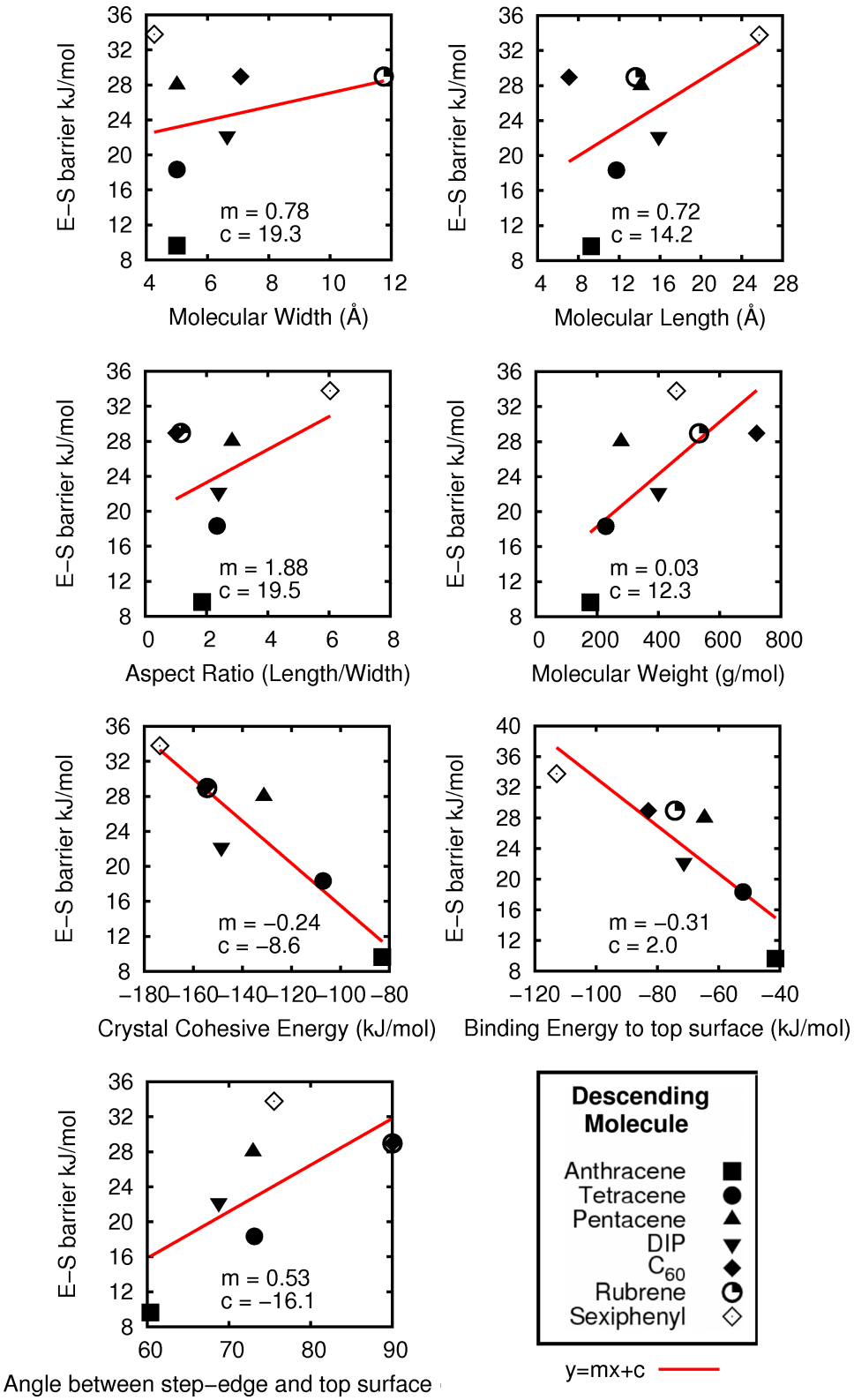

Figure 4.7: Correlations of the self–Schwöebel barrier against seven molecular variables.

values are numerically close to each other and so the correlations will not be greatly affected. Molecular weight, crystal cohesive energy and minimum binding energy are more straightforward.

Examination of Figure 4.7 shows that there is no simple linear relationship between the Schwöebel barrier and any single metric for the set of molecules studied, though the crystal cohesive energy and binding energy come the closest to providing a linear (or at least a simple) relationship. Several other observations can be made about Figure 4.7: (a) the acene homologous series (anthracene, tetracene and pentacene) shows a large degree of correlation for many of the metrics we selected (b) depending on how you interpret the correlation for a given metric, in general, rubrene and C_{60} tend to be outliers.

Also plotted on Figure 4.7 are the linear regression best fits and the value of parameters m and c in $y = mx + c$. The molecular length and width produce scattered plots that unsurprisingly do not lead to very good predictions of the Schwöebel barrier. The geometric complexity of the molecules precludes such simple parameters as width and length from solely governing the relationship and even the ratio of length and width fares little better although the planar fused ring molecules (anthracene, tetracene, pentacene and DIP) do fall on the same line. Both the molecular weight and the angle that the step forms with the top surface produced correlations which were unconvincing but indicative of expected trends. It would be predicted that larger molecules would have larger Schwöebel barriers because larger molecules will usually have more interactions with a surface and therefore have more to lose as they fall off the step. Also, larger bulkier molecules (assuming a certain degree of rigidity) would be expected to be less agile when navigating the step edge. The correlation for the angle that the step forms with the top surface is complicated further because of the difficulty in defining this angle (as described in Section 4.4.1) but the general trend seems to be that a steeper step edge

produces a higher Schwöebel barrier.

The two most promising correlations, CCE and binding energy, both indicate something about the ability of the molecule to form favourable interactions (within the crystal and on the top surface respectively). A linear correlation with these variables suggests that the Schwöebel barrier is simply a function of the original interaction strength and that the molecule will always have to lose a certain proportion of that energy (30% in the case of the binding energy) as it navigates the step edge. DIP and pentacene are the only molecules that produce qualitatively inaccurate predictions based upon these metrics *i.e.,* DIP has a higher binding energy/CCE than pentacene but produces a lower barrier. The deviations from the best fit line are less than 5 kJ/mol in the case of the binding energy correlation.

4.4 Hetero–step–edge barriers

While the step–edge barriers that a molecule experiences as it traverses a surface composed of its own type are important, there are many important industrialisations where the ultimate morphology of an interfacial layer between dissimilar materials, a hetero–interface, plays an important and, perhaps a critical, role in determining the properties of the device. Hetero–step–edge barriers are of particular importance, for example, when considering the growth of organic heterojunctions for use in photovoltaic devices. Recent research has focused on using C_{60} as the acceptor layer with a variety of other molecules as the donor [22, 23, 24]. Yet this is still a relatively new technology and there remains a lot of unexplored territory.

In an attempt to widen the concept of step–edge, Schwöebel, barriers, we introduce the concept of a ‘hetero–’ step–edge barrier and we consider one subtly altered

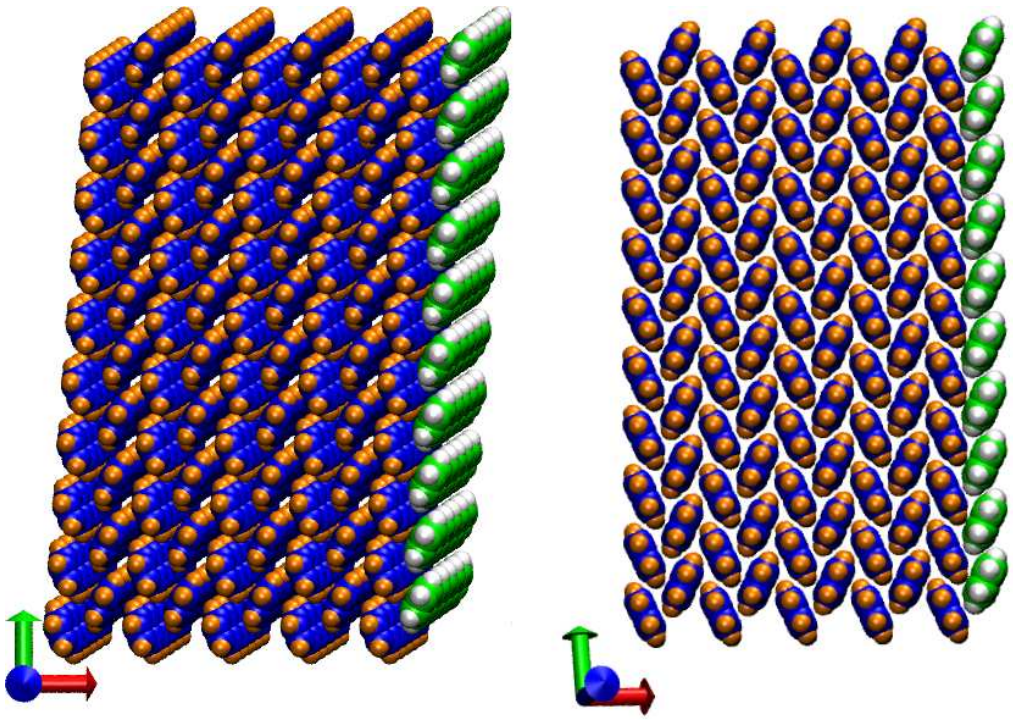

Figure 4.8: The two different pentacene surfaces considered to test the effect of the type of step–edge. The exclusion of the green and white molecules creates a different orientationally–disposed step–edge (pentacene-α) to that if the green and white molecules are included (pentacene-β). The step–edges are shown as views from directly above (left panel) and down the molecular axes (right panel).

step–edge. There are no calculations of these hetero–Schwöebel barriers during growth in any heterojunction formation situation.

We calculate the hetero–Schwöebel barriers of all seven molecules studied in the preceding chapter on four surfaces that we have already studied in some detail in other studies — namely, pentacene, tetracene, DIP and rubrene. Pentacene and tetracene were chosen because of the similarities in their unit cells and crystal structure — we expect to find almost identical results between the two but select them to confirm that we can predict when surfaces will behave similarly. The behaviour of DIP and rubrene differ significantly from the acenes and provide enough variety to justify any postulated correlations of hetero–Schwöebel barriers.

We also studied a different pentacene step–edge from the one studied in the preceding chapter. This second pentacene step–edge, which we will call pentacene-α, was included to test the effect of the precise type of step–edge that a descending molecule may encounter, an effect that was not considered in the preceding chapter for pentacene. The only difference between the two pentacene step–edges is exactly which molecule in the unit cell forms the step surface, see Fig 4.8. This difference in step–edges was considered for sexiphenyl in the previous chapter and depends on which of the {100} planes is chosen to cut the step–edge.

4.4.1 Correlations of Schwöebel barriers with physical metrics

The introduction of hetero–Schwöebel barriers means that any metric we use to correlate the barriers across different molecular systems is likely to include intrinsic information about both the molecule descending the step–edge and the nature of the step–edge itself. Referring to our experiences with self–Schwöebel barrier in the preceding chapter

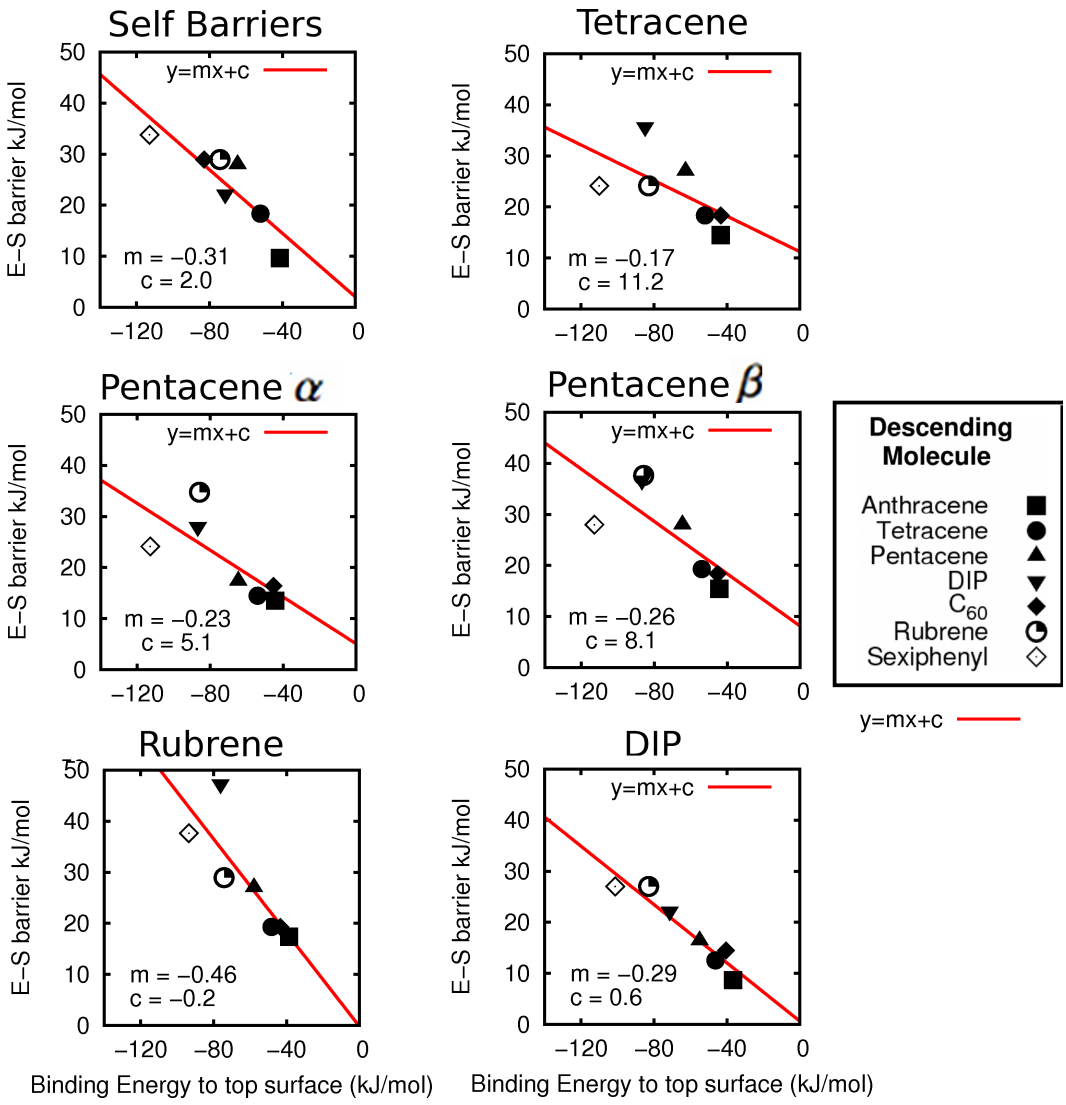

Figure 4.9: Correlation of the Ehrlich–Schwöebel barrier with the binding energy on the top surface for the self–Schwöebel barriers and hetero–Schwöebel barriers. The bold title on each sub–figure refers to the type of surface and step–edge over which the adsorbed molecule is descending. The barrier for each of the seven descending molecule types is shown on every surface using symbols provided in the accompanying key on the right–hand side.

and the correlations across molecule types, the only metric we have already used which satisfies this concept of including the cross–interaction of the diffusing (ultimately, descending) molecule and the underlying surface is the binding energy of the descending molecule to the top surface. Note that this was also one of the most promising correlations for the self–Schwöebel barrier determined in the preceding chapter. While another option could be a combination of two or more of the other metrics we considered, our results with the binding energy were sufficiently encouraging to preclude any such study at this time. These results are now described in some detail.

In Figure 4.9, we show the correlation of both the self– and hetero–Schwöebel barriers versus the binding energy for all seven diffusing/descending molecules over each of the four different surfaces (pentacene, anthracene, rubrene and DIP). As the figure shows, the general roughly linear correlation of Schwöebel barrier against binding energy with Schwöebel barrier holds up well across all surfaces. As expected, there is a consistently linear relationship within the acene homologous series across all surfaces. It also shows, encouragingly, that the results for all seven targeted molecules are almost identical for the pentacene and tetracene surfaces (except when rubrene is the descending molecule). The results also show that, as a general rule, the size of the step–edge barrier for sexiphenyl is consistently and significantly lower in value than its bonding energy to the surface suggests. We attribute this departure to its ability to bend and adapt its conformation as it navigates the step–edge. This is responsible for skewing the linear fit away from the other molecules for the tetracene, pentacene-α and pentacene-β surfaces in particular. The difference between the steepness of the correlations for the two pentacene surfaces (α and β) highlights the complexity of the system we are dealing with, and the sensitivity of the barriers to slight changes in the surfaces.

There are two points of concern amongst this data: firstly, the $\approx$ 13 kJ/mol discrep-

ancy between the Schwöebel barriers for rubrene on tetracene and rubrene on pentacene and, secondly, the higher than expected barrier for DIP on rubrene. That rubrene should be involved in both of these unexpected results should not be a surprise considering it is conformationally the most complex molecule we are studying. The low value of the Schwöebel barrier of rubrene on tetracene is a case where the Schwöebel barrier that we calculated for this trajectory is lower than some of the 2D diffusion barriers we observed for other trajectories of rubrene on tetracene and so the concept of a Schwöebel barrier is not really applicable.

In Figure 4.10 we consolidate all our results onto one graph of Schwöebel barrier versus binding energy in pursuit of a universal relationship, and in Figure 4.11 we modify the results in Figure 4.10 to add the results from the only other previous values of organic molecule Schwöebel barriers available in the literature (for PTCDA and sexiphenyl). Figure 4.11 shows that the PTCDA result would lie on a linear relationship through our data, but the result for sexiphenyl does not. Our concerns over the sexiphenyl results have already been thoroughly discussed in the preceding chapter. It can be seen from Figure 4.10 that, although we can correlate the binding energy with the Schwöebel barrier reasonably well over the entire range of systems studied within an uncertainty of about 10 kJ/mol or less, there are clearly other variables contributing towards the Schwöebel barrier. For example, the rubrene step–edges consistently give higher Schwöebel barriers than DIP step–edges. We can postulate reasons for this, although quantification becomes problematic. One of these variables is the angle which the step forms with the top surface. This was investigated experimentally by Hlawacek *et al.* for the sexiphenyl system in which a gradual standing up of molecules was observed experimentally from the first monolayer upwards until bulk–like conditions were observed. It is intuitive that the more severe the angle that the step forms with the surface (i.e. the more upright the step edge), the higher the barrier. However, we have yet

to quantify this with all of our results due to the difficulty in defining a 'step angle.' Because the steps are constructed of molecules which are not geometrically simple (especially in the case of rubrene) the surfaces that they form exhibit local variations (*i.e.*, deviations from the surface plane) over the range of one unit cell thus complicating the measurement. The crystals can be thought of as exhibiting a fractal dimension greater than unity — depending on the scale of measurement the angle varies. For example, as can be seen from Figure 4.3, on a macro–scale the angle between (010) and (001) for rubrene is clearly 90^o whereas on an Å scale this is not the case and there is considerable variation along [010]. However it is clear, again from Figure 4.3, that the rubrene step presents a more severe angle than DIP.

4.4.2 Sexiphenyl on DIP trajectories

As we discussed above, when sexiphenyl is the descending molecule it consistently has a lower Schwöebel barrier than that predicted by the correlation we found with binding energy. As we have shown above, the flexibility of the sexiphenyl molecular backbone allows the molecule to navigate the step–edge more easily than might be experienced by a more rigid molecule, like pentacene, say. In the minimum energy pathway that sexiphenyl seeks to traverse the step–edge, the molecule still navigates the step–edge with its backbone almost parallel to the step–edge. When pentacene, tetracene or rubrene molecules formed the underlying terrace and step, we observed no trajectories where sexiphenyl preferentially oriented itself in an orthogonal approach to the step and none in which the molecule drapes itself continually over the step–edge (bending at each C-C bond).

However, when DIP molecules form the underlying terrace and step, we did observe

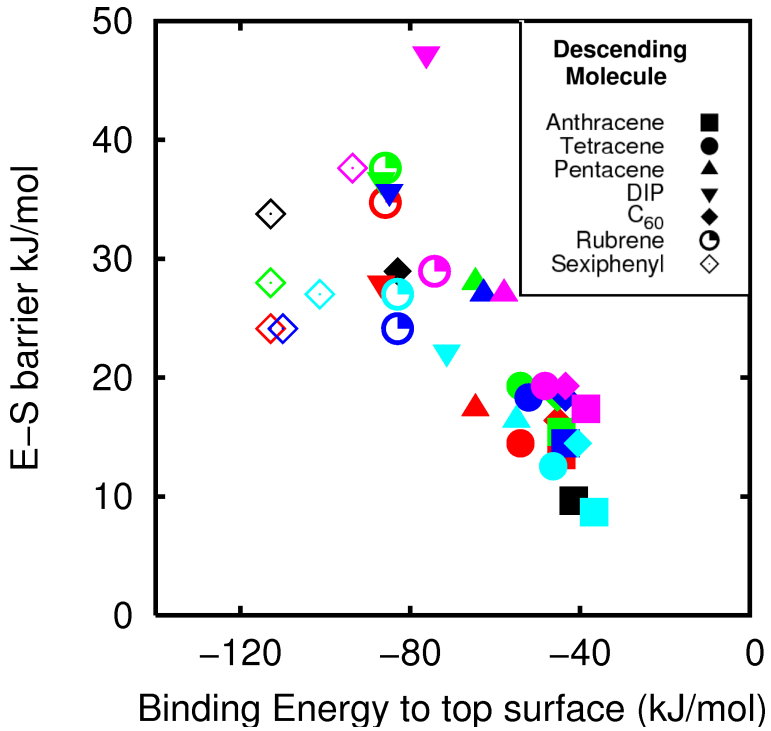

Figure 4.10: Relationship between binding energy and Schwöebel barrier for the entire set of systems studied in this work. The colour of the points refers to the material constituting the step–edge, whereas the point style denotes the descending molecule (see key). Black — Self– barrier; Dark Blue — Tetracene, Red — Pentacene-α, Green — Pentacene-β, Magenta — Rubrene, Light Blue — DIP.

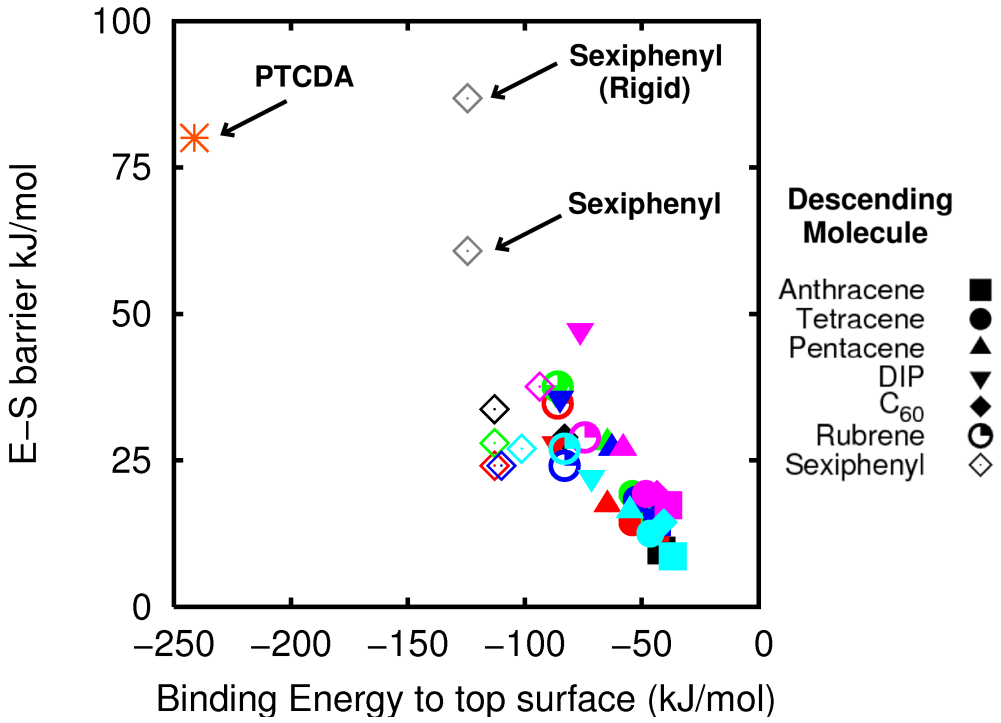

Figure 4.11: Data shown in Figure 4.10 with the inclusion of previous results in this field. Grey shows the results for sexiphenyl from Hlawacek *et al.*; orange denotes the results for PTCDA from Fendrich *et al.*. All other points are the same as in Figure 4.10.

one instance that produced such a trajectory, leading to a hetero–Schwöebel barrier of 40 kJ/mol. Whilst this descent, featuring a sexiphenyl molecule smoothly draped over the step–edge, was not the lowest energy trajectory (the lowest being 27 kJ/mol), the value of 40 kJ/mol is within an an accessible energetic range, and hence in dynamic situations molecules will occasionally adopt this draped descent. In Figures 4.12 and 4.13 we examine the energetics of both trajectories. In Figure 4.14, we show snapshots of the molecule as it drapes over the step edge. This is an important result in the context of the Hlawacek *et al.* paper as it shows that our search method *is* able to pick up such a trajectory if it is of low enough energy to occur. The reason that it was seen for DIP and not on other surfaces is because of the shape of the DIP molecule and how it forms step–edges. The relatively large molecular width of DIP means that more carbon atoms are exposed at the step–edge face and so the binding energy of the descending molecule is stronger (than it would be on the other surfaces we considered, for instance). When an orthogonally approaching molecule begins to poke itself over the edge of the step–edge, it feels a stronger energetic driving force from the proximal exposed C-atoms and the less steep step–edge that encourages the sexiphenyl molecule (with its greater rotational freedom) to bend round the step and pick up the energy advantage of the $\pi - \pi$ interactions. This example of an eventuality in which descending molecules can continuously drape themselves over steps) illustrates the kinds of molecules (orientationally more free molecules) and step–edges (less steep, π–cloud exposed) that are more likely to give rise to heavily bent descents.

4.5 The effect of using the MM3 model rather than MM3π

To examine the extent of some of the compromises that were made in the preceding sections to make the computational studies tractable, we have revisited some of these

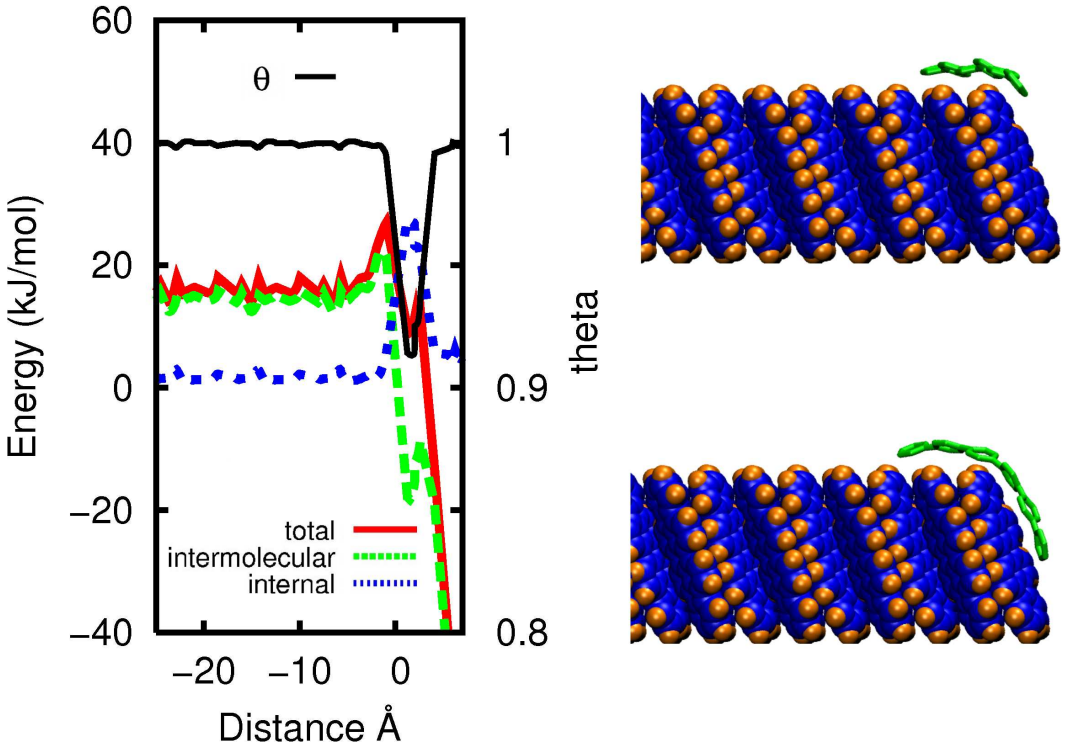

Figure 4.12: The energetic profile (left) and key snapshots (right) of the minimum energy trajectory for a sexiphenyl molecule to descend over a DIP step–edge. Note the relative invariance of the low energy path as the molecule traverses the terrace and the relatively small period of energy loss at the transition point.

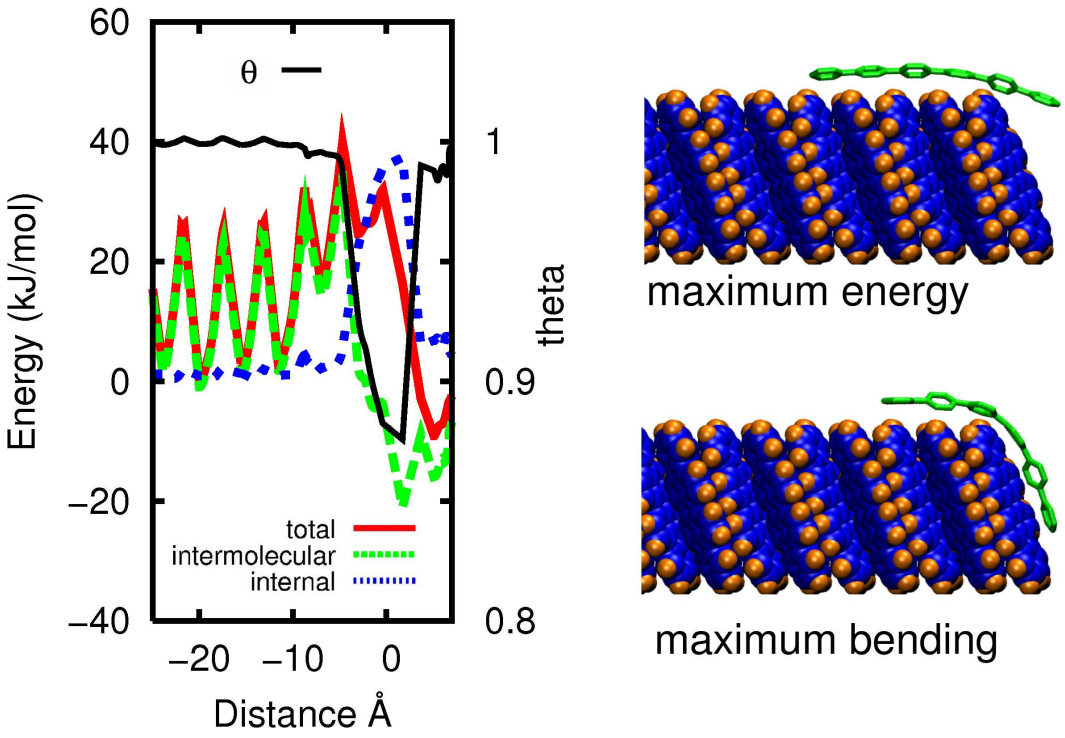

Figure 4.13: The energetic profile (left) and key snapshots (right) of an orthogonal trajectory of a sexiphenyl molecule (not the minimum energy path) as it descends over a DIP step–edge in which the 6P molecule gradually bends over the step–edge. Note the spikes in energy as the uncomfortably oriented molecule traverses the terrace and the relatively large period of energy loss during the descent.

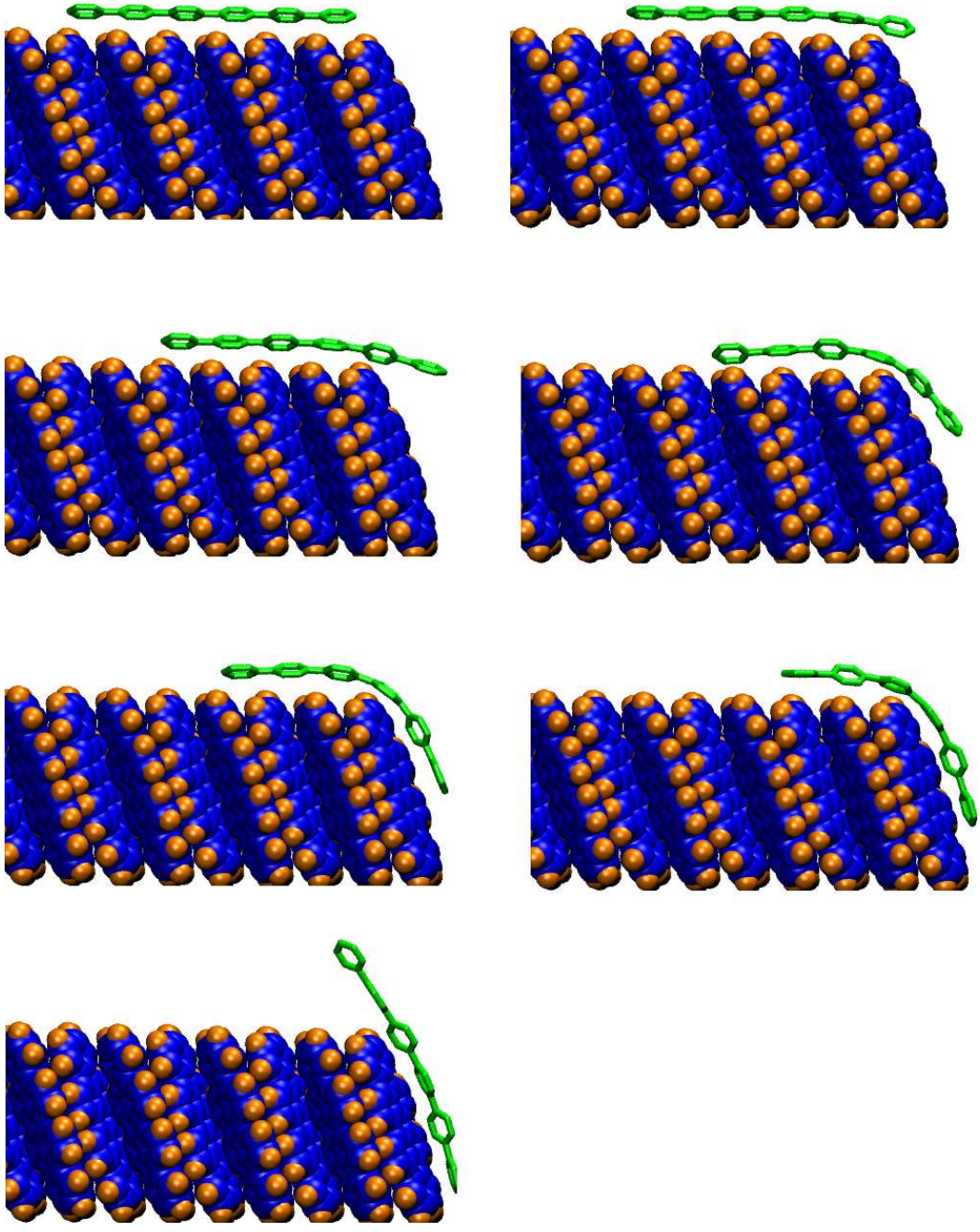

Figure 4.14: More detailed snapshots of the orthogonal trajectory from Figure 4.13

scenarios for a limited set of studies. All the subsequent calculations in this section are made for the pentacene surface and consider a pentacene molecule traversing the step (*i.e.*,, a self–Schwöebel barrier).

Our first study, involved comparing results for the pentacene self–Schwöebel barrier obtained using the MM3π and MM3 models. There were two main reasons for this comparison: (1) a practical consideration that the MM3π–modelled system takes a factor of 100 or so more to run than that of MM3 and hence, if sufficiently accurate step–edge barriers can be obtained using the more computationally efficient MM3 model, then the extra expense to run MM3π modelled systems would be unnecessary. (2) On the other hand, we have shown that, unless the MP2 correction to the MM3 model is used for π–conjugated molecules, an incorrect planar molecular structure of certain molecules will be predicted, specifically rubrene and sexiphenyl. For the five fused–ring molecules that we considered (the acenes, DIP and C60), the correct molecular structure is observed without the MP2 correction, but a smaller C=C bond length is observed ($\approx$0.05 Å smaller, depending on the locality). This results in a pentacene molecule which is 13.61 Å in length instead of 14.14 Å, but the intermolecular energy is largely unaffected.

The second study involved repeating all of our calculations for binding energies with both MM3 and MM3π models and running Schwöebel barrier searches. We found that all of the fused–ring molecules provided very similar results regardless of whether the MM3π was employed or not: All MM3 barriers were within 5 kJ/mol of the MM3π values. The MM3 potential also described the herringbone structure of pentacene without the expensive MP2 correction.

This encouraging result allows us to remove the π conjugation restriction from the whole system with no significant loss in accuracy and hence enabled us to “unfreeze” the

molecules constituting the step–edge to investigate whether any active role was played by the molecules in the step during molecule descent. For the rest of this chapter, we concentrate on pentacene and carry out various simulations with the standard MM3 potential.

4.5.1 Pentacene: Removing the restriction of a "frozen" step–edge

The entire procedure, described above, to quantify the Schwöebel barrier for pentacene was repeated with different sets of restrictions placed on the system so as to decouple the effects of choice of model and the disposition of the molecules forming the step–edge ("frozen" in place and unable to move in response to the presence of the descending molecule, or not). The cases we considered were:

- 1. Original case — All molecules forming the step–edge "frozen" in place. MM3π model used to describe the descending molecule.
- 2. All step molecules frozen. The MM3 model used for the descending molecule.
- 3. All step molecules free to move. The MM3π model used for the descending molecule.
- 4. All step molecules free to move. The MM3 model used for the descending molecule.

We show, in Figure 4.15, the minimum trajectories resulting from the four different cases. All of the trajectories, transition points and barriers are similar, again indicating that adding the MP2 correction is not necessary for pentacene in the Schwöebel barrier search. When the molecules constituting the step are free to move, we see no mechanism by which the molecules substantially affect (either to assist or hinder) the descent of

the molecule and the resulting step–edge barrier is only 5 kJ/mol lower when all the molecules are free to move and accommodate the descending molecule. The molecules in the step do not move significantly when the descending molecule passes by in close proximity.

4.5.2 Pentacene: Dynamics of step–edge descent

To investigate how the step–edge barrier was affected by thermal movement of the molecules or atoms, we performed Molecular Dynamic simulations of selected systems. In this way, we could study not only the minimum energy path, but observe the interplay of kinetic and thermodynamic aspects of step–edge descent.

All of the Molecular Dynamics simulations were carried out using the MM3 potential applied to all molecules in the system. The construction of a more complex step–edge with two layers was also required; the bottom layer frozen and the top layer was free to move. The top layer was thermalised to a temperature of 300 K for 40 ps in a constant–temperature simulation (NVT ensemble) to allow it to come to a quasi–equilibrium condition and then a single diffusing molecule on the upper surface was directed orthogonally towards the step–edge from a series of random starting points and orientations.

Because the step–edge barrier is significant compared to the thermal energy of the molecule, we cannot simply rely on the molecule to make a successful attempt to descend the step–edge of its own accord during the limited period of observation (order of nanoseconds) of the MD simulation. When the initial location of the molecule was constrained to lie within 5Å of the step and a constant–temperature, NVT, simulation was run at 300 K for longer time–scales (i.e. 10s of ns), the molecule free to diffuse

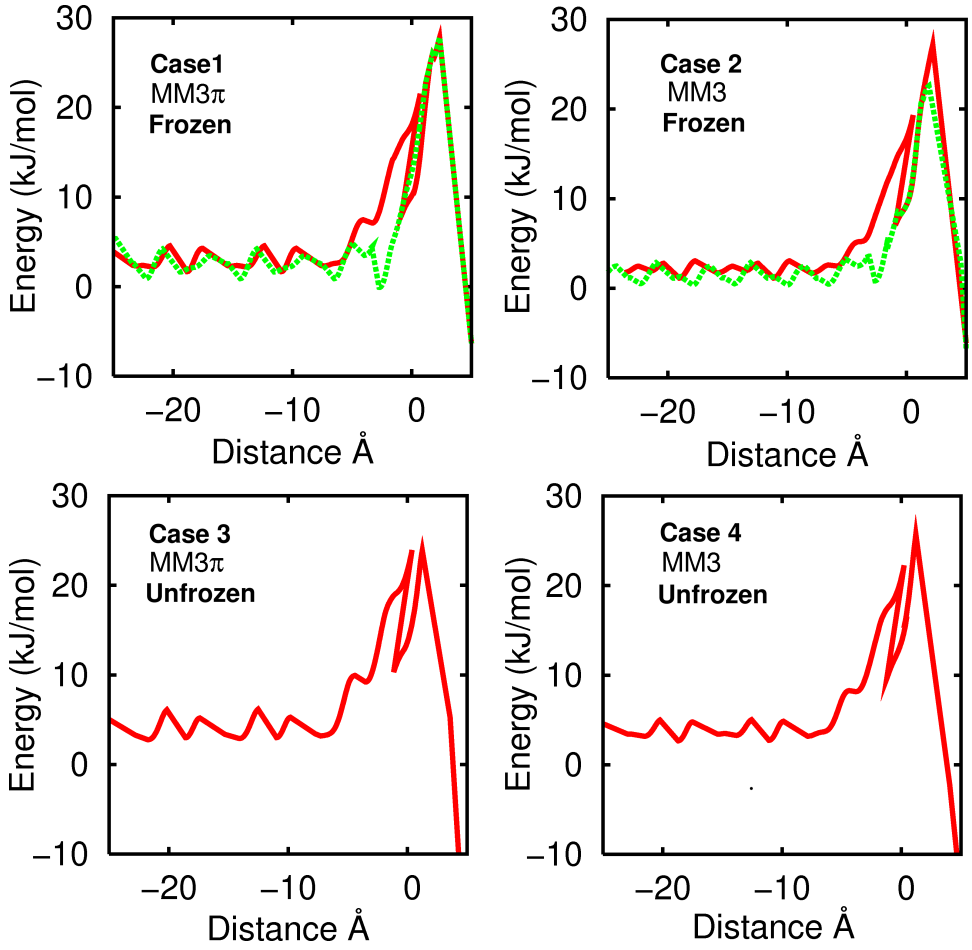

Figure 4.15: A comparison of the minimum energy Schwöebel barriers for the four test cases of constraint. For each graph, the label "Frozen" or "Unfrozen" refers to the disposition of the step–edge molecules and the labels MM3 and MM3π refer to the potential model used to describe the intermolecular interactions of the descending molecule.

over the terrace was not observed to fall down the step once. Assuming a Boltzmann relationship defined by an attempt frequency, ν_0, and an activation energy, ΔE_{ES}, given in the equation below, the molecule would need to approach the step–edge 2300 times for every successful descent. This estimate of the probability of observing a spontaneous descent was larger than the number of trials in our study.

$$\nu = \nu_0 e^{-(\Delta E_{ES}/k_B T)} \tag{4.1}$$

To finesse this problem, the diffusing molecule on the upper terrace was directed across the surface by imposing a harmonic potential on the central phenyl ring until it was within 10Å of the step–edge. At this point, the potential was then lifted and the system evolved under a microcanonical, constant–energy, NVE ensemble. At each random starting position (varying both rotational and translational initial conditions), eight simulations were carried out with varying force constants, thus varying the energy of approach to the step–edge. The lowest energy successful trajectories and highest energy unsuccessful trajectories were then analysed. All of the trajectories in Figures 4.16, 4.17, and 4.18 use the intermolecular energy between the descending molecule and the step edge on the ordinate axis. The internal energy of the molecule remains roughly constant and we see very little deformation in the step edge as the molecule approaches.

Figure 4.16 shows one of the many failed trajectories where the molecule approaches the step edge only to be repelled back away from it. The loss in binding energy is at least equivalent to that of the successful descents shown in Figure 4.17, indicating the importance of the molecule's approach in considering the likelihood of a successful descent. The two trajectories shown in Figure 4.17 are both successful descents; the red molecule descends in a more orthogonal orientation with a slightly higher loss in binding energy than the parallel green molecule, though the difference is marginal. We are not claiming

that these successful descents represent the global lowest energy descents because of the imposed directional bias that we place on the dynamic simulations. And, indeed, the loss in binding energy is higher than we observed in our static energy minimizations. In order to claim that we have observed the dynamics of such a global energy situation, we would need to sample the true diffusional paths available to the molecule; by biasing the progress of the molecule towards the step–edge, this is compromised.

In Figure 4.18, we demonstrate the difficulty of overcoming the step–edge energy barrier in dynamic simulations: All three molecular trajectories shown on the top graph (red, green, blue) start at the same position, but are accelerated towards the step edge with slightly different energies (ascending in energy from red to green to blue). All three trajectories become unstable around 18-19 ps and the molecule leaves the (001) surface briefly (by rotating onto its edge, rather than lying flat on the surface), resulting in a loss in binding energy with the surface. In the cases denoted in red and green, the molecule falls back flat onto the step–edge at a time–stamp of 22 ps, but still fails to fall off the edge. This is because, in both cases, the molecule hits the last row of molecules in the step–edge. In the case of the "blue" molecule, its slightly higher energy allows it the momentum to just clear the surface, enabling it to fall over the edge. Importantly, in all three cases, despite the high energies involved, the step edge maintains its structural integrity throughout. This provides further justification for the assumption that the molecules in the step edge are largely passive in any Schwöebel barrier descent mechanism and that the degrees of freedom of molecules in the step–edge can be frozen out.

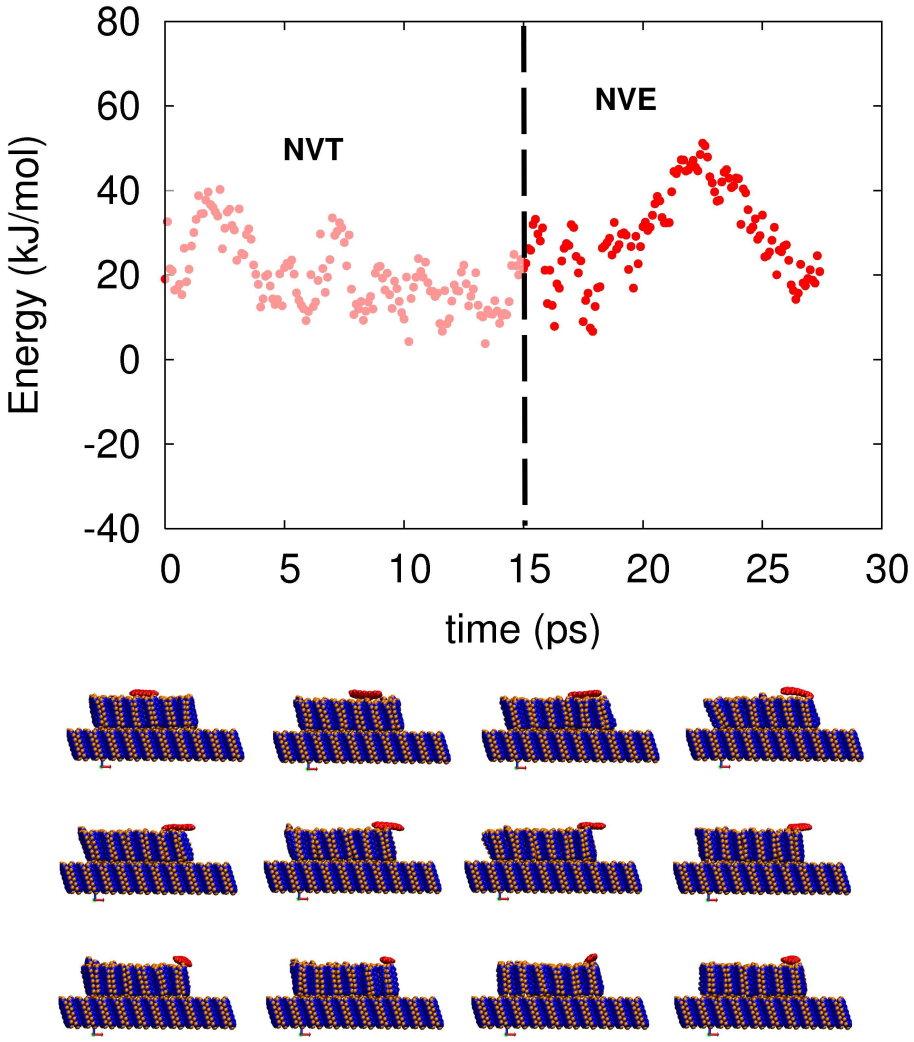

Figure 4.16: Time trajectory of a failed dynamic step–edge descent followed using Molecular Dynamics molecular simulations. The graph shows the intermolecular energy between the molecule and the step as a function of time. Before 15 ps, the system is held at thermal equilibration under constant–temperature, NVT, conditions. At 15 ps, the molecule is directed towards the step–edge with the aid of a harmonic potential placed on the middle phenyl ring. The energy of the system rises by about 10 kJ/mol as the molecule experience the step–edge barrier at about 22 ps. The snapshots shown below the energy–time plot are taken looking down the b-axis at 1 ps intervals from 16-27 ps and the molecules are colour–coded to correspond with the graph.

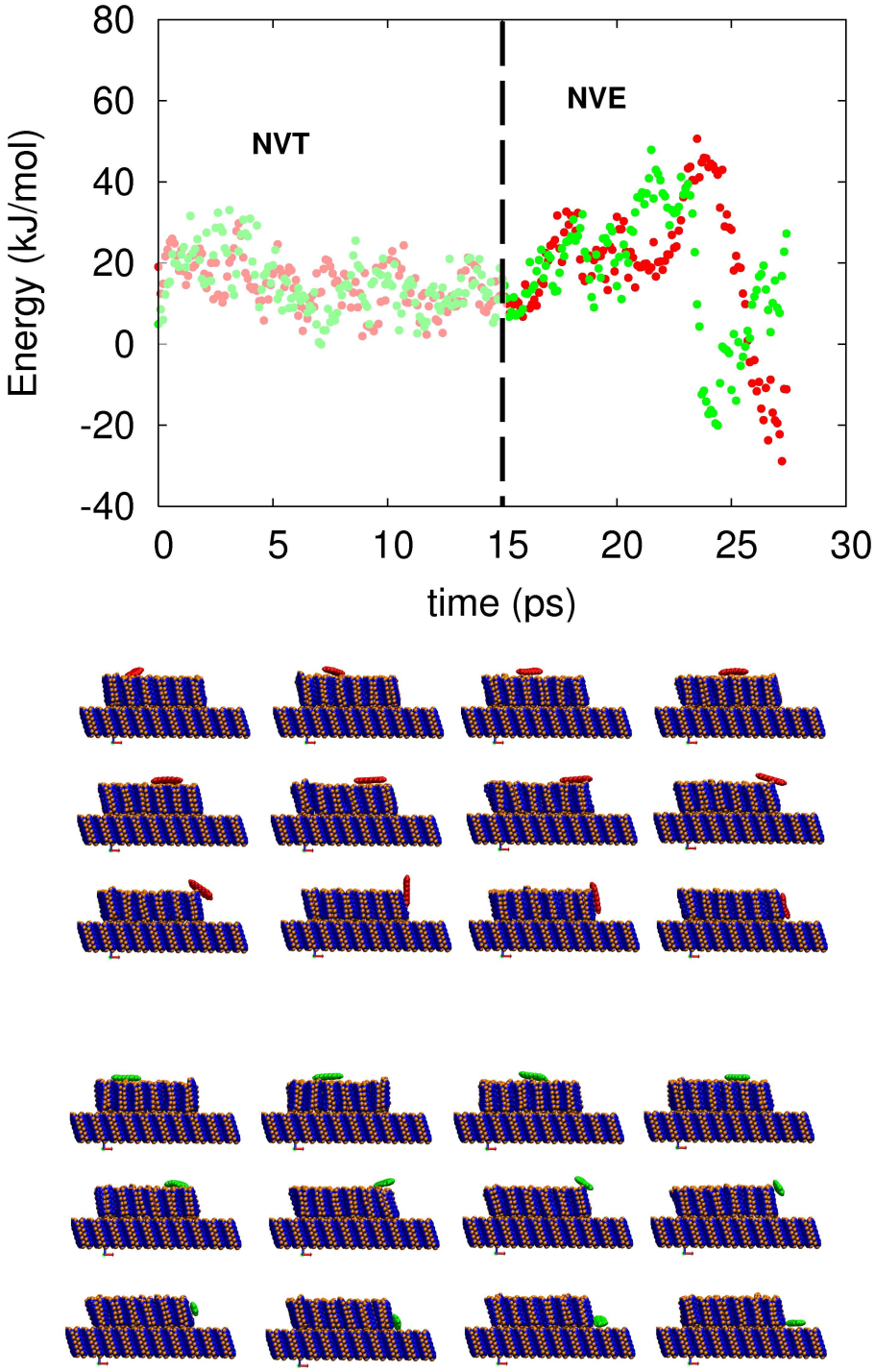

Figure 4.17: Two Molecular Dynamics simulation trajectories of two successful dynamic step–edge descents (one shown in red, the other in green, on the energy–time plot on the upper part of the figure). The energy rise at the step–edge is clearly larger than in the preceding figure (of over 20 kJ/mol) but, like the preceding figure, the maximum energy occurs at the tipping point (around 22-24 ps). The key is the same as that given in Figure 4.16 caption.

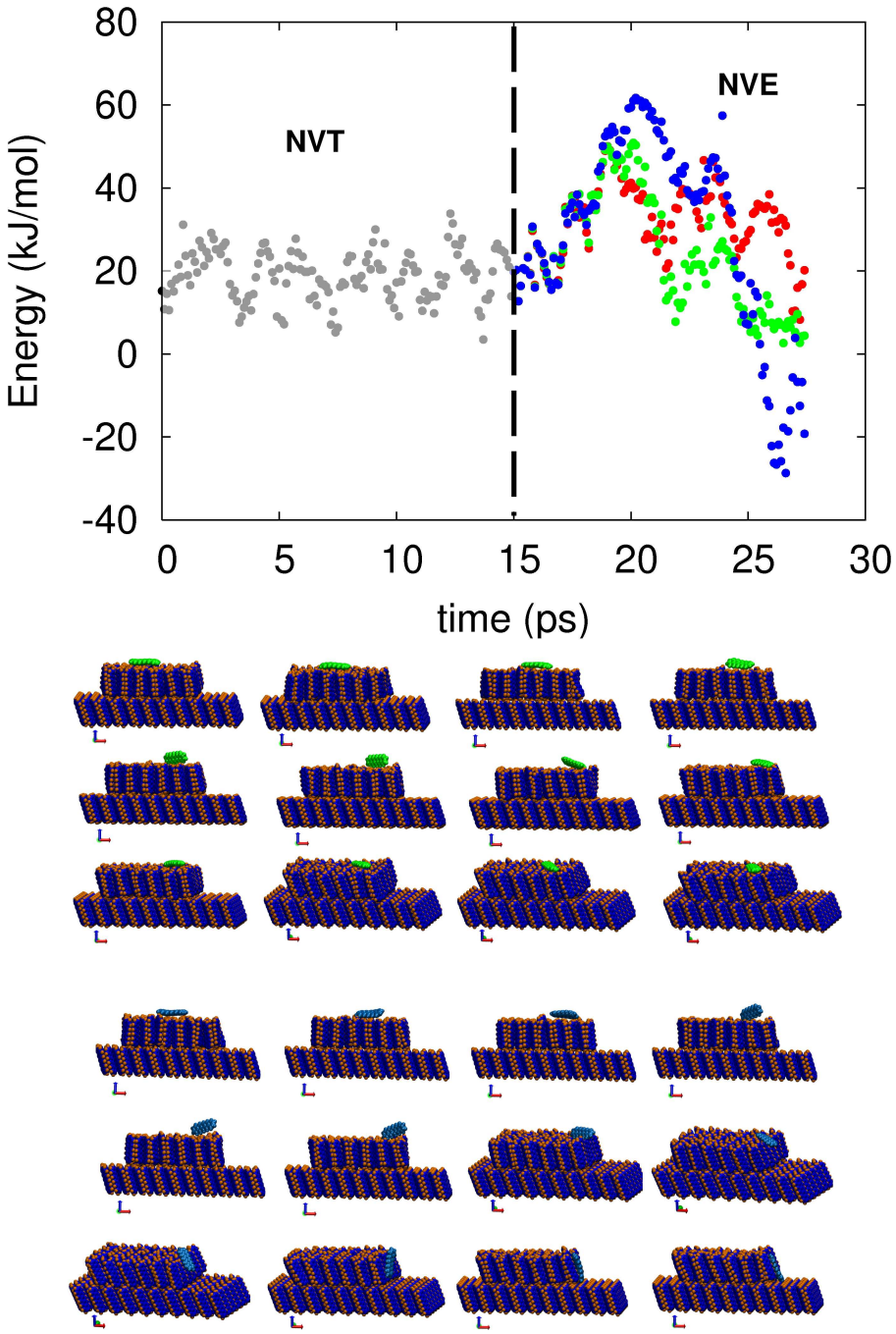

Figure 4.18: Three trajectories, all starting from the same position, but with different initial energies (red being the lowest in energy, followed by green, and then blue). The key is the same as in Figure 4.16 with the exception that the NVT portion trajectory is shown in grey. Snapshots of the red trajectory are not shown. Here again, the unsuccessful descents of the red and green molecules are seen to not experience a high enough energy rise to overcome the Schwöebel barrier, whereas the energy–time profile of the blue trajectory is able to do so and fall over the step edge.

4.6 Conclusions

By studying, in detail and for the first time, the Schwöebel barrier of seven small organic molecules on a number of different underlying surfaces, several important qualitative observations have been made, which we believe have led to a better understanding of the processes involved in step–edge descent. A roughly linear correlation was found which relates the binding energy to the Schwöebel barrier enabling researchers to estimate the Schwöebel barrier for either self– or hetero–interface situations without the need to perform the time–consuming and rather demanding molecular simulations described in this chapter. In general, the molecules lose about 40% of their binding energy as they descend a step edge, but this can be reduced in the case of molecules with flexible backbones, such as sexiphenyl. A "log–roll" mechanism was confirmed as the preferred step–edge descent in which the long molecular axis remains nearly parallel to the step edge. This mechanism is preferred for high–aspect ratio molecules.

Although most of the studies in this chapter consider the Schwöebel barrier of molecules descending one particular type of step–edge, our limited study of different step–edges showed that the steepness (as in the DIP step) and even subtle differences in molecular orientation (as in the two pentacene step–edges) can have a significant effect on the value of the Schwöebel barrier. It is obvious that the features of the step itself play an important part in determining the magnitude of the barrier. So it must be observed that alternate steps or kink sites should play an important role in the evolution of the film. This would be particularly apparent in the sub–monolayer regime of film growth as the small islands which form would not have particularly well defined step–edges. It also points to the difficulty of interpreting experimental estimates of step–edge barriers which have to arise from an ensemble average of different Schwöebel barriers depending on the details of the island density and type, making molecular sim-

ulation a far more attractive and definitive source of information about the way in which small organic molecules descend steps and assisting in the design of hetero–interfaces to promote smoother film growth.

BIBLIOGRAPHY

[1] Z. Bao and J. Locklin, eds., *Organic Field-Effect Transistors*. Optical Science and Engineering, CRC, **2007**.

[2] H. Klauk, ed., *Organic Electronics: Materials, Manufacturing, and Applications (Hardcover)*. Wiley-VCH, **2006**.

[3] S. R. Forrest, "The path to ubiquitous and low-cost organic electronic appliances on plastic," *Nature*, vol. 428, no. 6986, p. 911, **2004**.

[4] H. H. Fong, S. K. So, W. Y. Sham, C. F. Lo, Y. S. Wu, and C. H. Chen, "Effects of tertiary butyl substitution on the charge transporting properties of rubrene-based films," *Chem. Phys.*, vol. 298, no. 1-3, p. 119, **2004**.

[5] O. D. Jurchescu, A. Meetsma, and T. T. M. Palstra, "Low-temperature structure of rubrene single crystals grown by vapor transport," *Acta Crysta. B*, vol. 62, no. 2, p. 330, **2006**.

[6] B. Chapman, A. Checco, R. Pindak, T. Siegrist, and C. Kloc, "Dislocations and grain boundaries in semiconducting rubrene single-crystals," *J. Crystal Growth*, vol. 290, no. 2, p. 479, **2006**.

[7] R. B. Campbell, J. M. Robertson, and J. Trotter, "The crystal and molecular structure of pentacene," *Acta Crysta.*, vol. 14, no. 7, p. 705, **1961**.

[8] R. B. Campbell, J. M. Robertson, and J. Trotter, "The crystal structure of hexacene, and a revision of the crystallographic data for tetracene," *Acta Crysta.*, vol. 15, no. 3, p. 289, **1962**.

[9] A. C. Dürr, N. Koch, M. Kelsch, A. Rühm, J. Ghijsen, R. L. Johnson, J.-J. Pireaux, J. Schwartz, F. Schreiber, H. Dosch, and A. Kahn, "Interplay between morphology, structure, and electronic properties at diindenoperylene-gold interfaces," *Phys. Rev. B*, vol. 68, no. 11, p. 115428, **2003**.

[10] R. Mason, "The crystallography of anthracene at 95°K and 290°K," *Acta Crysta.*, vol. 17, no. 5, p. 547, **1964**.

[11] P. A. Heiney, J. E. Fischer, A. R. McGhie, W. J. Romanow, A. M. Denenstein, J. P. McCauley Jr., A. B. Smith, and D. E. Cox, "Orientational ordering transition in solid C_{60}," *Phys. Rev. Lett.*, vol. 66, no. 22, p. 2911, **1991**.

[12] A. C. Dürr, F. Schreiber, M. Münch, N. Karl, B. Krause, V. Kruppa, and H. Dosch, "High structural order in thin films of the organic semiconductor diindenoperylene," *Appl. Phys. Lett.*, vol. 81, no. 12, p. 2276, **2002**.

[13] J. E. Northrup, M. L. Tiago, and S. G. Louie, "Surface energetics and growth of pentacene," *Phys. Rev. B*, vol. 66, no. 12, p. 121404, **2002**.

[14] S. Verlaak, S. Steudel, P. Heremans, D. Janssen, and M. S. Deleuze, "Nucleation of organic semiconductors on inert substrates," *Phys. Rev. B*, vol. 68, no. 19, p. 195409, **2003**.

[15] D. Nabok, P. Puschnig, and C. Ambrosch-Draxl, "Cohesive and surface energies of π-conjugated organic molecular crystals: A first-principles study," *Phys. Rev. B*, vol. 77, no. 24, p. 245316, **2008**.

[16] J. H. Seo, D. S. Park, S. W. Cho, C. Y. Kim, W. C. Jang, C. N. Whang, K.-H. Yoo, G. S. Chang, T. Pedersen, A. Moewes, K. H. Chae, and S. J. Cho, "Buffer layer effect on the structural and electrical properties of rubrene-based organic thin-film transistors," *Appl. Phys. Lett.*, vol. 89, no. 16, p. 163505, **2006**.

[17] M. Haemori, J. Yamaguchi, S. Yaginuma, K. Itaka, and H. Koinuma, "Fabrication of highly oriented rubrene thin films by the use of atomically finished substrate and pentacene buffer layer," *Jpn. J. Appl. Phys.*, vol. 44, no. 6A, p. 3740, **2005**.

[18] S. Guha, W. Graupner, R. Resel, M. Chandrasekhar, H. R. Chandrasekhar, R. Glaser, and G. Leising, "Planarity of *para*-hexaphenyl," *Phys. Rev. Lett.*, vol. 82, no. 18, p. 3625, **1999**.

[19] A. S. Paraskar, A. R. Reddy, A. Patra, Y. H. Wijsboom, O. Gidron, L. J. W. Shimon, G. Leitus, and M. Bendikov, "Rubrenes: Planar and twisted," *Chem. Eur. J.*, vol. 14, no. 34, p. 10639, **2008**.

[20] R. Cantrell and P. Clancy, "A computational study of surface diffusion of C_{60} on pentacene," *Surface Science*, vol. 602, no. 22, p. 3499, **2008**.

[21] H. Liu, Z. Lin, L. V. Zhigilei, and P. Reinke, "Fractal structures in fullerene layers: Simulation of the growth process," *J. Phys. Chem. C*, vol. 112, no. 12, p. 4687, **2008**.

[22] P. Sullivan and T. Jones, "Pentacene/fullerene (C_{60}) heterojunction solar cells: Device performance and degradation mechanisms," *Organic Electronics*, vol. 9, no. 5, p. 656, **2008**.

[23] A. M. C. Ng, A. B. Djurisic, W.-K. Chan, and J.-M. Nunzi, “Near infrared emission in rubrene:fullerene heterojunction devices,” *Chem. Phys. Lett.*, vol. 474, no. 1-3, p. 141, **2009**.

[24] S. Yoo, W. J. P. Jr., B. Domercq, S.-H. Han, T.-D. Li, S. C. Jones, R. Szoszkiewicz, D. Levi, E. Riedo, S. R. Marder, and B. Kippelen, “Analysis of improved photovoltaic properties of pentacene/C_{60} organic solar cells: Effects of exciton blocking layer thickness and thermal annealing,” *Solid-State Electronics*, vol. 51, no. 10, p. 1367, **2007**. Special Issue: Papers Selected from the NGC2007 Conference.

CHAPTER 5

MOLECULAR–SCALE EVENTS IN HYPERTHERMAL DEPOSITION OF ORGANIC SEMICONDUCTORS FROM EXPERIMENT AND MOLECULAR SIMULATION

5.1 Introduction

This chapter examines one possible way of overcoming the Ehrlich–Schwöebel barrier for the archetypal small organic molecule, pentacene. We examine here the dynamics of adsorption of pentacene using Molecular Dynamics simulations and compare the results to experimental sticking coefficients provided by Professor James R. Engstrom and his students. As mentioned in Chapter 1, examination of the growth of pentacene using energetic sources that create far–from–equilibrium conditions has recently attracted interest as a way to modulate the structure and morphology of the deposited thin films [1, 2, 3, 4, 5] to a more desirable 2D fashion. We continue this investigation by studying additional, more detailed, aspects of the hyperthermal collision such as the molecular orientation of the molecule as it strikes the surface. The fundamental questions that we seek to address here are: What mechanisms contribute to growth and how do they depend on controllable variables such as the incident kinetic energy and the angle of incidence?

5.1.1 Background

Pentacene is the subject of intense current scrutiny for research into organic semiconductors due to its relatively low cost and electrical properties rivalling those of amorphous silicon [6, 7]. Pentacene is of potential use in devices used to create solar cells

and in flexible display technologies. However, the production of devices exhibiting single crystal electrical properties has proven challenging. The deposition of small organic molecules is notoriously sensitive to many variables such as deposition rate [8], temperature [9, 10] and the nature of the substrate [11]. There is considerable interest in controlling the growth modes of pentacene [12, 13] because of its tendency to form undesirable 3-D structures that adversely affect device performance. A number of approaches have been utilized to increase the molecular ordering within the film and promote 2D morphologies such as post–fabrication annealing [14, 15] or exploration of soluble derivatives [16, 17] for use in spin coating. However, one of the most successful methods has been to deposit molecules hyperthermally by accelerating the incident molecules, using an inert carrier gas, to kinetic energies of the order of a few eV. This technique has been used extensively on atomic/ionic substances, such as copper [18] and silicon [19], and over a large range of incident energies on the order of 100 eV, but only recently for organic molecules [20].

When considering the variables involved in hyperthermal deposition, the geometry of the pentacene molecule provides a rich phase space, immediately bringing orientational and rotational aspects into the equation. The molecular level processes which define the final morphology of the film are still little understood, but local annealing, direct insertions and increased molecular mobility are thought to play a role. Casalis *et al.* [5] attributed the hyperthermal growth of better quality pentacene films on Ag(111) at low substrate temperatures (200K) to the local annealing triggered by the collision of the incident molecule with the surface and observed a decreasing quality of film as the substrate temperature was increased. Killampalli *et al.* [2, 1] studied the nucleation of pentacene on inert silicon dioxide based substrates and postulated the existence of insertion events or an increased inter–layer transport efficiency at higher energies. They found a critical nucleus size of four molecules. The same system was also studied by

Wu *et al.* [4] who found a smaller critical nucleus size of 2–3 molecules, depending on the incident energy. They stated that quite different growth modes can be achieved using a much reduced deposition rate. Their study attributed the 2D structure observed in the sub–monolayer film to the increased diffusive length of a high energy incident molecule landing on the 2nd layer enabling it to retain enough kinetic energy to overcome a Ehrlich–Schwöebel barrier at the step–edge and join the sub–monolayer. Toccoli *et al.* [3] characterized field effect transistors fabricated from hyperthermally deposited films on silicon dioxide and found an linear increase of field effect mobilities with incident energies up to 6.5 eV together with improved film quality. Despite this considerable experimental scrutiny, a clear picture of the molecular processes that are thought to govern the observed rich variety of behaviour remains elusive. This situation provides some impetus for a computational approach that can tease apart the various processes at play in a more controlled manner than is possible experimentally.

Modelling energetic beam deposition and growth in a molecular simulation offers insight that is difficult, if not impossible, to obtain experimentally. Jacobsen *et al.* [21, 22] developed a computational approach to model the energetic beam deposition of Cu on Cu by incorporating Molecular Dynamics simulations (for the collision) into a Kinetic Monte Carlo framework (describing the diffusion events). Unfortunately the computational complexity of this hybrid approach limited it, in practice, to the deposition of only 1–2 layers of growth of an atomic species in a tractable length of simulated time. For small organic molecules, the additional complications arising from the size and anisotropy of the molecules render this method computationally prohibitive. The local effects of the collision are typically on the order of ps, whereas thermal diffusion is a continuous process occurring over the lifetime of the film. In effect, deposition events are instantaneously altering the initial configuration for which longer–term processes are taking place, but **not** altering their intrinsic rates due to rapid thermal equilibration.

5.2 Sticking coefficients: comparison to experimental data

All of the following experimental data were collected by the group led by Professor J. R. Engstrom at Cornell University [23]. These data have been published in previous articles [2, 24]. What follows is a brief summary of the experimental technique they used in order to allow comparison with the simulation data and to provide a brief overview of the results and their relevance. For a more detailed and comprehensive explanation of the experimental techniques and analysis, please refer to the previously published articles.

5.2.1 Explanation of experimental data

N_2 was used as a carrier gas to produce beams where the mean kinetic energy of pentacene lies in the range, E_i = 1.5–6.7 eV. In comparison, the two–body interaction potential between two pentacene molecules has a well depth of only 0.6 eV [25]. The angle of incidence of the depositing molecules was varied from θ_i = 0–75°, measured from the surface normal. The high incident beam to background flux ratio (> 10^3) facilitates experiments where multiple exposures can be produced on a single substrate by simply translating the sample. In the sub–monolayer regime, the coverage was assessed using *ex situ* atomic force microscopy. In the multilayer regime *ex situ* ellipsometry was used.

5.2.2 Experimental sticking

Figure 5.1 (a) shows the relative probabilities of adsorption measured for pentacene incident on clean SiO_2 as a function of the incident kinetic energy for three different angles

of incidence. The probability has been normalized to the highest growth rate observed for these conditions, while the incident flux was kept constant (including compensating for the change in the angle of incidence) to ± 5%. As expected for a process that involves dissipation of incident kinetic energy, at all angles, the probability of adsorption decreases with increasing incident kinetic energy. Of course, for these incident kinetic energies, the only processes available to the incident molecules involve momentum exchange with the surface atoms, and excitation of internal degrees of freedom— penetration or electronic excitation of the lattice can be ruled out. As described elsewhere [2], these data can be scaled using a function that weighs both perpendicular and parallel momentum nearly equally, suggesting a rather complex gas–surface interaction.

Figure 5.1 (b) shows the relative probability of adsorption for pentacene on a pentacene substrate, as deduced by thickness (D) versus exposure time (t) data obtained from *ex situ* ellipsometry. Here, the data have been fitted to a quadratic and the minimum thickness in the fit was always greater than 2 monolayers (in most cases, the probability is an average over the coverage range 2 ML < D < 10 ML). Again, the probability has been normalized to the highest growth rate observed for these conditions, while the incident flux was kept constant. Interestingly, for both sub–monolayer and multilayer growth rates at E_i = 1.5 eV and $\theta_i = 0^\circ$ or 45°, we observe the same absolute growth rate within ± 5%. This observation would seem to suggest that, even at this incident energy, the absolute probability of adsorption is near unity. In this multilayer regime, the probability of adsorption also decreases with incident kinetic energy for all angles of incidence, but it decreases much less rapidly. For many conditions the adsorption probability of pentacene on pentacene is greater than that for pentacene on SiO_2, consistent with better mass–matching conditions for the former. However, attempts to use energy scaling arguments for these data were quite unsuccessful, suggesting that in addition to simple momentum exchange and trapping that new mechanisms may be

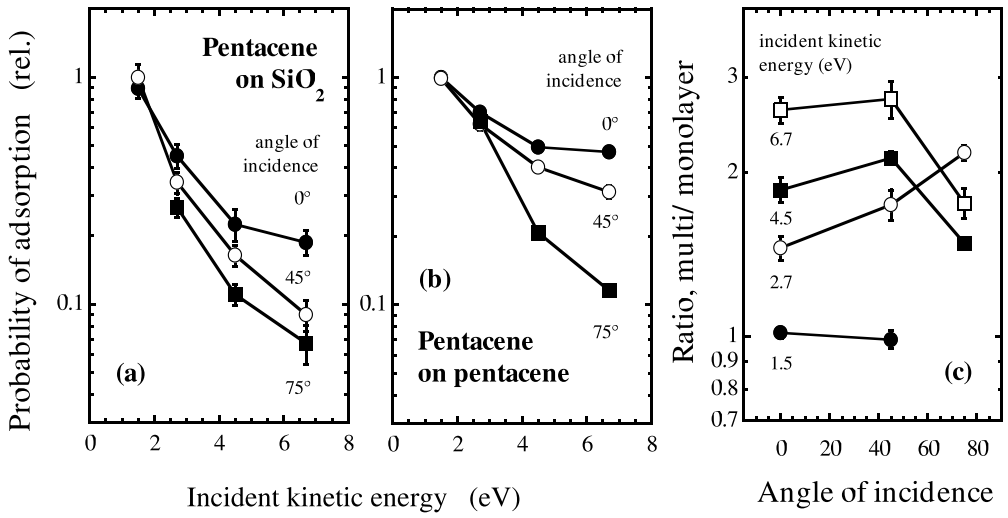

Figure 5.1: The relative probability of adsorption of pentacene in (a) the sub–monolayer and (b) multilayers as a function of incident kinetic energy, E_i, for three values of θ_i. (c) The ratio of adsorption of multilayer to monolayer adsorption.

involved for pentacene interacting with pentacene thin films.

In Figure 5.1 (c) the ratio of the adsorption probability observed in the multilayer regime to that observed for the monolayer regime is plotted. Here the data are plotted as a function of the angle of incidence and fixed incident kinetic energy. As indicated above, at the lowest incident kinetic energy examined here, there is no difference between the probability of adsorption on the two surfaces, and the ratio is unity. Interestingly, at a fixed angle of incidence, except for one case (E_i = 2.7 eV, $\theta_i = 75^\circ$), this ratio grows with increasing incident kinetic energy. At fixed incident energy, again excepting the one datum, the ratio is about constant as θ_i increases from 0° to 45°, and then decreases as it increases to $\theta_i = 75^\circ$. These data are most reminiscent of a direct activated process (such as dissociative adsorption [26]), where the probability increases with increasing incident kinetic energy and decreases with increasing angle of incidence.

5.3 Simulation methodology

To illuminate the possible mechanisms and molecular–level processes involved in hyperthermal deposition, we explore the short–term collisions of a single pentacene molecule with a pentacene surface. We used the non–reactive empirical MM3 potential [27, 28, 29] to model the collision of pentacene molecules in the proximity of a pentacene (010) step–edge using Molecular Dynamics. The system shown in Figure 5.2 involved 6,948 atoms, consisting of 121 molecules that were free to move under the influence of the intermolecular forces and a bottom layer of 72 molecules (6×6 unit cells) fixed in pentacene's 'bulk phase'. The system was thermalised at 300 K for 100 ps, except for the incident molecule. The incident molecule was cooled rotationally and vibrationally to 0 K before being directed at the surface with an incident energy E_i. The

time evolution of the system is governed by the Beeman algorithm using the TINKER software package. Each simulation was run for 10 ps; this time–frame was generally found to be sufficient for the molecular collision to occur and the system to thermalise. Longer runs were made in the rarer cases where thermalisation required more time.

All collisions between the single incident molecule and the surface were performed in the NVE ensemble to avoid any complications due to the velocity corrections used to scale the temperature to a desired value. This approach was validated through our observations that the incident energy dissipated rapidly amongst the internal energy of the molecules and not raise the system temperature more than 5 K, even transiently (Figure 5.3). To justify freezing the bottom layer and thus creating a large temperature gradient in the system, pairs of simulations were examined where, in one case, the bottom layer was free to move and, in the other, fixed. A comparison of these two cases led to no significant difference in the general behaviour of system (allowing for deterministic differences due to the different degrees of freedom). The distance between collision point and the plane of the fixed atoms was approximately 30 Å which was enough to allow an efficient dissipation of the incident kinetic energy to other molecules in the system through lateral interactions. The bottom layer, when allowed to move, was found to interact very weakly with the layer above and maintained its lateral integrity throughout, resisting any great deformation in the x-y plane. This was due to the strong **intra**–layer bonding relative to the **inter**–layer bonding, as predicted by surface energy calculations [30]. Single molecules in the bottom layer were displaced vertically from their neighbours by no more than 2 Å.

The [010] direction of the step–edge was chosen for these studies since it has been predicted by DFT and force field methods to be relatively stable [31, 32, 30, 33], and this has been reinforced by experimental evidence pointing towards its prevalence during the

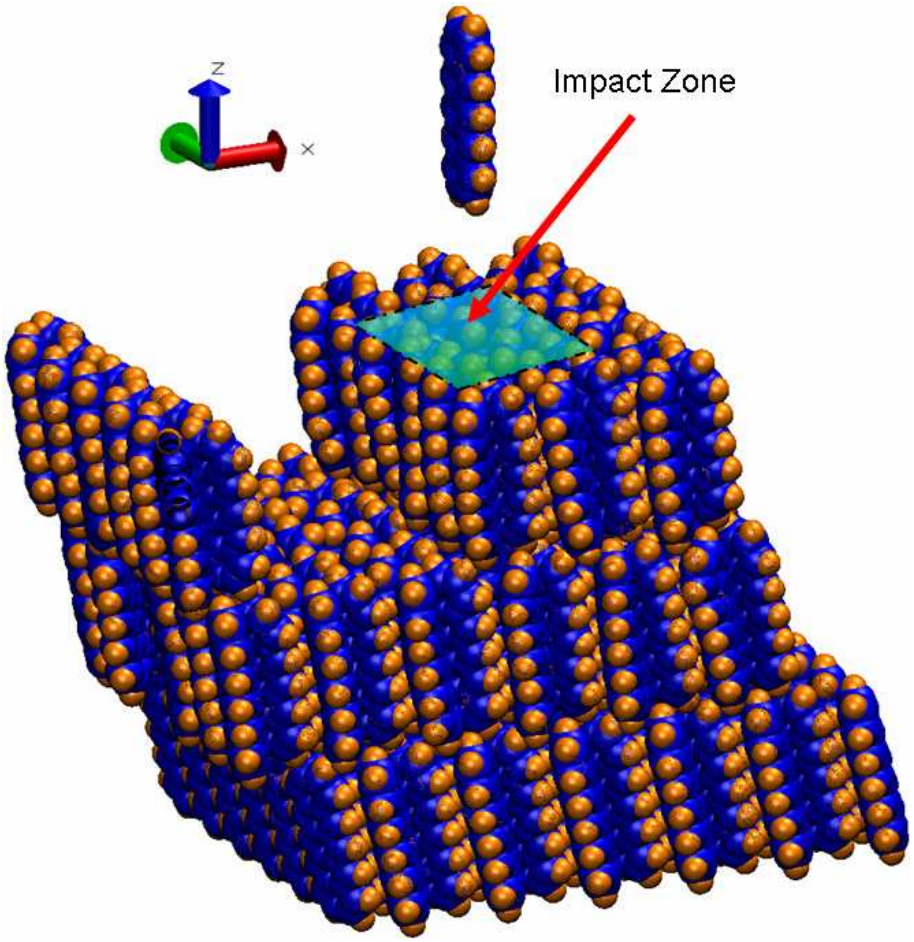

Figure 5.2: Schematic of the simulated system. Bottom layer fixed in the bulk phase configuration with all other molecules free to move. All collisions occur within the 'impact zone' marked on the figure. Periodic boundary conditions are imposed in the x-y plane and are 'infinite' in the z direction.

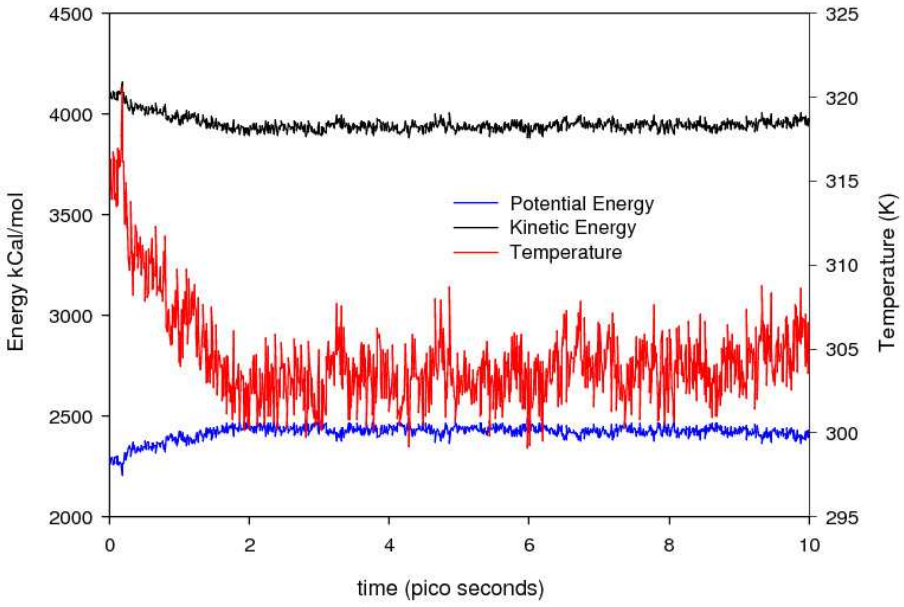

Figure 5.3: Evolution of the kinetic and potential energies and the temperature for a typical simulation over the course of 10 ps and an incident energy, E_i = 10 eV.

growth of thin films of crystalline pentacene [30]. In this work, the lattice parameters [a, b, c] were [6.06 Å, 7.9 Å, unrestricted] meaning that the (010) step–edge was parallel to the short lattice parameter in the x-y plane.

The MM3 potential was used because it is known to accurately model organic molecules, including pentacene [32] in both crystalline and gaseous forms and also has a large degree of transferability. Intermolecular interactions in the MM3 model consist of dipole–dipole and van der Waals (vdW) forces, and constraints for the internal structure of the molecules are applied using 'mechanical' terms such as bond stretching and bending, torsional, and out of plane bending contributions. A recent development in the MM3 potential included a Möller–Plesset 2nd–order Self Consistent Field correction for conjugated π systems (resulting in a slightly larger equilibrium C=C bond length). In practice, the computational penalty of this correction has limited its use to systems containing 50 atoms or less. The π correction has little effect on the intermolecular interactions (the only intermolecular interactions implemented in the potential are vdW and dipole–dipole interactions) and no noticeable difference was observed in the outcome due to its inclusion in test collisions. Verlaak *et al.* [32] developed a parameterisation that works well for relaxed molecular crystals but is untested for dynamic situations. We have also compared the MM3 potential to *ab initio* methods for intermolecular interactions of acenes (members of the same homologous series as pentacene). MM3 was found to predict similar energies to the much more computationally expensive MP2/6-31g(d) but to run orders of magnitude faster in simulation time. The cohesive energy of the crystal (1.3 eV) and surface energies predicted by Northrup *et al.* [31] using DFT methods were found to match, within a few percent, with our results using the MM3 potential. The distinctive herringbone structure is also accurately predicted, with unit cell axes in good agreement with experimental values. Despite the incident energy of the molecule being hyperthermal, these energies are not considered high enough to cause

errors in the short–ranged vdW repulsive term.

The TINKER software package was used to carry out the collisions and subsequent Molecular Dynamics simulations using the MM3 potential. VMD[34] was used to visualize the trajectories.

5.3.1 Results: Simulation of hyperthermal collisions

Adsorption can occur in one of two major locations on the surface, on terraces or at, or near, step–edges. Accordingly, the simulations considered both situations: two collision points were chosen, one on the step–edge and one 11 Å away from the step–edge, representative of collisions on a terrace. At each collision point, we varied the angle of incidence of the randomly oriented incoming molecule (θ_i = 0°, 30°, 45°, 60° from the surface normal) and its energy of incidence (E_i = thermal to 10 eV). At each angle, energy and position, at least 25 trajectories were simulated, resulting in a very large number (850 simulations) in which the behaviour of the system was documented. Given that Molecular Dynamics is a deterministic tool, this large number of "computer experiments" covers a wide range of typical energetic fluctuations in the nature of the surface.

In Figure 5.4, we plot the absolute probability of adsorption as a function of the incident kinetic energy for a pentacene molecule incident on (a) a terrace and (b) a step for three angles of incidence. To facilitate comparison to experiment, the ordinates are identical to those of Figure 5.1, whereas the abscissa are somewhat enlarged to account for the larger range of energies examined in simulation. Only those trajectories that lead to a net increase by one of the number of molecules representing the surface were counted as adsorption events (*vide infra*). As may be seen, there are strong similarities between the results from simulation and experiment. First, consistent with the experi-

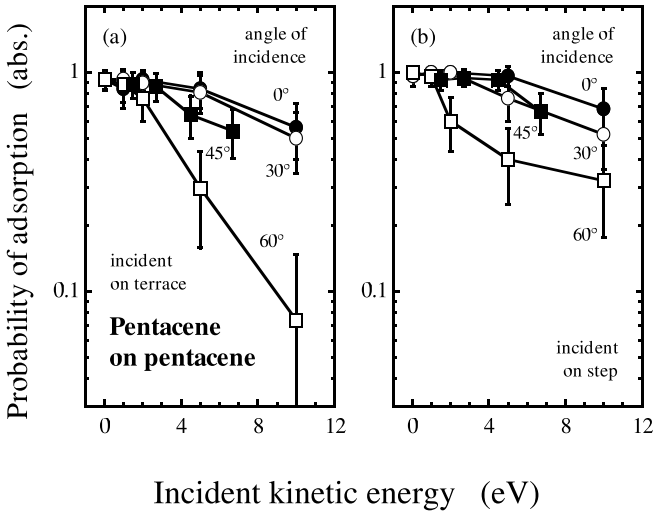

Figure 5.4: The probability of adsorption of pentacene on a pentacene surface obtained from Molecular Dynamics simulations on (a) the terrace and (b) the step–edge as a function of incident kinetic energy, E_i, for four values of θ_i. Error bars denote 90% confidence intervals calculated by the Adjusted Wald Method.

mental results for pentacene on pentacene [Figure 5.1(b)], incoming molecules incident at the two angles closest to the surface normal exhibit a gradual decrease in the probability of adsorption with increasing incident kinetic energy. Experimental results at E_i = 6.7 eV give the probability of adsorption to be 0.47 (at 0°) and 0.31 (at 45°). Similarly, simulation results at the somewhat higher value of E_i = 10 eV give the probability of adsorption to be 0.56–0.68 (0°) and 0.50–0.52 (30°). Since experimental and simulation results can often differ by orders of magnitude, this similarity is striking. In addition, the simulation results support the experimental claim that the absolute probability of adsorption at E_i = 1.5 eV and θ_i = 0° and 45° is nearly unity. Perhaps the most interesting observation is the growing deviation between the data sets for glancing incidence and that nearly normal to the surface at high incident kinetic energies: Experimental studies at E_i = 4.5 eV show a decrease by a factor of 1.2 and then by a factor of 1.9 as θ_i increases from 0° to 45° and then 45° to 75°. Simulation results for impacts on terrace site, at the same incident energy, E_i = 5 eV, decrease by a factor of 1.04, and then 2.7 as θ_i increases from 0° to 30°, and then 30° to 60°. Similarly, agreement occurs at a higher incident energy of 6.7eV where experimental results decrease by factors of 1.5 and 2.7 as θ_i increases from 0° to 45° and then 45° to 75°, and simulation results decrease by factors of 1.12 and 6.7 as θ_i increases from 0° to 30°, and then 30° to 60°. When comparing simulation and experiment, it is important to realize that simulation shows that the impact site (terrace or step–edge) plays a role in adsorption probability. For instance, simulated impacts on the step–edge produces a drop in adsorption with more glancing angles of incidence and at high energy, but it is less dramatic than on the terrace, particularly at the highest energies studied here, E_i= 10 eV. These differences in adsorption probability between terrace and step–edge can be attributed, in part, to the increased exposure of the face of the step at acute values of θ_i during the experiments. The simulations do not account for such events, though one could imagine a different

behaviour if the collision point was at the bottom of a step–edge.

We have harnessed the power of molecular simulation to consider discrete trajectories, not just ensemble averages. This allowed us to calculate the fraction of molecules having a given fate (adsorbed, scattered, *etc.*) Molecules that adsorb, for instance, can be subdivided depending on where they end up in the crystal, namely (i) on top of the topmost layer (where they prefer to lay flat to maximize the weak van der Waals interaction), (ii) in, or part of, the topmost layer that forms the upper step, and (iii) in the layer below, which forms the lower terrace. Molecules that scatter can be divided between those that (iv) interact only with the surface or those that (v) penetrate the surface before exiting. Here 'penetration' is defined by trajectories where the centre of mass has penetrated below the (001) surface plane. Figure 5.5 shows example trajectories of all five possibilities.

In Figure 5.6, we plot the probability of the five outcomes as a function of incident kinetic energy, and the results are placed in six groups representing the three angles of incidence and the two impact points (step and terrace) that we considered. Results for impacts on the terrace site for molecules incident along the surface normal show that insertion into the topmost layer appears for energies as low as 1 eV, and becomes an increasingly important pathway to adsorption as E_i increases. This corresponds to an increase in direct insertion events, as opposed to molecules falling over the step–edge. Indeed, at 10 eV, we see that the second layer below the surface has been penetrated and occupied, and that only 20% of the molecules that have been adsorbed are lying on the topmost surface. For these same conditions, the outcomes change considerably for impact on the step–edge: At modest incident energies (1–2 eV), most of the molecules have been incorporated into the first layer. There are two factors likely contribute to this change: First, due to fewer nearest neighbours for molecules at the step, they are

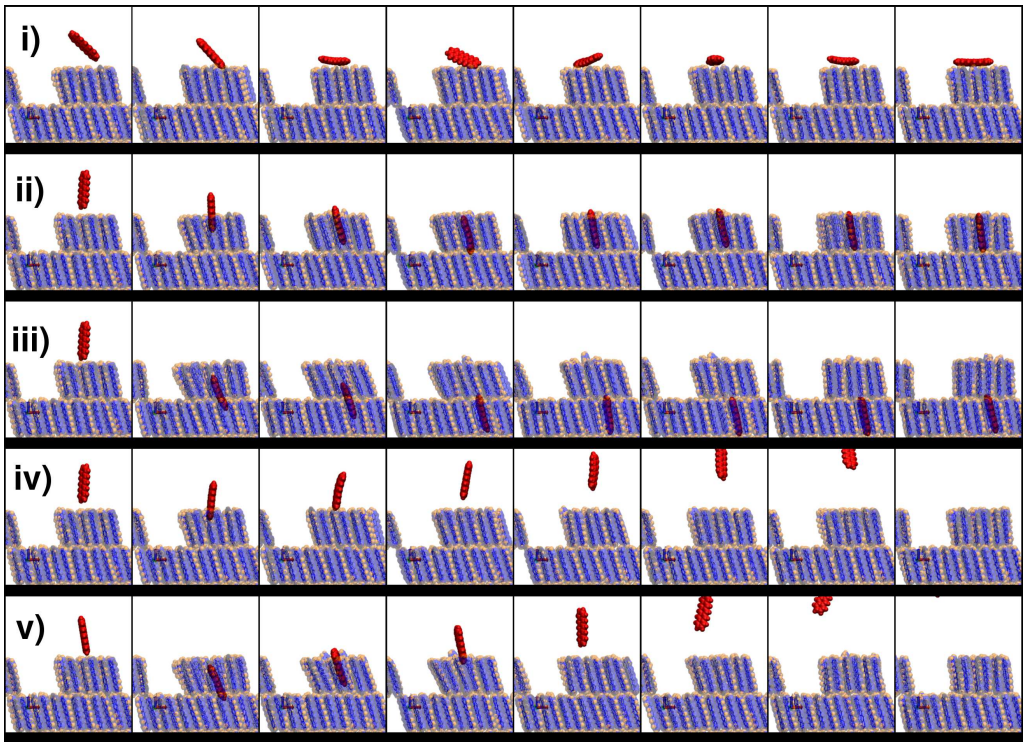

Figure 5.5: Example trajectories and outcomes of an incident pentacene molecule (shown in red) on a pentacene surface (i) to lie on top of the topmost layer, (ii) insertion into the topmost layer that forms the upper step, and (iii) insertion into the lower terrace. Molecules can also scatter by (iv) interacting only with the surface layer and those (v) that penetrate the surface before exiting. All trajectories comprise snapshots taken every 1.4 ps looking down the step–edge. Here $\theta_i = 0^\circ$ for all cases and E_i = (i) thermal, (ii) 2 eV, (iii) 10 eV, (iv) 1 eV, (v) 10 eV

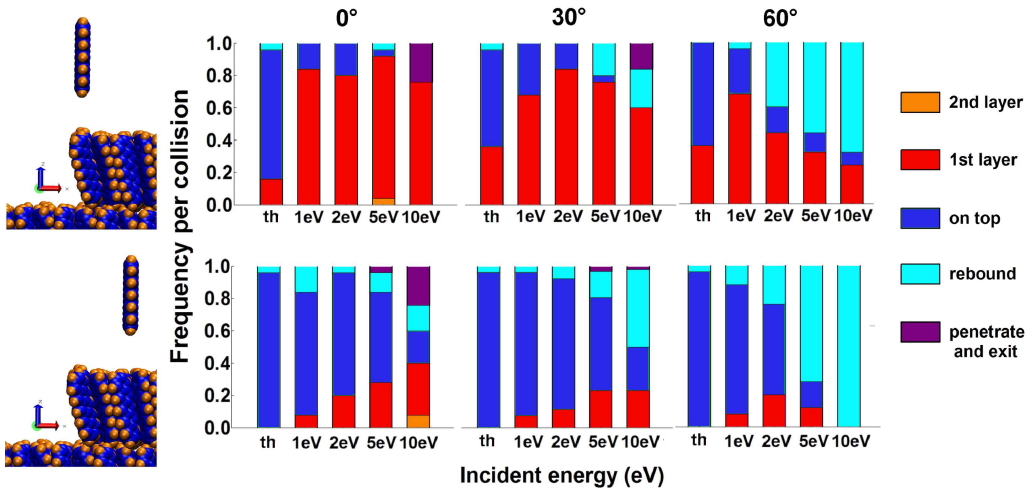

Figure 5.6: Destination of the incident molecule as a function of incident kinetic energy and at three incident angles (θ_i = 0°, 30°, 60 °) for collisions at the step edge (top row) and on the terrace (bottom row)as indicated by the schematic on the left hand side. The colour key for the outcome of a deposition event is shown on the right hand side.

more easily displaced by the incident molecule, leading to more direct insertions into the topmost layer. Second, impacts near the step–edge also lead to collisions where the impacting molecule is deflected towards the terrace below, in a process akin to 'downward funnelling' [35]. The disruption caused to the step–edge by the incident molecule made the distinction between these two mechanisms often unclear, yet both were observed.

As we move away from normal incidence, we observed important changes in the outcomes. On terrace sites, the changes are most significant at incident kinetic energies of 5 and 10 eV. At these high energies and the most glancing angle, we see that the adsorption probability has decreased significantly. More importantly, the fraction of molecules that exit without penetrating the surface has increased greatly as θ_i increases from 0° to 60°. The reasons for this are probably associated with the anisotropy of the (001) surface and the fact that penetration is easier from molecules incident along the surface normal, particularly for molecules whose long axis is also along this same direction which we will discuss in Section 5.3.2. Another factor is that collisions at increased angles of incidence tend to be more glancing (due to self–shadowing of nearest neighbours), representing larger impact parameters. Such collisions are less efficient, leading to poor dissipation of the molecule's incident kinetic energy, and hence scattering from the surface. Collisions near the step–edge change this picture rather dramatically. First, the concept of the surface normal at the step–edge is not well defined, and 'head–on' small impact parameter collisions are more likely. In consequence, adsorption is much more probable at glancing angles and high incident kinetic energy. We also see that it is more likely that molecules incident at the step site end up in, or become part of, the topmost layer.

It should be clear from these results that direct insertions of pentacene into existing terraces on the surface of the growing crystal are an important mechanism and help

reconcile the experimental observations made concerning the difference between the dynamics of growth in the monolayer regime and that observed in the multilayer regime (Figure 5.1). Given the lack of a suitably accurate intermolecular potential model for amorphous (Si) oxide material, we did not attempt to simulate adsorption on clean SiO_2. There is no unique periodic surface for amorphous materials to recreate and thus it should be noted that factors such as the role of the substrate (*e.g.*, its effective mass and its stiffness) may contribute to the observed differences. This could be investigated in future simulation studies of model systems.

In any event, our results raise new questions concerning the thin film growth of pentacene and related systems using energetic molecular beams. First, interstitials (Figure 5.7) are formed as a result of insertion; what is their fate? Second, as direct insertion does not lead to the formation of ad–molecules on terraces (which eventually contributes to roughening), can sufficiently high incident kinetic energy promote 2D versus 3D growth? Concerning the first, our preliminary calculations indicate that the interstitials that are formed are stable for at least 5 ns (long for MD simulations of these complex systems). But, since this time scale differs from the characteristic time scale of film growth by a factor of 10^{10}, the long–term stability of these defects remains an open question.

Concerning the second, the most direct answer comes from an experimental determination of the evolution of surface roughness as a function of incident kinetic energy. There are reports in the literature of spectacular changes that occur as the incident kinetic energy of pentacene is increased above ~5 eV. These reported changes with E_i (angle of incidence was not examined) include those in surface morphology [3], and electronic properties of the deposited layers [3], and even the size of the critical nucleus [4]. The authors of these works cite a “sort of local annealing” as being responsible for these

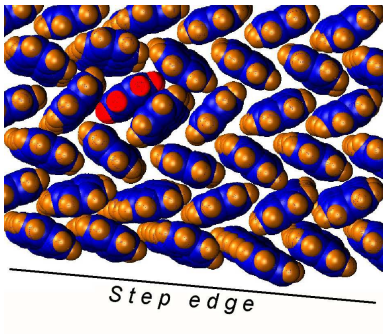

Figure 5.7: Interstitial formed after an incident molecule (shown with red hydrogen atoms) has inserted itself into a terrace.

effects. More strikingly, there is an abrupt change in the properties of the film at a critical incident energy: changing E_i from 5.5 to 6.5 eV [3] or from 5.0 to 6.4 eV [4] are apparently sufficient to produce these effects. Such a dramatic leap in properties with incident kinetic energy is difficult to understand. Indeed, our molecular simulation results (Figures 5.4 and 5.6) show no such abrupt transitions, nor the sudden appearance of new mechanisms with increasing E_i. For example, at normal incidence and on the terrace, the fraction of molecules that incorporate into the first layer increases smoothly as E_i is increased from 1 to 10 eV. Ideally, this issue may be resolved by a study (using experiment and simulation) of the evolution of surface roughness with thickness as a function of incident kinetic energy. Experimentally, in preliminary studies using *ex situ* AFM only modest changes in the evolution of surface roughness were found as E_i is varied from 1.5 to 6.7 eV [36]. These *ex situ* measurements have recently been supported by studies using *in situ* real–time synchrotron x–ray scattering [37].

5.3.2 Effect of angle and orientation on hyperthermal deposition of pentacene

The rotational and vibrational properties of organic molecules in a hyperthermal beam is of current interest to experimentalists. The supersonic expansion of a mixture of benzene molecules and a helium carrier has been shown to produce a rotationally relaxed 'Frisbee–like' flight of the benzene molecules under certain conditions [38], yet how these orientational factors affect the collision is unknown. In the last section we compared experimentally measured sticking probabilities of pentacene on pentacene to those generated from a simulated system of pentacene deposition events on pentacene using Molecular Dynamics. We found that both estimates of the sticking coefficient were very

similar in value. However, no attention was paid to the orientation of the molecule as it hits the surface. Here we investigate the role of molecular orientation when combined with varying incident energies (E_i) and angles (θ_i).

Vertical orientation collisions with velocity normal to the surface ($\theta_i = 0°$).

The collisions of a vertically oriented molecule (as in Figure 5.2) were studied for 25 randomly generated collision points (Fig 5.8) within the target zone. At each point, five incident kinetic energies (E_i = thermal, 1 eV, 2 eV, 5 eV and 10 eV) were supplied to the molecule directed at the surface. The final destinations of the incident molecules were recorded and are shown in Figure 5.9(a) as a function of E_i. A clear difference in behaviour was noticed between the thermal molecules which preferred to dock on top of the step, and hyperthermal molecules where the energetics made other destinations more likely. At hyperthermal energies, fewer than 1 in 10 molecules are left on top of the step due to transfer of molecules downward, or molecules rebounding (*i.e.*, leaving the system through desorption). In cases where the molecule did end up in the first layer (the layer constituting the step), the vast majority of such instances occurred through a direct insertion mechanism leading to interstitial molecule formation. Only for collisions directly on the step–edge were molecules observed to fall off the step and join the layer below by overcoming the Ehrlich–Schwöebel barrier.

In contrast, at high energies such as E_i = 10 eV, a significant proportion of the molecules became inserted into the 2nd layer by "channelling" through the first layer. This occurred increasingly frequently at distances further from the step–edge as the molecules in the vicinity of the collision point were more constrained by the presence of their neighbours and, consequentially, the incident molecule found it harder to move laterally. The maximum frequency of incident molecules leaving the system, a con-

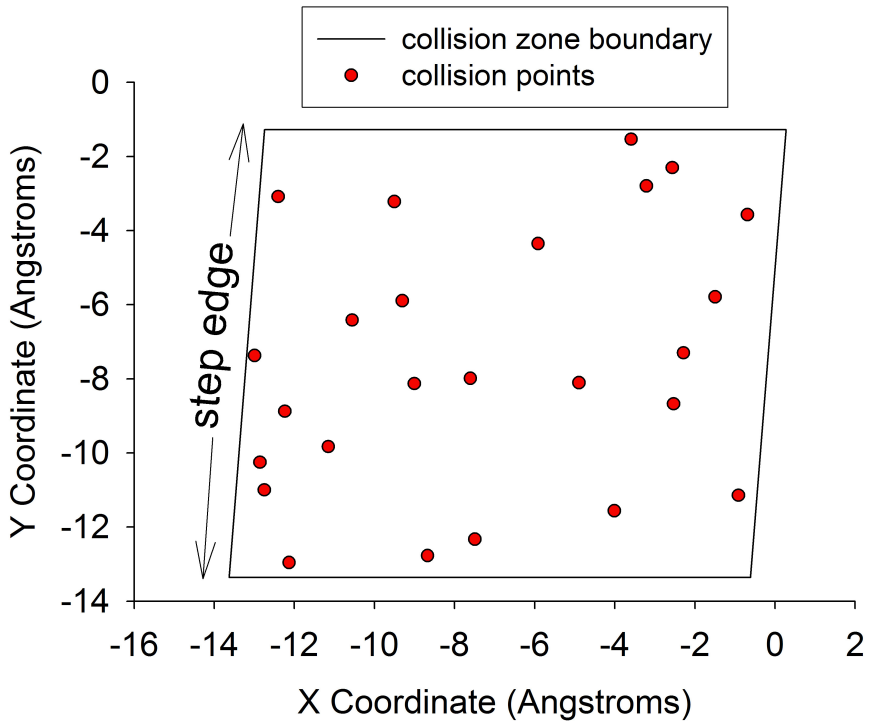

Figure 5.8: Collision points generated within the impact zone (as illustrated in Figure 5.2) for collisions of vertically oriented molecules with the surface.

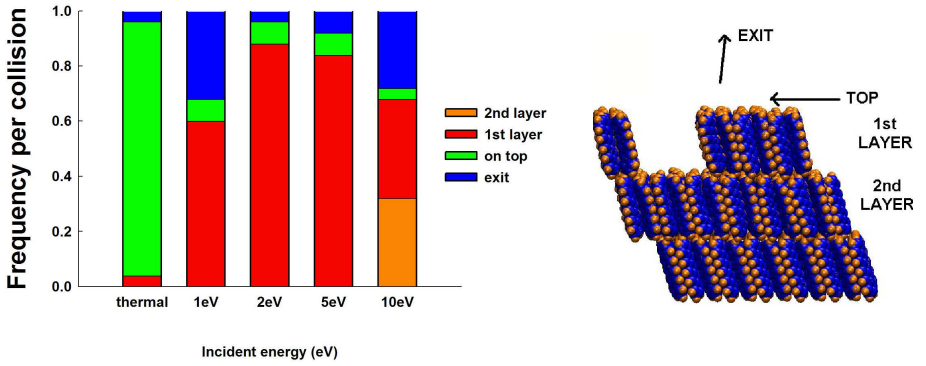

(a) (b)

Figure 5.9: (a) The destination of vertically oriented incident molecules shown as a histogram for all the incident energies studied here; colour key as shown on the right hand side of the histogram. (b) the schematic illustrates possible destinations of the incident molecules.

tributing factor to the experimentally measurable sticking factor, occurred at E_i = 1 eV. The reasons for this were not obvious from Figure 5.9(a) until the exact mechanisms of ejection are examined.

At E_i = thermal, 1 eV and 2 eV, all incident molecules that were ejected from the system did so as a result of rebounding off the top (001) surface of the step, more than 5 Å from the step–edge itself. The further from the step edge at which the collisions occurred, the more stable and therefore the more resistant the surface with respect to penetration. In this work, a "penetration" of the surface is said to occur when the centre of mass of the incoming molecule passes through the (001) surface of the step. None of the molecules had sufficient energy to penetrate the molecular crystal and simply rebounded out of the system. At E_i = 5 eV and 10 eV, **all** of the incident molecules which were subsequently ejected did manage to penetrate the surface. The molecules were then rejected by the molecules in the molecular crystal by rebounding off the layer below and being channelled back up through the crystal structure (essentially "bouncing" off the "mattress" provided by the fixed bottom layer).

Random orientation collisions, velocity normal to surface ($\theta_i = 0°$).

We froze the atomic vibrations and rotational energies of the molecule and altered the orientation of the molecule as it hit the molecular surface. The collisions were carried out on the same impact zone as before but at just three collision points a) on the step–edge, b) 5 Å from the step edge and c) 11 Å from the step–edge. The random orientation of the molecule combined with its large long axis (approx. 14 Å) ensured that the actual point of contact of the molecule with the surface varied even though the centre of mass collision trajectories remained the same. By averaging data over the three collision points, we were able to compare directly to the vertical orientation results. Fig-

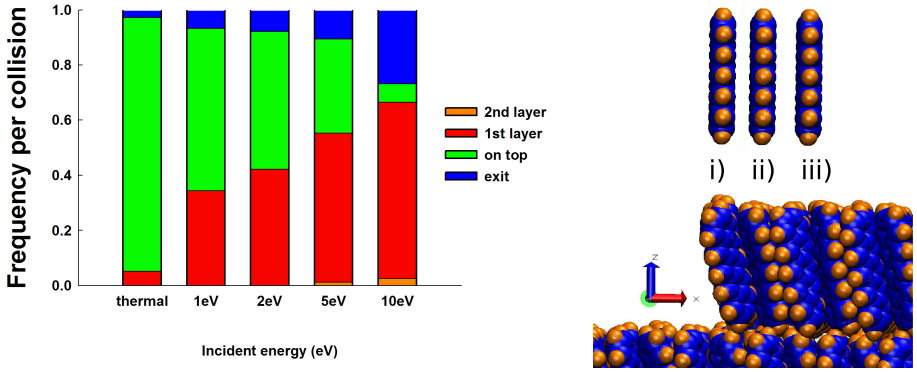

(a) (b)

Figure 5.10: (a) Destination of randomly oriented incident molecules as a histogram for different incident energies; colour key as given on the right hand side of the histogram. (b) Illustration of the three initial positions chosen for the collisions as a function of orientation. The centre of mass is i) on the step–edge, ii) 5 Å and iii) 11 Å from the step–edge. For clarity, the molecules are shown in the vertical position parallel to the step. Twenty five random orientations sharing the same centre of mass are generated for each case.

ure 5.10 shows a quite different dependence on E_i to the vertically oriented case for the destination of the incident molecule. There is a smoother, more gradual transition across energies from the thermal case where, again, almost all molecules remain on top of the step, to the high energy collisions where molecules are ejected from the system or are incorporated into the existing crystal structure by insertion. For E_i = 1 eV collisions, in contrast to that for vertically aligned molecules where ejections were a disproportionately high occurrence, the random orientations reduce the number of ejections at 1 eV to fit within the general trend of an increase of ejections with increasing E_i.

The angles ϕ and φ categorize the orientation of the molecule: ϕ measures the angle from verticality; thus, $\phi = 0^\circ$ represents a vertical molecule. φ is the angle that the molecular plane forms with the surface normal, $\varphi = 90^\circ$ represents a molecule lying parallel to the surface. In Figures 5.11 to 5.16 we plot the occurrence of specific 'events' for all collisions at 'point iii', 11 Å from the step–edge and for all collisions at 'point i', *on* the step–edge, as a function of orientation. The situation was far more varied for collisions 11 Å from the step–edge. Figure 5.11 shows that all the molecules that were able to penetrate the surface occurred where E_i = 2 eV or above and relatively vertical ($\phi \leq 30^\circ$) in orientation or, were displaying a leading edge to the surface ($\varphi \leq 20^\circ$). As the molecules strayed from a vertical orientation, greater incident kinetic energy was needed to penetrate the surface. Figure 5.12 shows a concentration of vertically oriented ($\phi \leq 20^\circ$), E_i = 1 eV molecules being ejected from the system. The same orientations which caused penetrations of the surface for E_i = 2 eV molecules caused the E_i = 1 eV molecules to rebound back out of the system. This can be attributed to the stiffness of the molecule as the momentum is carried along its vertical axis. The molecules did not topple over after hitting the surface and therefore the attractive interactions with the surface were restricted to van der Waals forces between hydrogen atoms. (A simple analogy would be dropping a rigid object such as a pen onto a carpeted floor. When the

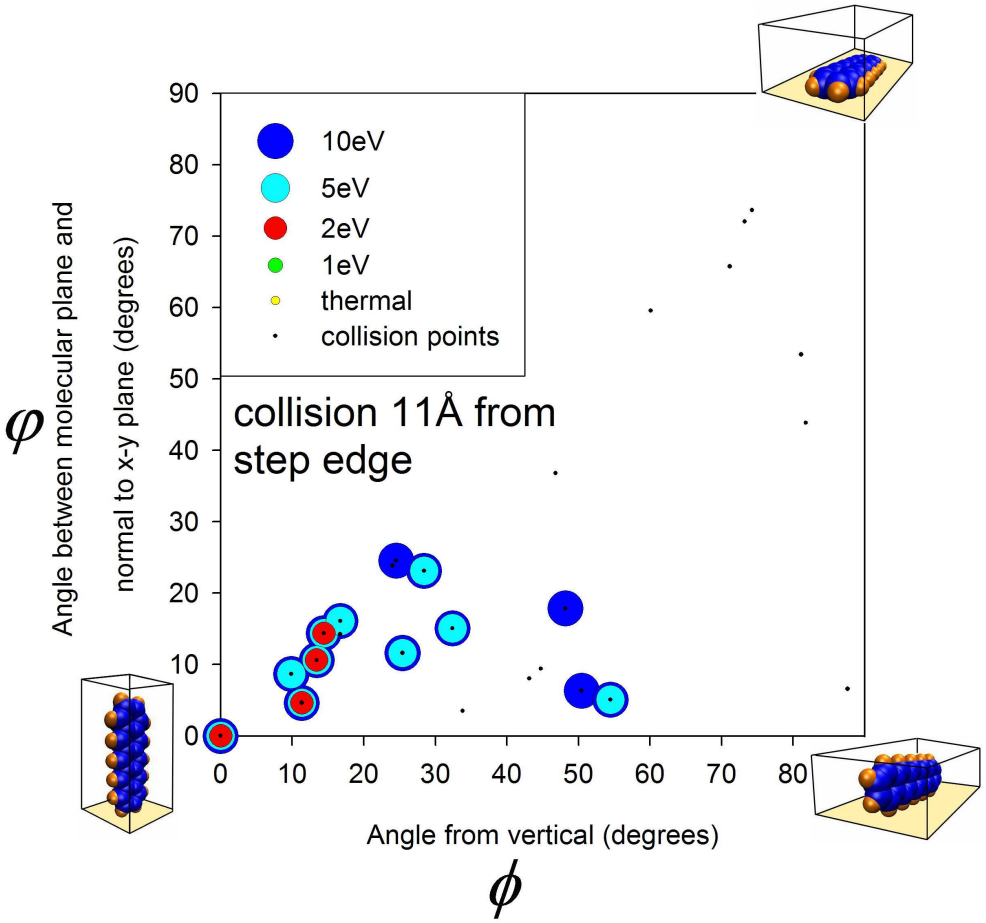

Figure 5.11: Molecules penetrating the (001) terrace as a function of the angles ϕ and φ for collisions 11 Å from step–edge. Cartoons at the vertices represent the orientations representative of the molecule at the respective corners of the graphs: Vertically oriented molecules are found at the origin, horizontally oriented molecules with a leading edge facing the surface at the bottom right, and horizontal molecules with the molecular plane parallel to the surface are shown in the top right hand corner. All collision points are marked for completeness. A successful occurrence of the event is marked by a coloured circle representing the energy of the incident molecule.

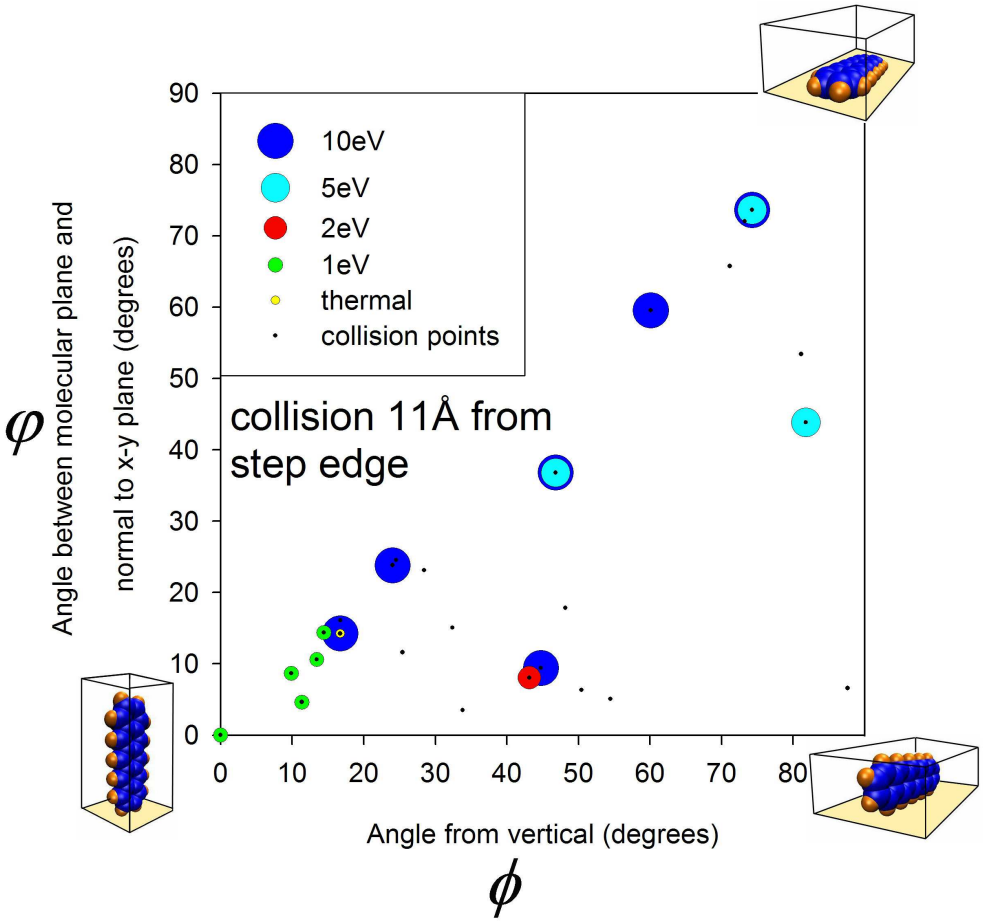

Figure 5.12: Molecules ejected as a function of angles ϕ and φ for collisions 11 Å from the step–edge.

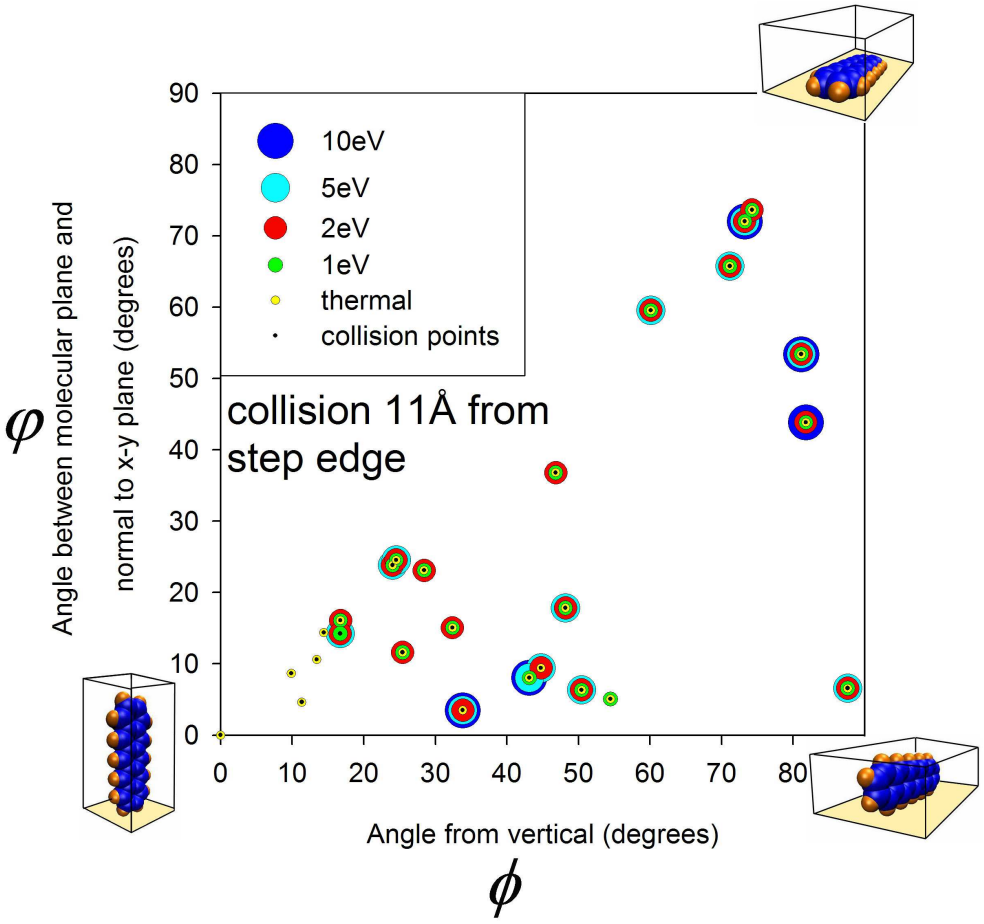

Figure 5.13: Molecules remaining on (001) terrace as a function of angles ϕ and φ for collisions 11 Å from the step–edge.

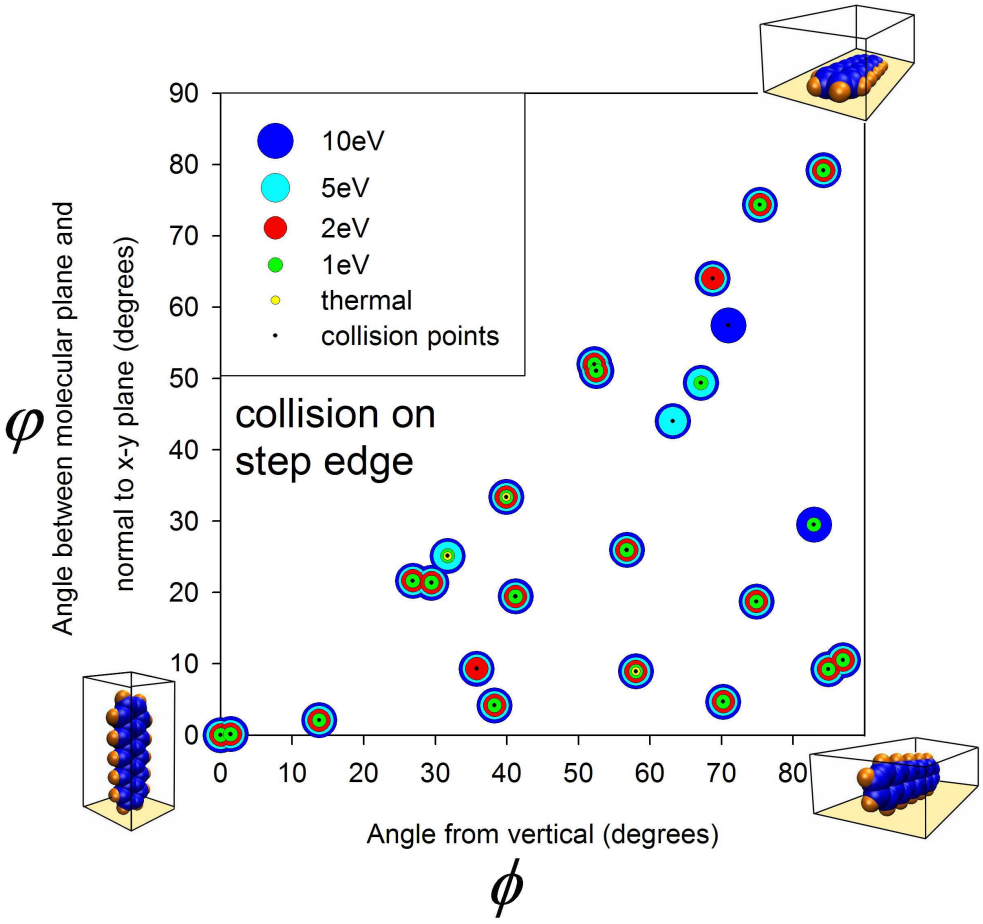

Figure 5.14: Molecules penetrating the (001) terrace as a function of angles ϕ and φ for collisions at the step–edge.

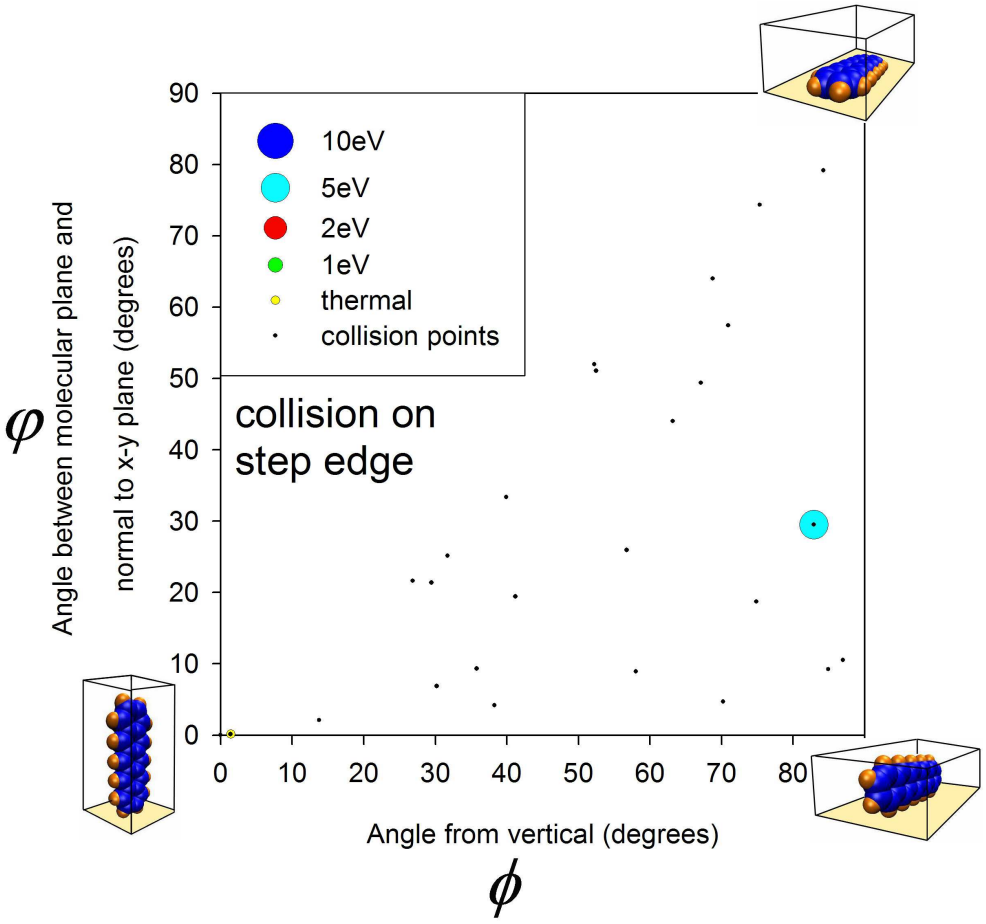

Figure 5.15: Molecules ejected as a function of the angles ϕ and φ for collisions at the step–edge.

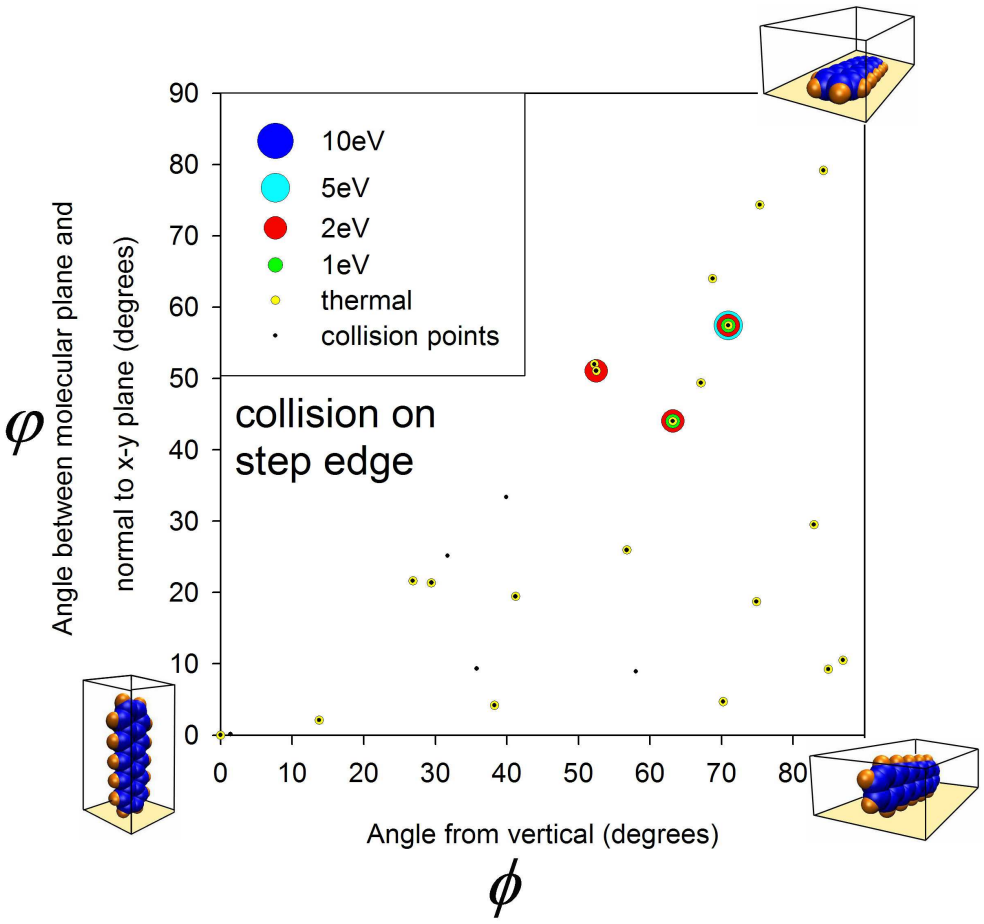

Figure 5.16: Molecules remaining on the (001) terrace as a function of angles ϕ and φ for collisions at the step–edge.

pen is oriented at angles close to normal it bounces off with just the leading end having made contact with the carpet. If the pen is oriented further from normal then the pen falls over during the collision and bounces back only after having had both ends touch the carpet.) If the initial collision could not burrow into the surface then the reactive force dominates and the molecule is forced back off the surface. When the orientation is far enough from normal that the molecule can fall over during the collision, then more of the molecule becomes exposed to the surface attractive forces and the chances of it sticking are increased. Figure 5.13 reinforces the finding that, if molecules are vertically oriented ($\phi \leq 20^\circ$), only molecules of thermal energy will remain on top of the step–edge leading to 3–D growth.

As reported earlier in the chapter, collisions on the step–edge were dominated by molecules penetrating the step –a sort of *downward funnelling* effect of the step–edge. [39, 40] The distinction between direct insertion events and molecules falling down the step becomes unclear due to the disruption caused to the step by the arrival of the incident molecule. Figure 5.14 includes all incident molecules which were transported downwards into the 1st layer and consists of nearly all incident hyperthermal energies and values of ϕ and φ except for thermal collisions. Figures 5.15 and 5.16 show the only molecule leaving the system at E_i = 5 eV and the prevalence of thermal molecules which remain on top of the step, respectively. There was no obvious orientational bias observed for collisions at the step–edge.

Random orientation collisions, velocity non–normal to the surface (θ_i = 30° and 60°).

We studied the effect of molecular orientation on the fate of molecules with incident angles 30° and 60°. At these values of θ_i, the effect of molecular orientation was found

not to be significant and θ_i itself was the far more dominant variable probably due to the relatively upright orientation of the pentacene molecules within the crystal structure. As described earlier, increasing θ_i was found to minimize the number of direct insertion events and lead to more ejections from the system by rebounding off the top surface. In this study we noticed other rarer events, such as surface molecules being scattered by the incident molecule, or being transported up or down a layer. These events did not occur frequently enough to warrant numerical study.

5.4 Justification of assumptions and simulation methods

5.4.1 Single molecule *ab initio* calculations.

To investigate the suggestion that fragmentation of pentacene could play a role at higher incident energies, we have complemented our MD studies with *ab initio* calculations to estimate the strain imposed on molecules within the system and confirm that we are not operating within a bond–breaking regime. To test the internal strain on molecules we extracted the trajectories of a number of molecules with high kinetic energy as they underwent a collision with the pentacene surface and examined the internal energy of each molecule. Every 0.1 ps for the first 2 ps, where the distortions were most evident (up to 30° out of plane bending), the isolated single point energies of the incident molecule were calculated using two methods, firstly the MM3 potential itself and secondly *ab initio* MP2 calculations using Gaussian03 [41]. Although not a strictly fair comparison due to the energetic minima of the molecule for MP2/6-31g(d) calculations resulting in a slightly longer average bond length, the deviations from a planar molecule seemed to outweigh this. A typical collision trajectory is shown in Figure 5.17 where, for both

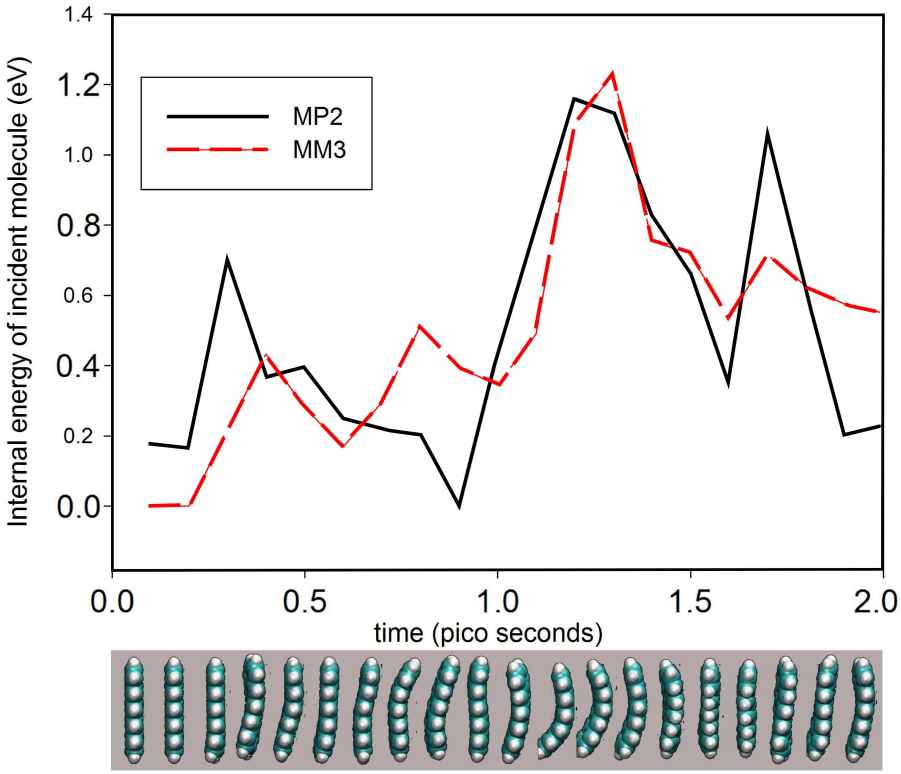

Figure 5.17: Evolution of the internal energy of a single incident molecule as a function of time, given a 10 eV incident kinetic energy, calculated with both the semi–empirical MM3 potential and the ab initio MP2/6-31g(d) model. The time evolution follows the particle throughout its collision with a surface showing the molecular distortion that occurs at around 1 ps. The molecular configuration of the incident molecule is shown below the graph at times corresponding to the energy–time plot given above.

methods of calculation, the maximum in energy occurred for the same highly distorted molecule around 1.2 - 1.3 ps. This maximum was an increase of 1.2 eV per molecule from the minimum configuration; thus, considering the covalent bond strength in the pentacene system is on the order of 5 eV, the impact energy is not enough to cause the internal fragmentation of the molecule. An alternative would be to employ the reactive AIREBO potential [42] to test the limits of the system in this regard, but we are confident that collisions of 10 eV incident kinetic energy are not within the fragmentation regime for pentacene.

5.4.2 Thermalisation and diffusion in simulations

Table 5.1: Destination of incident molecule for 5 incident energies.

energy(eV)	ejected	inserted	adsorbed
thermal	0	0	10
1	1	0	9
2	0	1	9
5	1	3	6
10	3	3	4

We analysed the thermalisation and diffusion properties of our system using a bulk surface (*i.e.*, with no step–edge present). The surface consisted of three layers of 5x5 unit cells (5400 atoms in total). Again, the bottom layer was frozen in bulk coordinates and the top two layers were free to move. For each incident energy (E_i = thermal, 1 eV, 2 eV, 5 eV, 10 eV), ten molecules were fired at the bulk pentacene surface. All incident molecules were randomly orientated but the incident angle was always 0^o. The results are summarized in Table 5.1 and Figure 5.18. When considering these results it must be remembered that there are a maximum of only ten trajectories at each incident energy and, thus, the statistical error will be relatively high.

Table 5.1 shows the destination of the incident molecules. The results are consistent

with our ‘bulk’ collision point in previous sections. Figure 5.18a shows the average displacement of molecules still on the surface after 50 ps. For molecules that adsorb on the surface, the average displacement is largest for the 10 eV collisions (45 Å) but not greatly larger than the thermal collisions (25 Å) remembering that pentacene is 15 Å in length). When insertions are also considered, this value decreases significantly because the inserted molecules remain static in an interstitial site and the average displacement is more or less constant over all energies. Importantly, looking at Figure 5.18b, the increased displacement of the higher energy molecules is due to the movement in the first 25 ps. From visualizations of these trajectories it is apparent that this is when the molecule is not ‘bound’ to the surface but is on a secondary bounce. It would be hard to describe this as surface diffusion but more a part of the collision event itself. After 10 ps there is very little difference in the trend of displacement versus time across all energies. The temperature of the system was also stable by 10 ps with none of the system temperatures rising above 310 K.

5.5 Conclusions

By a comparison of Molecular Dynamics simulations of pentacene hyperthermal deposition and experimental results, we have examined the dynamics of adsorption of pentacene on both an inorganic substrate (SiO_2) and an organic substrate. There are significant differences between the kinetics of growth in the monolayer regime (on SiO_2), and that in the multilayer regime (which are greatest at normal incidence and increasingly so with increasing incident kinetic energy).

Results from Molecular Dynamics are almost quantitatively identical to experiment and explain that direct insertion of molecules into the topmost layer contributes signifi-

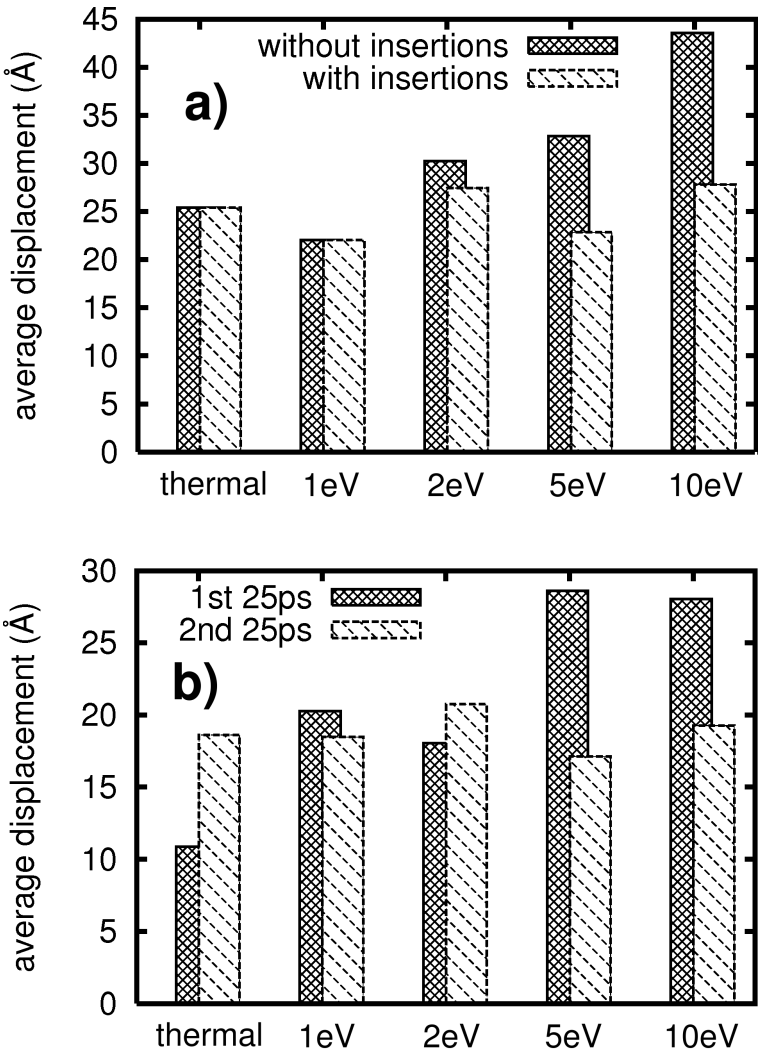

Figure 5.18: Average displacement (in Angstroms) for molecules remaining on the surface with $\theta_i = 0$ a) after 50 ps and b) a comparison of the first and second 25 ps.

cantly. Moreover, the ability of molecules to insert into the topmost layer is more facile near step–edges. Such insertion events may be expected to play a role in the dynamics of growth, possibly promoting smooth layer–by–layer growth, but experimental observations to date are contradictory. On the other hand, insertion events might also trigger other effects due to the generation of interstitial species and the accompanying strain that is introduced.

The effect of molecular orientation on the deposition event of a pentacene molecule colliding with the pentacene (010) step–edge was also investigated. For incident angle $\theta_i = 0^\circ$, a vertical orientation of the molecule ($\phi \leq 20^\circ$) greatly enhanced direct insertions at all hyperthermal values of E_i. If direct insertion was not observed, then the incident molecule was ejected in preference to remaining on top of the step, hence promoting growth of 2–D films. For randomly orientated molecules, a more gradual transition to 2–D growth was observed with increasing E_i. A detailed characterization of the pentacene molecular beam is therefore necessary to determine the optimal energy at which to deposit. Where more glancing angles of incidence ($\theta_i = 30^\circ$ and 60°) were used, the orientational bias was lost and very few direct insertion events were observed. The proximity of the collision to the step–edge was also an important factor. A downward funnelling mechanism at the step–edge was observed for all hyperthermal energies with no particular molecular orientational bias. *Ab initio* calculations on distorted pentacene molecules extracted from the MD simulations confirmed that we are not operating in a bond–breaking regime where molecules would preferentially fragment upon impact. Further, we showed the instantaneous nature of the collision event by examining the diffusion of incident pentacene molecules on a bulk surface.

BIBLIOGRAPHY

[1] A. S. Killampalli and J. R. Engstrom, "Nucleation of pentacene thin films on silicon dioxide modified with hexamethyldisilazane," *Appl. Phys. Lett.*, vol. 88, no. 14, p. 143125, **2006**.

[2] A. S. Killampalli, T. W. Schroeder, and J. R. Engstrom, "Nucleation of pentacene on silicon dioxide at hyperthermal energies," *Appl. Phys. Lett.*, vol. 87, no. 3, p. 033110, **2005**.

[3] T. Toccoli, A. Pallaoro, N. Coppede, S. Iannotta, F. D. Angelis, L. Mariucci, and G. Fortunato, "Controlling field-effect mobility in pentacene-based transistors by supersonic molecular-beam deposition," *Appl. Phys. Lett.*, vol. 88, no. 13, p. 132106, **2006**.

[4] Y. Wu, T. Toccoli, N. Koch, E. Iacob, A. Pallaoro, P. Rudolf, and S. Iannotta, "Controlling the early stages of pentacene growth by supersonic molecular beam deposition," *Phys. Rev. Lett.*, vol. 98, no. 7, p. 076601, **2007**.

[5] L. Casalis, M. F. Danisman, B. Nickel, G. Bracco, T. Toccoli, S. Iannotta, and G. Scoles, "Hyperthermal molecular beam deposition of highly ordered organic thin films," *Phys. Rev. Lett.*, vol. 90, no. 20, p. 206101, **2003**.

[6] D. J. Gundlach, "Organic thin film transistors with field effect mobility $> 2cm^2/$ Vs," *57th device research conference digest.*, vol. 1, p. 164, **1999**.

[7] O. D. Jurchescu, J. Baas, and T. T. M. Palstra, "Effect of impurities on the mobility of single crystal pentacene," *Appl. Phys. Lett.*, vol. 84 (16), p. 3061, **2004**.

[8] S. Pratontep, M. Brinkmann, F. Nuesch, and L. Zuppiroli, "Correlated growth in ultrathin pentacene films on silicon oxide: Effect of deposition rate," *Phys. Rev. B*, vol. 69, no. 16, p. 165201, **2004**.

[9] C. Kim, K. Bang, I. An, C. Kang, Y. Kim, and D. Jeon, "Morphology and ellipsometry study of pentacene films grown on native Sio_2 and glass substrates," *Curr. Appl. Phys.*, vol. 6, p. 925, **2006**.

[10] T. Minakata, H. Imai, and M. Ozaki, "Electrical properties of highly ordered and amorphous thin films of pentacene doped with iodine," *J. of Appl. Phys.*, vol. 72, no. 9, p. 4178, **1992**.

[11] R. Ruiz, B. Nickel, N. Koch, L. C. Feldman, R. F. Haglund, A. Kahn, and G. Scoles, "Pentacene ultrathin film formation on reduced and oxidized Si surfaces," *Phys. Rev. B*, vol. 67, no. 12, p. 125406, **2003**.

[12] S. Zorba, Y. Shapir, and Y. Gao, "Fractal-mound growth of pentacene thin films," *Phys. Rev. B*, vol. 74, no. 24, p. 245410, **2006**.

[13] F. J. Meyer zu Heringdorf, M. C. Reuter, and R. M. Tromp, "Growth dynamics of pentacene thin films," *Nature*, vol. 412, p. 517, **2001**.

[14] M. T. Lloyd, A. C. Mayer, A. S. Tayi, A. M. Bowen, T. G. Kasen, D. J. Herman, D. A. Mourey, J. E. Anthony, and G. G. Malliaras, "Photovoltaic cells from a soluble pentacene derivative," *Organic Electronics*, vol. 7, p. 243, **2006**.

[15] D. Guo, S. Ikeda, K. Saiki, H. Miyazoe, and K. Terashima, "Effect of annealing on the mobility and morphology of thermally activated pentacene thin film transistors," *J. Appl. Phys.*, vol. 99, no. 9, p. 094502, **2006**.

[16] S. K. Park, C. C. Kuo, J. E. Anthony, and T. N. Jackson, "High-mobility solution-processed OTFTs," *International Electron Device Meeting Technical Digest*, p. 113, **2005**.

[17] O. Ostroverkhova, D. G. Cooke, S. Shcherbyna, R. Egerton, R. R. Tykwinski, J. E. Anthony, and F. A. Hegmann, "Band-like transport in pentacene and functionalized pentacene thin films revealed by sub-picosecond transient photoconductivity measurements," *Phys. Rev. B.*, vol. 71, p. 035204, **2005**.

[18] M. O. Jahma, M. Rusanen, A. Karim, I. T. Koponen, T. Ala-Nissila, and T. S. Rahman, "Diffusion and submonolayer island growth during hyperthermal deposition on Cu(100) and Cu(111)," *J. Chem. Phys.*, vol. 112, no. 14, p. 6472, **2005**.

[19] J. W. Rabalais, A. H. Al-Bayati, K. J. Boyd, D. Marton, J. Kulik, and W. K. Chu, "Ion-energy effects in silicon ion-beam epitaxy," *Phys. Rev. B*, vol. 53, no. 10, p. 781, **1996**.

[20] S. Iannotta and T. Toccoli, "Supersonic molecular beam growth of thin films of organic materials: A novel approach to controlling the structure, morphology, and functional properties," *J. Polymer Science Part B: Polymer Physics*, vol. 41, no. 21, p. 2501, **2003**.

[21] J. Jacobsen, B. H. Cooper, and J. P. Sethna, "Simulations of energetic beam de-

position: From picoseconds to seconds," *Phys. Rev. B*, vol. 58, no. 23, p. 15847, **1998**.

[22] J. M. Pomeroy, J. Jacobsen, C. C. Hill, B. H. Cooper, and J. P. Sethna, "Kinetic Monte Carlo–molecular dynamics investigations of hyperthermal copper deposition on Cu(111)," *Phys. Rev. B*, vol. 66, no. 23, p. 235412, **2002**.

[23] "http://www.cheme.cornell.edu/cheme/people/profile/group.cfm?netid=jre7."

[24] J. Goose, A. Killampalli, P. Clancy, and J. Engstrom, "Molecular-scale events in hyperthermal deposition of organic semiconductors implicated from experiment and molecular simulation," *J. Phys. Chem. C*, vol. 113, no. 14, p. 6068, **2009**.

[25] D. Choudhary, P. Clancy, R. Shetty, and F. Escobedo, "A computational study of the sub-monolayer growth of pentacene," *Adv. Funct. Mater.*, vol. 16, no. 13, p. 1768, **2006**.

[26] J. R. Engstrom, D. A. Hansen, M. J. Furjanic, and L. Q. Xia, "Dynamics of the dissociative adsorption of disilane on Si(100): Energy scaling and the effect of corrugation," *J. Chem. Phys.*, vol. 99, no. 5, p. 4051, **1993**.

[27] N. L. Allinger, Y. H. Yuh, and J. H. Lii, "Molecular mechanics. the MM3 force field for hydrocarbons. 1.," *J. Amer. Chem. Soc.*, vol. 111, pp. 8551–8566, **1989**.

[28] J. H. Lii and N. L. Allinger, "Molecular mechanics. the MM3 force field for hydrocarbons. 2. Vibrational frequencies and thermodynamics," *J. Amer. Chem. Soc.*, vol. 111, p. 8566, **1989**.

[29] J. H. Lii and N. L. Allinger, "Molecular mechanics. the MM3 force field for hydrocarbons. 3. The van der waals' potentials and crystal data for aliphatic and aromatic hydrocarbons," *J. Amer. Chem. Soc.*, vol. 111, p. 8576, **1989**.

[30] L. Drummy, P. Miska, D. Alberts, N. Lee, and D. Martin, "Imaging of crystal morphology and molecular simulations of surface energies in pentacene thin films," *J. Phys. Chem. B*, vol. 110, no. 12, p. 6066, **2006**.

[31] J. E. Northrup, M. L. Tiago, and S. G. Louie, "Surface energetics and growth of pentacene," *Phys. Rev. B*, vol. 66, no. 12, p. 121404, **2002**.

[32] S. Verlaak, S. Steudel, P. Heremans, D. Janssen, and M. S. Deleuze, "Nucleation of organic semiconductors on inert substrates," *Phys. Rev. B*, vol. 68, no. 19, p. 195409, **2003**.

[33] D. Nabok, P. Puschnig, and C. Ambrosch-Draxl, "Cohesive and surface energies of π-conjugated organic molecular crystals: A first-principles study," *Phys. Rev. B*, vol. 77, no. 24, p. 245316, **2008**.

[34] W. Humphrey, A. Dalke, and K. Schulten, "VMD – Visual Molecular Dynamics," *J. Molecular Graphics*, vol. 14, p. 33, **1996**.

[35] J. W. Evans, D. E. Sanders, P. A. Thiel, and A. E. DePristo, "Low-temperature epitaxial growth of thin metal films," *Phys. Rev. B*, vol. 41, no. 8, p. 5410, **1990**.

[36] A. Killampalli. PhD thesis, Cornell University, **2004**.

[37] S. Hong, A. Amassian, A. R. Woll, S. Bhargava, J. D. Ferguson, G. G. Malliaras, J. D. Brock, and J. R. Engstrom, "Real time monitoring of pentacene growth on SiO_2 from a supersonic source," *Appl. Phys. Lett.*, vol. 92, no. 25, p. 253304, **2008**.

[38] F. Pirani, D. Cappelletti, M. Bartolomei, V. Aquilanti, M. Scotoni, M. Vescovi, D. Ascenzi, and D. Bassi, "Orientation of benzene in supersonic expansions, probed by IR-Laser Absorption and by Molecular Beam Scattering," *Phys. Rev. Lett.*, vol. 86, no. 22, p. 5035, **2001**.

[39] J. W. Evans, D. E. Sanders, P. A. Thiel, and A. E. DePristo, "Low-temperature epitaxial growth of thin metal films," *Phys. Rev. B*, vol. 41, no. 8, p. 5410, **1990**.

[40] M. Li and J. W. Evans, "Theoretical analysis of mound slope selection during unstable multilayer growth," *Phys. Rev. Lett.*, vol. 95, no. 25, p. 256101, **2005**.

[41] M. J. Frisch, G. W. Trucks, H. B. Schlegel, G. E. Scuseria, M. A. Robb, J. R. Cheeseman, J. A. Montgomery, Jr., T. Vreven, K. N. Kudin, J. C. Burant, J. M. Millam, S. S. Iyengar, J. Tomasi, V. Barone, B. Mennucci, M. Cossi, G. Scalmani, N. Rega, G. A. Petersson, H. Nakatsuji, M. Hada, M. Ehara, K. Toyota, R. Fukuda, J. Hasegawa, M. Ishida, T. Nakajima, Y. Honda, O. Kitao, H. Nakai, M. Klene, X. Li, J. E. Knox, H. P. Hratchian, J. B. Cross, V. Bakken, C. Adamo, J. Jaramillo, R. Gomperts, R. E. Stratmann, O. Yazyev, A. J. Austin, R. Cammi, C. Pomelli, J. W. Ochterski, P. Y. Ayala, K. Morokuma, G. A. Voth, P. Salvador, J. J. Dannenberg, V. G. Zakrzewski, S. Dapprich, A. D. Daniels, M. C. Strain, O. Farkas, D. K. Malick, A. D. Rabuck, K. Raghavachari, J. B. Foresman, J. V. Ortiz, Q. Cui, A. G. Baboul, S. Clifford, J. Cioslowski, B. B. Stefanov, G. Liu, A. Liashenko, P. Piskorz, I. Komaromi, R. L. Martin, D. J. Fox, T. Keith, M. A. Al-Laham, C. Y. Peng, A. Nanayakkara, M. Challacombe, P. M. W. Gill, B. Johnson, W. Chen, M. W. Wong, C. Gonzalez, and J. A. Pople, "Gaussian 03, Revision C.02." Gaussian, Inc., Wallingford, CT, 2004.

[42] S. J. Stuart, A. B. Tutein, and J. A. Harrison, “A reactive potential for hydrocarbons with intermolecular interactions,” *J. Chem. Phys.*, vol. 112, no. 14, p. 6472, **2000**.

CHAPTER 6

CONCLUSIONS AND FUTURE WORK

6.1 Accomplishments

The incredibly rich field of small organic molecular electronics, whilst still being a relatively new concept, has exploded in research activity in recent years. The more traditional inorganic semiconductor building blocks have established manufacturing techniques with well defined problems associated with patterning, lithography and annealing whereas the small organic molecule community has been forced by materials' constraints to take a different approach: Beyond the thermal budget associated with processing these molecules, the anisotropy of orientational preference to stack that is associated with these molecules, combined with the larger particle size (compared to atomic Si and SiGe systems, say) and their weak intermolecular interactions creates many obstacles in the quest to produce consistent, reproducible, commercial devices, even as these very same qualities are responsible for the inherent richness and diversity of the field of small organic molecules.

This thesis has attempted to illuminate some of the properties of these systems through molecular modelling. Previously there was very little understanding of even very basic issues of thin film growth of small organic molecules, for instance, the combination of transport, thermodynamics and kinetics, that occur for deposition and growth of thin films of these molecular crystals, here observed through Molecular Dynamics trajectories [1]. Even the observation that single planar molecules such as pentacene (and most of the other molecules studied here) lie down on the (001) surface, rather than stand up, when diffusing was not established beyond a static energy minimization picture. The latter observation has led to further investigation within our group on the

diffusive properties of organic molecules (see Cantrell *et al.* [2]) which, in turn, has opened up further areas of study of heterojunctions. The hyperthermal deposition simulations of pentacene, described in this thesis, have also led to further work within our research group, investigating the role of Self Assembled Monolayers either to assist or frustrate the growth of more exotic organic thin films than pentacene.

Some of the specific achievements described in this thesis can be summarised as follows:

1. Understanding the Ehrlich–Schwöebel barrier of organic molecules

Firstly, a detailed examination of the Ehrlich–Schwöebel barrier of the small organic molecule, sexiphenyl, which has the rotational freedom to twist and bend, led to the generally applicable conclusion that the nature of this barrier for molecular systems is far richer than had been previously understood. While the barriers for atomic systems can be represented by one value, it was shown that, for molecular systems, step-edge energy barriers depend sensitively on approach angle to the step-edge and that this, in turn, depends sensitively on the ability of the molecule to explore rotational degrees of freedom. As an example, sexiphenyl was used to explore how the degree to which the molecule was allowed to twist and bend affected the value of the Ehrlich–Schwöebel barrier. The adequacy of the empirical molecular mechanics MM3π model was established by comparison to numerous DFT models before using MM3π to represent the minimum energy path of sexiphenyl over a step-edge. The conformational flexibility of sexiphenyl led to a complicated mechanism of descent over a step-edge involving a combination of bending and twisting of the molecule that rigid models failed to capture, yet which only had a small effect on the magnitude of the barrier. A lower bound of 32.5 kJ/mol for the energy barrier at the commonly encountered (100) step-edge was reported. Also shown

was the importance of selecting a sufficiently representative intermolecular potential model and of employing an appropriately conducted search mechanism.

Secondly, the same search method was employed for six other commonly encountered organic molecules of differing size and shape (anthracene, tetracene, pentacene, diindenoperylene, rubrene and C_{60}) in an attempt to better understand the some of the underlying mechanisms of the step-edge barrier. The self-Schwöebel barriers were found to correlate well with both the Crystal Cohesive Energy and the binding energy to the top surface. We are the first to consider the heteroepitaxial barriers that occur when a molecule diffuses over a surface of a different type of molecule. We found that a correlation with the binding energy correlation was again a good measure of the step-edge barrier and will know allow researchers to estimate these barriers, reasonably accurately, without having to perform any molecular simulations and based solely on the geometric and energetic characteristics of the molecule . Several general rules for step-edge descent were discovered, primarily, the preference of long planar molecules to log-roll over the step-edge at angles that are within about 20 degrees off parallel to the step-edge.

2. Modelling the hyperthermal deposition of pentacene molecules

Significant insight into the molecular-level processes involved in the hyperthermal deposition of pentacene was achieved through Molecular Dynamics simulations. Experimental results from the Engstrom group over a similar range of incident energies (0-10 eV) and angles (30–90^o) revealed a change in the dynamics of growth of pentacene on SiO_2 compared to that on pentacene itself (at incident energies at and above 2 eV, the rate of growth accelerates, moving from the sub–mono-layer to the multilayer regime). Molecular-scale insight from simulation attributed a significant contribution to this effect to molecular insertion events into the topmost layer of the pentacene thin film.

Insertion also occurred on terrace sites at incident kinetic energies as low as 1 eV and is, we predict, more likely at step-edges than on terraces, though this detailed information is beyond the ability of experiments to confirm at this time.

The factors affecting the behaviour of an incident pentacene molecule colliding with the pentacene (010) step-edge were also examined with particular attention paid to the effect of molecular orientation in conjunction with incident kinetic energy (E_i) and angle (θ_i) of the incoming molecule and proximity of the collision of the incoming molecule to the step-edge. We predicted that ideal 2–D growth, manipulated through the experimentally controllable parameters, E_i and θ_i, could be enhanced if the molecular orientation within the beam could be controlled. For $\theta_i = 0°$, when the momentum of the incident molecule is aligned along the long axis of the molecule, downward inter–layer transport of the incident molecule is dominant for all hyperthermal energies. When the molecular orientation is random, higher energies must be employed to achieve the same degree of downward inter–layer transport. For non–zero values of θ_i, the mechanism for 2–D growth moves away from direct insertions thus reducing the bias on molecular orientation.

6.2 Future work

The large volume of fundamental energy barriers and probabilities for molecular events that were generated for these archetypal small organic molecules is ideal to be used as the input for a Kinetic Monte Carlo simulation. Such a framework is currently being devised within the Clancy group. The MM3(π) potential has been shown to provide an accurate description of the potential energy of the systems studied here at reasonable computational cost and is therefore a powerful tool. However, as has been shown in the

preceding chapters, the search method/framework is as important, if not more so, in discovering accurate energy barriers in complex systems. An incorporation of the potential into either a well researched Nudged Elastic Band or Transition Path Sampling [3] based framework would hopefully lead to a more robust method in finding molecular level energy barriers. In order to implement such a system it may be necessary to interface with Allinger's original code in C rather than the TINKER [4] modelling package (which has just undergone a new release). Although the tools within are TINKER are useful, they are not altogether easily adaptable due to the self-contained nature of the package.

In summary, this thesis has highlighted the complex nature of a representative set of small organic molecules and has advanced our fundamental understanding of the *dynamics* of organic molecular systems. This advance has been achieved largely through use of the semi-empirical MM3π potential. By careful comparison of the ability of many semi-empirical intermolecular potential energy models to those of more accurate *ab initio* calculations, we have shown the efficacy of these relatively simple models. Previous work has not recognized the ability of these models to capture the intricacies of these systems. Estimating how far this good correlation can be extended to molecules that contain atom types beyond carbon and hydrogen would be an interesting next step.

However, despite the success of semi-empirical ("all-atom") models, they are still computationally intensive enough that there is still a very considerable incentive to explore to what extent we can exploit a more coarse-grained approach, such as ellipsoidal potentials of the Gay–Berne variety [5] for materials processing simulations of film growth and the extent to which such models are able to retain key properties of the system. This endeavour is still at a fairly primitive stage and represents an interesting extension of the work described in this thesis.

BIBLIOGRAPHY

[1] J. Goose, A. Killampalli, P. Clancy, and J. Engstrom, "Molecular-scale events in hyperthermal deposition of organic semiconductors implicated from experiment and molecular simulation," *J. Phys. Chem. C*, vol. 113, no. 14, p. 6068, **2009**.

[2] R. Cantrell and P. Clancy, "A computational study of surface diffusion of C_{60} on pentacene," *Surface Science*, vol. 602, no. 22, p. 3499, **2008**.

[3] C. Dellago, P. Bolhuis, and P. Geissler, "Transition path sampling," *Advances in Chemical Physics*, vol. 123, no. 1, **2002**.

[4] J. W. Ponder, "Tinker - software tools for molecular design," **2004**.

[5] R. Everaers and M. R. Ejtehadi, "Interaction potentials for soft and hard ellipsoids," *Phys. Rev. E*, vol. 67, no. 4, p. 041710, **2003**.